Robust Time-Optimal Control for the One-Dimensional Optical Lattice for Quantum Computation

by

Botan Khani

A thesis
presented to the University of Waterloo
in fulfillment of the
thesis requirement for the degree of
Master of Science
in
Physics - Quantum Information

Waterloo, Ontario, Canada, 2011

I hereby declare that I am the sole author of this thesis. This is a true copy of the thesis, including any required final revisions, as accepted by my examiners.

I understand that my thesis may be made electronically available to the public.

Abstract

Quantum information is a growing field showing exciting possibilities for computational speed-up and communications. For the successful implementation of quantum computers, high-precision control is required to reach fault-tolerant thresholds. Control of quantum systems pertains to the manipulation of states and their evolution. In order to minimize the effects of the environment on the control operations of the qubits, control pulses should be made time-optimal. In addition, control pulses should be made robust to noise in the system, dispersion in energies and coupling elements, and uncertain parameters.

In this thesis, we examine a robust time-optimal gradient ascent technique which is used to develop controls of the motional degrees of freedom for an ensemble of neutral atoms in a one-dimensional optical lattice in the high dispersion regime with shallow trapping potentials. As such, the system is analyzed in the delocalized basis. The system is treated as an ensemble of atoms with a range of possible quasimomenta across the first Brillouin zone. This gives the ensemble of Hamiltonians, indexed by the quasimomenta, a distinct spectra in their motional states and highly inhomogeneous control Hamiltonians. Thus, the optical lattice is seen as a model system for robust control.

We find optimized control pulses designed using an ensemble modification of gradient-ascent pulse engineering robust to any range of quasimomentum. We show that it is possible to produce rotation controls with fidelities above 90% for half of the first Brillouin zone with gate times in the order of several free oscillations. This is possible for a spectrum that shows upwards of 75% dispersion in the energies of the band structure. We also show that NOT controls for qubit rotations on the entire Brillouin zone fidelities above 99% were possible for 0.6% dispersion in energies. The gate times were also in the order of several free oscillations. It is shown that these solutions are palindromic in time due to phase differences in some of the energy couplings when comparing one half of the Brillouin zone to another. We explore the limits of discretized sampling of a continuous ensemble for control.

Acknowledgements

I would like to express gratitude to my advisor Professor Frank Wilhelm for his patience, guidance, and wisdom. I would also like to thank members of my thesis committee who have volunteered their time to oversee my committee or defence, Professor Anton Burkov and Professor Adrian Lupaşcu, and Kevin Resch.

I would also like to give gratitude to my colleagues Dr. Jay Gambetta, Dr. Seth Merkel, and Felix Motzoi who have been wonderful in exchanging ideas. I would also like to acknowledge the camaraderie amongst the graduate students in the windowless room at the Institute for Quantum Computing, the many intellectually stimulating conversations that are struck and the fascinating perspectives of physics and science that their diverse backgrounds bring. I would like to thank Nathan Killoran for providing me with code to draw Bloch sphere diagrams that I used in this thesis. Finally, I would like to express gratitude to all those who have worked hard in building the Institute for Quantum Computing, and the researchers whose contributions to quantum technologies move us forward.

Dedication

This is dedicated to God almighty, the bringer of life and death. To worship Him is to worship truth, justice, and wisdom.

Table of Contents

List of Figures

Chapter 1

Introduction

Quantum information is a burgeoning field promising to provide some remarkable gains in computational speed, increased security in cryptography, as well as introducing the ability to break present cryptography schemes [33, 29, 40, 96, 68]. The field of quantum information pertains to the study of performing information processing in the realm of quantum physics. The possibility of quantum-based computing was introduced through a series of discoveries. One significant such discovery was in 1961 when Landauer argued that all information is physical since a physical process must occur to store and erase it [69]. In 1982, Feynman considered the idea of quantum computers as quantum simulators [33]. Another idea put forth from Feynman in 1985 was the possibility of quantum computation through controlled evolution of atomic quantum states [34]. That same year, Deutsch published a paper that introduced a fully quantum model of computation [26]. He argued that a quantum computer could simulate any finite physical system exactly and simulate any discrete stochastic classical processes. In 1998, DiVincenzo laid out the criteria by which quantum computers would function [28].

Very important to the field were discoveries of specific quantum algorithms in the early 1990s that showed the potential for quantum-based computers to have tremendous increases in computational speedup versus contemporary classical computers. One such algorithm was discovered by Peter Shor in 1994 in which he showed that a quantum algorithm was more efficient than a classical one. Complexity is defined as how the number of elementary operations required to perform the necessary computation changes as a function of the number of input bits. This particular algorithm showed that order-finding problems, such as factoring a number or finding a discrete logarithm could be performed on a quantum computer with a complexity that was super-polynomially better than the best known classical algorithms of the time [96]. As data security systems using public key encryption

schemes relied on the difficulty of factoring prime numbers for keeping encrypted information secure, a quantum algorithm had shown that they were vulnerable. Subsequently, great interest is still placed in the field of quantum information.

Another significant contribution to the field arrived in 1995 with the publication of Grover's search algorithm [45]. This algorithm showed that quantum computers could enjoy wide use in applications such as database searches. Although the improvement in computational speed is not as dramatic as Shor's algorithm, it is significant nonetheless. An important development in quantum computing was that quantum systems could be simulated by quantum computers more efficiently than classical computers, as postulated by the strong Church-Turing thesis [26]. This provides wide opportunities for scientific studies of physical systems that would otherwise have been too difficult to simulate, leading to new discoveries in physics and chemistry. Other significant algorithms showing vast improvements in quantum over classical computational speed followed, including: quantum Fourier transforms [4, 47], generalizations of specific hidden subgroup problems [32], quantum random walks [17], etc. Essentially, the field shows great promise as many discoveries continue to be made.

With the theories showing the vast capabilities and benefits of quantum information, the main challenge rests in the physical implementation of a quantum computer. A basic requirement for a quantum computer is that it must be able to prepare and maintain a series of well-defined quantum bits, or qubits, where a quantum state is stored as a superposition of two pure states in each qubit that may or may not be coupled. The quantum computer must then be able to perform a complete set of coherent quantum evolutions, or gates, in order to do computation on a qubit or series of coupled qubits. The state of the qubit must then be able to be physically measured. Lastly, the number of qubits a quantum computer can operate on must be scalable so that the computer can be made more complex.

When it comes to physical implementations, there are a variety of choices to experiment with: ion traps [20], neutral atom traps [44], cavity quantum electrodynamics (QED) [31, 103], photonics [63], liquid and solid state nuclear magnetic resonance (NMR) [112], superconducting qubit devices [21], topological quantum computing [84], etc. Each implementation has its own advantages and disadvantages. Regardless of their attributes, they must satisfy the basic requirements of a quantum computer. The main challenge common to some implementations such as superconducting qubits for quantum computation is improving coherence times. Coherence is the property of a state being preserved within a system. Decoherence is the opposite where information from a state within a system is spread to the external environment. Information that has leaked into the environment is both exceedingly difficult to measure and can not be computed by the quantum computer, thus being considered lost. With the advent of fault tolerant quantum error correction

codes by Shor and DiVincenzo in 1996, it was shown that quantum computers could tolerate finite noise allowing complex quantum algorithms to be performed effectively [30]. This was greatly improved upon by Laflamme and Knill with the development of a general theory of quantum error correction [64] and also by Gottesman with the introduction of stabilizer codes in 1997 [41].

The problem of decoherence is inherent to the nature quantum systems. Coherent quantum effects are effectively observable when coupling to the environment, that is everything that is external to the qubit, has been abated to minimize noise. In practice it is not possible to have a perfectly isolated qubit as it would preclude the ability to control and measure it, thus some noise will always be present. Despite the best efforts of experimentalists and theorists alike, gates can not be performed at present with precision high enough to satisfy required error correction thresholds. The solution requires more advanced designs [79], improved error correction codes, more advanced hardware, and performing qubit operations fast and precise enough to avoid issues with decoherence.

Another problem presented in quantum systems is imperfect knowledge of the system, imperfect hardware, and inhomogeneity in the state or controls of the system itself. Some implementations such as superconducting qubits require precise nanoscale fabrication of the device [65]. As a result, some parameters of the system may be significantly different from the intended design and are difficult to measure, leaving a parameter that may have a large uncertainty. In systems such as charge qubits, the quantized energy levels depends on a particular parameter that is prone to fluctuate between runs of the experiment, thus requiring robustness [65]. Other implementations of quantum computers such as some condensed matter systems contain an ensemble of systems with dispersion in energies [3]. A practical apparatus measuring and controlling the qubit may also be imperfect. Better hardware and engineering for quantum systems can be done though imperfections will always remain. However, being able to perform high precision qubit operations in the presence of imperfections through robust control would address these issues.

Research into quantum control aims to help resolve the problem of decoherence and deal with imperfections. Interest in the control of quantum systems has been present for over 60 years since the advent of experimental NMR spectroscopy [67, 35]. Coherent control of quantum systems is necessary in preparing states and evolving gates. Not limited to the burgeoning field of quantum computing, applications of quantum control to research and industry are widespread and include NMR spectroscopy and imaging, research in atomic trapping, metrology, and nanotechnology. In the beginning, quantum control techniques had centred around simple analytic pulses designed for idealized models of systems such as Rabi pulses for rotating the state of a qubit or Ramsey fringes for measuring a qubit's frequency [1, 100]. More sophisticated control techniques emerged as research in NMR

further advanced and the immediate need in quantum computing for high precision controllability arose [67]. These control techniques addressed many of these issues in quantum control. One such issue was the application of fast control pulses. For this, time-optimal numerical control methods allowed for pulses with short times. Since almost any quantum system is generally too complex for optimal control to be calculated analytically, numerical algorithms such as gradient ascent pulse engineering [59], Kaya-Huneault methods [58], real-embedding [49], Krotov [66], and genetic algorithms [56] are relied upon. Another issue is preventing unwanted transitions or couplings to quantum levels in a system that have a higher rate of decoherence than the qubit itself. Analytic pulse shaping methods such as derivative removal by adiabatic gate (DRAG), or stimulated Raman adiabatic passage (STIRAP) work to prevent such transitions while remaining time-optimal [52, 81, 38].

Other control methods seek to isolate the qubit by effective removal of coupling to the environment. The environment can not be controlled directly and behaves unpredictably with a system on short time scales. However, techniques derived from bang-bang control such as CPMG and dynamical decoupling utilize sufficiently fast pulses to effectively decouple the qubit hamiltonian from the environment by exploiting an effective time-reversal of its evolution with the bath environment [106, 91, 105, 104, 86, 14]. Dynamical decoupling can also be applied while performing quantum gates [61]. The only drawback is that they do not suppress the pure energy relaxation type of decoherence. However schemes such as the quantum Zeno effect can effectively eliminate relaxation by repeated measurements [78]. Other techniques to isolate a qubit from the environment include encoded protection from coupling errors and using decoherence-free subspaces [74, 102, 9].

Another important issue to be resolved by quantum control is robust control. Improved qubit controls would address incomplete knowledge of the system and imperfect hardware. This manifests as uncertainties in the parameters of the system, imperfectly executed control pulses, calibration errors, and dispersions in the energies. Controls that can be designed to be robust to these imperfections would allow for the high precision gates that are the requisite for a quantum computer. There are a variety of methods for designing robust control sequences which includes the composite for off-resonance with a pulse sequence (CORPSE) method [80], the broadband excitation by optimized pulses (BEBOP) [99], the band-selective uniform response pure-phase (BURP) [39], and modifications to standard time-optimal control methods such as gradient ascent pulse engineering [72].

A promising physical implementation for quantum computers is that of superconducting qubits. These devices rely on the non-linear effect of the Josephson junction and the phenomena of superconductivity to produce macroscopic quantum states consisting of a large quantity of electrons [21]. They do not require rigorous mechanical control for function unlike atomic traps and can be designed with desired parameters unlike molecules

used in NMR. Also, in situ tunability of energy couplings and non-linearity is possible. The most attractive feature of superconducting qubits is that the design and fabrication of the devices have much in similarity to the semiconductor chips mass produced by the computer industry. As a result, fabrication of the devices is possible with available technology. In addition, placing a qubit in a superconducting cavity mimics the effects of cavity quantum electrodynamics and helps shield it from noise sources while providing strong measurement and control coupling to the qubit. Most of all, they show great potential for scalability as multiple qubits can be coupled to a single cavity [108, 37].

The main challenges in such devices is their calibration in order for them to respond desirably to shaped control pulses. They also require ultra cold temperatures only producible within dilution refrigerators. In addition, their coherence times are much shorter than other implementations of quantum computers, on the order of a few ns to tens of μs. Initially, superconducting qubits had very few qubit operations that could be performed within their decoherence times. As an example, in 2002 the best performing charge qubit had a decoherence time of 0.5 μs and a qubit relaxation time of 1.8 μs [107]. However, as design engineering and fabrication improved along with more clever designs that were crafted, decoherence times improved significantly. By 2005 the highest decoherence time was 4 μs with a qubit relaxation time of 1 μs [6]. At present, a group in Yale has shown qubit relaxation times of up to 60 μs and superposition coherence times of 20 μs [85]. Taking into account the frequency of Yale's qubit, well over a million single-qubit rotations are possible during the coherence time, making it one of the best quantum devices at present. With the pace of improvements made in coherence times, superconducting qubits may be the first implementation to provide a fully scalable quantum computer. They certainly hold merit as potential candidates for quantum computing in the long-term future.

Superconducting qubit devices undoubtedly will require robustness to dispersions, noise, and imperfect hardware. One challenge would then be to provide high precision control pulses robust to errors. However, a challenging physical system for quantum computation should be selected, one that would be both difficult to control yet possible to benchmark control pulses in experiment. One such system is a one-dimensional optical lattice. They are also considered a candidate for a quantum computer [27] owing to their long coherence times and ease of scalability [68]. The one-dimensional optical lattice is a lattice of ultra cold atoms trapped by a standing potential of light along one axis in a vacuum chamber. The qubit state can then be encoded into the vibrational state of the atom. Controlling the system as a whole is a significantly difficult challenge since each atom may have its own position and quasimomentum with respect to the trapping potential well it sits in. Applying lasers on the entire system to wiggle the atoms or change the height of their trapping potential barriers is simple in experiment. However, having them perform high-precision

operations is not trivial if possible at all, especially for quantum computing. The reason is that the controls must be designed to be robust to the range of possible energies the atoms may have. Also, the atoms interact differently to the lasers depending on their vibrational state. As a result, there is inhomogeneity in both the energies and controls of the atoms. One recent proposal has suggested the use of global controls of atoms in addition to single atom addressability to perform high precision gates [94]. However, the need for robust control remains. Thus, if robust control can be demonstrated on a system as challenging as the optical lattice, than it is possible to apply robust control to many other systems.

This research pertains to the robust control of the optical lattice. In particular, robust time-optimal control using a modified gradient ascent algorithm for optimization over a discrete sample of an ensemble parameter. For complex problems such as controlling an ensemble it is generally difficult to find control sequences analytically. An alternative is to use techniques from optimal control theory where control pulses are developed using powerful numerical approaches [90, 66, 55, 59]. These numerical techniques are highly flexible since they are independent of the type of quantum system considered and can be adapted to many constraints such as the need for robustness. Optimal control theory has been applied to the problem of robust or ensemble control in many different contexts like NMR [72, 10, 98, 111], many-body entanglement [87], spin-chains [109], and spin systems [93].

In this thesis, it is shown that optimal control can perform high-fidelity gates in the presence of significant energy and coupling dispersion. In Chapter 2, a description of the physical model of the optical lattice is presented. In Chapter 3, an introduction to the use of time-optimal control theory is given with a description on robust control. In Chapter 4, the results are presented in detail. These results show the quality of robust control pulses designed by numerical gradient pulse engineering methods with limited resources. A description of an interesting result is given where higher fidelity gates were possible with shorter durations for high dispersion.

Chapter 2

Physical model: The optical lattice

2.1 Introduction

Optical lattices [7] are a candidate for quantum computing [27] since they are naturally scalable and provide long coherence times [68]. They are also useful for the simulation of strongly correlated many-body and other condensed matter systems [71, 8, 7]. Simulations of such systems can in turn be used to compute otherwise intractable problems such as antiferromagnetic transitions [97] and conductor to insulator transitions [53, 42], to name a few. Particles are bound in a lattice structure arrangement by optical wavelengths of light. The simplest one-dimensional optical lattice can be created by two counter-propagating beams of coherent light to create a standing wave potential. A local vapour cloud of neutral atoms is trapped in one dimension by light-induced forces with a binding potential that is proportional to the light intensity while being free to move in the other two spatial dimensions. The atoms are consistently kept at very low temperatures to ensure minimal energy fluctuations so that they remain bounded in the potential of the relatively weak trapping lasers and that their quantum mechanical nature may be observed and exploited. Investigating this system provides the opportunity to study a difficult control problem for quantum computation where the qubits are encoded into the vibrational states of the atoms [12, 16, 76, 94].

One of the advantages of optical lattices are the possibilities for control; however finding control sequences to perform desired operations is very difficult. The eigenstates of a periodic potential give a band structure where states within the bands are distinguished by quasimomentum (Fig. 2.1) and the coupling strength between states is also dependent on quasimomentum. The control task that is being set out for discussion is to perform a

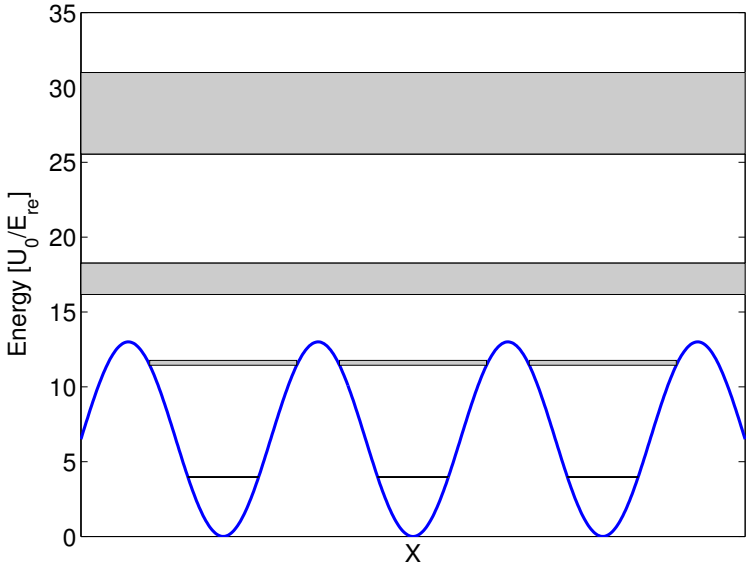

Figure 2.1: The first four energy bands (highlighted in grey) for a 1-D optical lattice are shown in the localized basis for potential depth $r = 13$ and compared to the sinusoidal trapping potential. Refer to Fig. 2.2.

single-qubit gate between atoms in the lowest two Bloch bands. These gates are naturally vertical, i.e., they connect states with equal quasimomenta since the eigenvalues e^{ika} of the discrete displacement operator are described by the quasimomenta k. The only controls available over the atoms are a global set that adjust the phase and intensity of the control laser, thus acting on all atoms. These controls do not affect the discrete displacement symmetry so that the quantum number k is not changed. The challenge is to control an ensemble of particles in parallel for preparing quantum states or performing gates despite undergoing different evolutions. This problem is mathematically equivalent to that of robust control [101, 19, 81, 89, 18, 92, 54, 73].

The purpose of this research is to investigate theoretical control sequences for the optical lattice in the broader scope of being able to further control the quantum system in the context of the gate model of quantum computing. In this Chapter, the physics of the one-dimensional optical lattice and the corresponding global controls are discussed, giving detail to the calculations of the eigenenergies of a system with a periodic potential and the control couplings in appropriate basis. In Section 2.2 & 2.3 the one-dimensional lattice model and

its band structure is introduced while developing a language connecting it to quantum control theory. The properties of the dispersion in the system and the anharmonicity of the eigenenergies as a consequence of weak binding potentials are observed in Section 2.4. The relation of this system to the charge qubit is given in Section 2.5. In Chapter 3 a description of how this inhomogenous system can be treated within control theory is developed. The results of this numerical control treatment are shown in Chapter 4.

2.2 Physics of the Optical Lattice

2.2.1 Static Model

We consider a physical model of a one-dimensional optical lattice similar to the experimental apparatus of the Steinberg group [76, 57, 77]. In their apparatus, the optical lattice potential is generated by two vertical counter-propagating lasers with an incidence angle of 49.6° and is loaded with ^{85}Rb atoms from an optical molasses at 10 μK. Since the densities of the atoms are 10^5 per lattice plane along with no transversal trapping, it can be assumed that there are no inter-atomic interactions. In addition, the coherence lengths of atoms are smaller ($\approx$ 60 nm) than the distance between wells ($\sim$1 μm) so that it can be assumed there is no coherence between wells. The lattice lasers are placed one above the other in the direction of gravity so that the Landau-Zener tunnelling rates are kept minimal [82]. In addition, excited atoms that fall out of the lattice tend to become spatially separated from bound atoms, thus minimizing inter-atomic interactions [82, 5]. However, the horizontal optical lattice has been considered here. One of the advantages to horizontal optical lattices is the availability of higher excited states for more qubits or as resource states for quantum operations. The Hamiltonian for an alkali atom interacting with an ideal optical lattice potential in 1-D is given by

$$H_0 = \frac{p^2}{2m} + U_0 \sin^2 k_L x \tag{2.1}$$

where m is the mass of the atom, k_L is the wave number of the lattice laser light and U_0 is the lattice potential depth. The potential is assumed uniform since the region of interest is small. Given that there are over 10^5 lattice sites in the region of interest the lattice is assumed to be infinite in length. Re-scaling this Hamiltonian gives

$$H_0 = \frac{p^2}{2m} + rE_{re} \sin^2 k_L x \tag{2.2}$$

Here $E_R = \hbar\omega_{re} = \hbar^2 k_L^2/2m$ is the recoil energy (i.e. the kinetic energy the atom gains by absorbing a lattice photon). In experiments, the depth is typically 18-30E_R, though a wider range was considered for this numerical study. At these lattice depths for typical atomic densities the atoms are essentially non-interacting and thus we can simplify the model by considering the evolution of a single atom interaction [76]. Finally, for the purposes of analysis, by letting

$$\begin{aligned} \tilde{\hbar} &= 1 \\ \tilde{x} &= k_L x \\ \tilde{t} &= \omega_{re} t \\ \tilde{p} &= -i\tilde{\hbar}\frac{\partial}{\partial \tilde{x}}, \end{aligned} \tag{2.3}$$

the Hamiltonian is expressed in a dimensionless form given by

$$\tilde{H}_0 = \tilde{p}^2 + r\sin^2\tilde{x} = \tilde{p}^2 + \frac{r}{2}(1 - \cos 2\tilde{x}), \tag{2.4}$$

where r is the lattice potential depth in units of recoil energies and $\tilde{p}$ is now the momentum in units of $\hbar k_L$. In order to analyze this system the eigenenergies and wavefunctions must be calculated. A Hamiltonian that contains a periodic potential has a well-known solution that can be derived using Bloch's theorem or Mathieu's functions, which will be referred to as Bloch solutions and Mathieu solutions, respectively. Choosing either method of deriving solutions is a matter of preference and of computational tools available since the solutions are mathematically equivalent. Mathieu solutions must be calculated using either algebraic approximation or numerical approaches [36]. Bloch solutions must be calculated through the use of similarity transformations in linear algebra which also must also be computed numerically for large systems (see Subsection 2.2.3). In any case, the resulting solutions using Wannier functions can also be derived to give Wannier states in the localized basis although they were not used in this research other than to verify the solutions of Bloch states.

2.2.2 Mathieu solutions

The Mathieu method for solving the static Hamiltonian of the one-dimensional optical lattice involves solving Schrödinger's equation explicitly. Letting $p = \hat{p} - p_0$, where p_0 is

the equivalent of quasimomentum k and $\hat{p} = -i\frac{d}{dx}$, the eigenstates can be solved as follows

$$H\psi(x) = E\psi(x)$$

where $\psi(x) = \psi(x + 2\pi)$.

$$\begin{aligned}
\left[(\hat{p} - p_0)^2 - r\cos^2 x\right]\psi(x) &= E\psi(x) \\
\left(-\frac{d^2}{dx^2} + 2ip_0\frac{d}{dx} + p_0^2\right)\psi(x) - r\cos^2(x)\psi(x) &= E\psi(x) \\
\psi''(x) - 2ip_0\psi'(x) + (E + r\cos^2(x) - p_0^2)\psi(x) &= 0
\end{aligned} \tag{2.5}$$

This equation can be reformulated into Mathieu's differential equation by assuming $\psi(x) = e^{ip_0x}g(x)$. The first term of the expression becomes

$$\begin{aligned}
(e^{ip_0x}g(x))'' &= (ip_0e^{ip_0x}g(x) + e^{ip_0x}g'(x))' \\
&= e^{ip_0x}[-p_0^2g(x) + 2ip_0g'(x) + g''(x)]
\end{aligned}$$

and the second term of the expression becomes

$$-2ip_0(e^{ip_0x}g(x))' = e^{ip_0x}[2p_0^2g(x) - 2ip_0g'(x)]$$

Thus

$$\begin{aligned}
(e^{ip_0x}g(x))'' - 2ip_0(e^{ip_0x}g(x))' + (E + r\cos^2 x - p_0^2)e^{ip_0x}g(x) &= 0 \\
e^{ip_0x}g''(x) + (E + r\cos^2 x)e^{ip_0x}g(x) &= 0 \\
g''(x) + \left(E + \frac{1}{2}r + \frac{1}{2}r\cos 2x\right)g(x) &= 0
\end{aligned} \tag{2.6}$$

Thus Eq. (2.6) is in the form of Mathieu's differential equation. This is solved by a Mathieu function $\mathrm{me}_\mu(q = -\frac{r}{4}, x)$, where μ is the exponential term. Thus the wavefunction for band level n is

$$\psi_n(x) = \frac{1}{\sqrt{2}}e^{ip_0x}\mathrm{me}_{-2[p_0 - k(n,p_0)]}\big(-\frac{r}{4}, x\big) \tag{2.7}$$

where

$$k(n,p_0) = \sum_{l=\pm 1} (\text{int}(2p_0 + l/2) \text{mod } 2) \times (\text{int}(p_0) + l(-1)^n[(n+1)\text{div } 2])$$

and int(a) rounds a to the nearest integer, a mod b is the modulus of a and b, and a div b is the integer divisor of a divided by b.

2.2.3 Bloch solutions

Bloch's solution utilizes the periodicity of the Hamiltonian by exploiting the symmetries of the potential and the fact that the Hamiltonian is invariant to spatial translations of integers of primitive lattice vectors. Bloch showed that Hamiltonians with periodic functions have periodic modulated plane wave solutions describing the wavefunction of a particle in a lattice. The length of a reciprocal primitive lattice vector for our Hamiltonian is $K = \frac{2\pi}{a}$, where a is the primitive lattice vector.

Proof

This proof to Bloch's theorem gives a more intuitive description. Beginning by defining the translation operator[1]:

$$T(\vec{G})f(\vec{r}) = f(\vec{r} + \vec{G}). \tag{2.8}$$

where $\vec{G}$ is a primitive lattice vector that translates by integers of lattice spacings.

In the first part of this proof, the translation operator is shown to commute with the Hamiltonian and thus both have simultaneous eigenvalues. The translation operator acts on a periodic Hamiltonian $H(\vec{r})$ with periodic eigenstate $\psi(\vec{r})$ to give

$$\begin{aligned} T(\vec{G})H(\vec{r})\psi(\vec{r}) &= H(\vec{r}+\vec{G})\psi(\vec{r}+\vec{G}) \\ &= H(\vec{r})\psi(\vec{r}+\vec{G}) \\ &= H(\vec{r})T(\vec{G})\psi(\vec{r}). \end{aligned} \tag{2.9}$$

Thus operating on a Hamiltonian gives

$$T(\vec{G})H(\vec{r}) = H(\vec{r})T(\vec{G}). \tag{2.10}$$

[1]This proof is based directly on the one shown on pg. 134 of Ashcroft and Mermin [2].

Also observe that applying multiple translation operations is independent of the order,

$$T(\vec{G})T(\vec{G}')\psi(\vec{r}) = \psi(\vec{G}+\vec{G}') = T(\vec{G}')T(\vec{G})\psi(\vec{r}). \tag{2.11}$$

Thus, the translation operator commutes with the Hamiltonian and as a consequence they share the same eigenbasis, i.e.

$$\begin{aligned} H\psi &= \epsilon\psi \\ T(\vec{G})\psi &= \lambda(\vec{G})\psi. \end{aligned} \tag{2.12}$$

so that $\lambda(\vec{G})$ is a simultaneous eigenvalue of the translation operator and the Hamiltonian.

In the second part of this proof, the solution to the eigenvalues and eigenstates are given. Observe that one set of translation operations can be written as

$$\begin{aligned} T(\vec{G})T(\vec{G}')\psi &= \lambda(\vec{G})T(\vec{G}')\psi \\ &= \lambda(\vec{G})\lambda(\vec{G}')\psi. \end{aligned} \tag{2.13}$$

and it can also be equivalently written as

$$\begin{aligned} T(\vec{G}')T(\vec{G})\psi &= T(\vec{G}+\vec{G}')\psi \\ &= \lambda(\vec{G}+\vec{G}')\psi. \end{aligned} \tag{2.14}$$

Thus, since the following relation must hold true

$$\lambda(\vec{G}+\vec{G}') = \lambda(\vec{G})\lambda(\vec{G}'), \tag{2.15}$$

the eigenvalues can be calculated using a suitable x_i to be

$$\lambda(\vec{a_i}) = e^{2\pi i x_i}. \tag{2.16}$$

where $\vec{a_i}$ is a primitive lattice vector.

Consider expressing the eigenvalues in terms of the primitive lattice translation vector,

$$\vec{G} = n_1\vec{a_1} + n_2\vec{a_2} + n_3\vec{a_3}, \tag{2.17}$$

where n_i is some integer. The eigenvalues become

$$\lambda(\vec{G}) = \lambda(\vec{a_1})^{n_1}\lambda(\vec{a_2})^{n_2}\lambda(\vec{a_3})^{n_3}. \tag{2.18}$$

Thus

$$\lambda(\vec{G}) = e^{i\vec{k}\cdot\vec{G}}, \tag{2.19}$$

where $\vec{k}$ is expressed in terms of the reciprocal lattice vectors $\vec{b_i}$

$$\vec{k} = x_1\vec{b}_1 + x_2\vec{b}_2 + x_3\vec{b}_3, \tag{2.20}$$

and $\vec{b_i} \cdot \vec{a_j} = 2\pi\delta_{ij}$.

Therefore the solution to Schrödinger's equation gives

$$T(\vec{G})\psi = \psi(\vec{r}+\vec{G}) = \lambda(\vec{G})\psi = e^{i\vec{k}\cdot\vec{G}}\psi(\vec{r}), \tag{2.21}$$

and $\psi(\vec{r})$ must be periodic in $\vec{G}$.

Bloch Solution

For our Hamiltonian in Eq. (2.4), according to Bloch's theorem we can assume that the eigenstates have the form

$$\Psi_n^{(k)}(x) = \langle x|\ \psi_n^{(k+Km)}\rangle = \psi_n^{(k+Km)}(x)e^{i(k+Km)x}, \tag{2.22}$$

where for some integer l

$$\left\langle (\frac{2\pi}{k}l + x \right|\ \psi_n^{(k)}\rangle = \langle x|\ \psi_n^{(k)}\rangle \tag{2.23}$$

and n indicates the state band level, k is the reciprocal lattice quasimomentum, $K = 2k_L$ is the primitive reciprocal lattice vector, m is an integer (Brillouin zone) lattice site number, and $\psi_n^{(k)}(m\pi x) = \psi_n^{(k)}(x)$ for all integers m. Essentially the wavefunction describing a particle with a one-dimensional periodic Hamiltonian is a wavefunction for a free particle with a periodic modulation. The resulting wavefunctions can be calculated using the central matrix method or the Bloch method [2, 62]. Here the quasimomentum will remain preserved for any control fields that are added to this Hamiltonian. As shown in the proof of Bloch's theorem, since the discrete translation operator commutes with the Hamiltonian, it shares its eigenbasis with the eigenstates of the one-dimensional optical lattice. As a result, the discrete translation operator commutes with the controlled Hamiltonian shown later in Eq. (2.29) so the e^{ika} of the discrete displacement operator are described by the quasimomenta k, and the quasimomentum is conserved for the control fields considered in Section 2.3. This allows us to express the Hamiltonian of the entire system as an ensemble of effective Hamiltonians over all quasimomenta where the Hamiltonian for a

given quasimomenta is:

$$\tilde{H}_0^{(k)} = (\tilde{p} - k)^2 + \frac{r}{2}(1 - \cos 2\tilde{x}), \tag{2.24}$$

satisfying $H_0^{(k)} \left|\psi_n^{(k)}\right\rangle = E_n^{(k)} \left|\psi_n^{(k)}\right\rangle$. Here one period of the potential is defined by choice of units to range from $-1 \leq x \leq 1$ for simplicity. Thus, having k restricted to the first Brillouin zone, the overall wavefunction for the entire ensemble system would be:

$$\Psi^{(k)}(x) = \sum_{m,n} \psi_n^{(k+Km)} e^{i(k+Km)x} \tag{2.25}$$

Following up to solving the eigenvalues analytically, the Hamiltonian from Eq. (2.4) is first rewritten in terms of the Fourier components of a generalized periodic potential,

$$\tilde{H}_0 = \tilde{p}^2 + \sum_g U_g e^{i\nu g\tilde{x}} \tag{2.26}$$

where ν is the minimum discrete frequency and U_g are the Fourier coefficients.

The eigenenergies can be solved using the proceeding wavefunction in Eq. (2.25) and Hamiltonian in Eq. (2.26) in Schrödinger's equation (The $\tilde{}$ symbol signifying dimensionless units will be dropped herein for brevity).

$$\begin{aligned}
0 &= H_0^{(k)}\Psi_n^{(k)}(x) - E_n^{(k)}\Psi_n^{(k)}(x) \\
0 &= \left(p^2 + \sum_g U_g e^{i\nu g x}\right) \sum_m \psi_n^{(k+Km)} e^{i(k+Km)x} - E_n^{(k)} \sum_m \psi_n^{(k+Km)} e^{i(k+Km)x} \\
0 &= \left(-\frac{\hbar^2}{2m}\frac{\mathrm{d}^2}{\mathrm{d}x^2} + \sum_g U_g e^{i\nu g x}\right) \sum_m \psi_n^{(k+Km)} e^{i(k+Km)x} - E_n^{(k)} \sum_m \psi_n^{(k+Km)} e^{i(k+Km)x} \\
0 &= \left(\frac{\hbar^2}{2m}(k+Km)^2 - E_n^{(k)}\right) \sum_m \psi_n^{(k+Km)} e^{i(k+Km)x} + \sum_{g,m} U_g e^{i(\nu g+k+Km)x} \psi_n^{(k+Km)} \\
0 &= \left(\frac{\hbar^2}{2m}(k+Km)^2 - E_n^{(k)}\right) \sum_m \psi_n^{(k+Km)} e^{i(k+Km)x} + \sum_{g,m} U_g e^{i(k+Km)x} \psi_n^{(k+Km-\nu g)}.
\end{aligned}$$

Since the periodicity of the lattice is determined by the periodicity of the potential, the magnitude of the primitive reciprocal lattice vector is equal to the smallest Fourier com-

ponent of the potential with non-zero frequency. I.e. $K = \nu$ so that the equation becomes

$$\begin{aligned}
0 &= \left(\frac{\hbar^2}{2m}(k+Km)^2 - E_n^{(k)}\right)\sum_m \psi_n^{(k+Km)} e^{i(k+Km)x} + \sum_{g,m} U_g \psi_n^{(k+K(m-g))} e^{i(k+Km)x} \\
0 &= \sum_m \left[\left(\frac{\hbar^2}{2m}(k+Km)^2 - E_n^{(k)}\right)\psi_n^{(k+Km)} e^{i(k+Km)x} + \sum_g U_g \psi_n^{(k+K(m-g))} e^{i(k+Km)x}\right] \\
0 &= \left(\frac{\hbar^2}{2m}(k+Km)^2 - E_n^{(k)}\right)\psi_n^{(k+Km)} + \sum_g U_g \psi_n^{(k+K(m-g))}
\end{aligned} \tag{2.27}$$

Denoting $\lambda^{(k)} = \frac{\hbar^2}{2m}(k+Km)^2$,

$$(\lambda^{(k)} - E_n^{(k)})\psi_n^{(k+Km)} + \sum_g U_g \psi_n^{(k+K(m-g))} = 0 \tag{2.28}$$

Result (2.28) is known as the **central equation** [62]. It only admits solutions whereby wavefunctions with quasimomenta k and quasimomenta that differ by K are admitted. This equation is written in a linear algebraic form to solve for the eigenvalues $E_n^{(k)}$ and eigenfunction $\psi_n^{(k+Km)}$.

$$\begin{pmatrix}
\ddots & & & & \\
\dots & (\lambda^{(k)} + U_0) - E_n^{(k)} & U_1 & U_2 & \dots \\
\dots & U_{-1} & (\lambda^{(k)} + U_0) - E_n^{(k)} & U_1 & \dots \\
\dots & U_{-2} & U_{-1} & (\lambda^{(k)} + U_0) - E_n^{(k)} & \dots \\
 & & & & \ddots
\end{pmatrix}
\begin{pmatrix}
\vdots \\
\psi_n^{(k+K(m-1))} \\
\psi_n^{(k+K(m))} \\
\psi_n^{(k+K(m+1))} \\
\vdots
\end{pmatrix} = 0$$

where m is the Brillouin zone number. Diagonalizing this matrix with respect to $E_n^{(k)}$ gives the eigenenergies and eigenstates for a particle with of fixed quasimomentum k and energy level n.

2.3 Dynamics Model

In a typical experimental setup [82], two lasers are placed at an angle of 49.6° to trap the atoms. These same lasers are used as control beams by directing their beams through

acousto-optic modulators where their relative phases can be controlled, allowing the trapping potential to spatially shift atoms along the axis of the lattice. The amplitude of the lasers can also be controlled, allowing modulation of the trapping potential depth. Following our horizontally oriented model of Steinberg's one-dimensional optical lattice, we introduce the system controls as two parameters $\eta(t)$ and $\phi(t)$ controlling the depth of the potential and the position of wells, respectively. Rewriting Eq. (2.24) in terms of these new variables we obtain,

$$H^{(k)}(t) = (p-k)^2 + r[1+\eta(t)]\sin^2\left(x + \frac{\phi(t)}{2}\right). \tag{2.29}$$

Here, the ˜ symbol has been dropped for brevity.

For the purpose of computing the time evolution of the system, the Hamiltonian in Eq. (2.29) is expressed in a form separating the time-dependent and independent variables:

$$\begin{aligned} H^{(k)}(t) =& (p-k)^2 + \frac{r}{2}\left[1+\eta(t)\right]\left[1-\cos\left(2x+\phi(t)\right)\right] \\ =& H_0^{(k)} - \frac{r}{2}\left[1-\cos(2x)\right] + \frac{r}{2}\left[1+\eta(t)\right]\left[1-\cos\left(2x+\phi(t)\right)\right]. \end{aligned} \tag{2.30}$$

Using the trigonometric identity $\cos(\phi+\theta) = \cos(\phi)\cos(\theta) - \sin(\phi)\sin(\theta)$

$$H^{(k)}(t) = H_0^{(k)} + \frac{r}{2}\left[1-(1+\eta(t))\cos\phi(t)\right]\cos(2x) + \frac{r}{2}(1+\eta(t))\sin\phi(t)\sin(2x) + \frac{r}{2}\eta(t). \tag{2.31}$$

In order to express the Hamiltonian in the standard form for quantum control (i.e. $H(t) = H_0 + \sum_p u_p(t)H_p$) we reparameterize the control fields in terms of

$$\begin{aligned} \alpha(t) =& \frac{r}{4}\Big[1-[1+\eta(t)]\cos\phi(t)\Big], \\ \beta(t) =& -\frac{r}{4}\Big[[1+\eta(t)]\sin\phi(t)\Big]. \end{aligned} \tag{2.32}$$

so that the total control Hamiltonian (neglecting the global phase $\frac{r}{2}\eta(t)$) is

$$\begin{aligned} H^{(k)}(t) &= H_0^{(k)} + 2\alpha(t)\cos(2x) - 2\beta(t)\sin(2x) \\ &= H_0^{(k)} + \alpha(t)(e^{2ix} + e^{-2ix}) + i\beta(t)(e^{2ix} - e^{-2ix}). \end{aligned} \tag{2.33}$$

In order to control a system with an ensemble of atoms spread over quasimomentum, the

system control fields $\alpha(t)$ and $\beta(t)$ must be found to perform desired quantum operations independent of k.

The remaining dynamic terms of the optical lattice Hamiltonian may be projected analytically into the Bloch basis using the following analysis.

Calculation of dynamic terms in the Bloch basis

The calculation of the dynamic terms of the Hamiltonian in the Bloch basis are straightforward as follows. Letting $k_L = 1$ so that $K = 2$,

$$\begin{aligned}
\langle \psi_{n'}^{(\hat{k}')} | e^{i2\hat{x}} | \psi_n^{(\hat{k})} \rangle &= \lim_{t\to+\infty} \int_{-t}^{t} \mathrm{d}x\mathrm{d}x' \langle \psi_{n'}^{(\hat{k}')} | x' \rangle \langle x' | e^{2i\hat{x}} | \hat{x} \rangle \langle \hat{x} | \psi_n^{(\hat{k})} \rangle \qquad \text{By resolution of identity} \\
&= \lim_{t\to+\infty} \int_{-t}^{t} \mathrm{d}x\mathrm{d}x' \Psi_{n'}^{*(\hat{k}')}(\hat{x}) e^{2i\hat{x}} \delta(\hat{x} - x') \Psi_n^{(\hat{k})}(\hat{x}) \\
&= \lim_{t\to+\infty} \int_{-t}^{t} \mathrm{d}x \sum_{m'} \psi_{n'}^{*(\hat{k}'+2m')} e^{-i(\hat{k}'+2m')\hat{x}} e^{i2\hat{x}} \sum_{m} \psi_n^{(\hat{k}+2m)} e^{i(\hat{k}+2m)\hat{x}} \\
&= \lim_{t\to+\infty} \int_{-t}^{t} \mathrm{d}x \sum_{m'm} \psi_{n'}^{*(\hat{k}'+2m')} \psi_n^{(\hat{k}+2m)} e^{-i(\hat{k}'+2m')\hat{x}} e^{i2\hat{x}} e^{i(\hat{k}+2m)\hat{x}} \\
&= \sum_{m'm} \psi_{n'}^{*(\hat{k}'+2m')} \psi_n^{(\hat{k}+2m)} \lim_{t\to+\infty} \int_{-t}^{t} \mathrm{d}x e^{i2(m-m'+1)\hat{x}} e^{i(\hat{k}-\hat{k}')\hat{x}} \\
&= \sum_{m'm} \psi_{n'}^{*(\hat{k}'+2m')} \psi_n^{(\hat{k}+2m)} \delta(m - m' + 1) \delta(\hat{k} - \hat{k}') \\
&= \sum_{m} \psi_{n'}^{*(\hat{k}+2m+1)} \psi_n^{(\hat{k}+2m)},
\end{aligned} \tag{2.34}$$

where the $\hat{}$ symbol has been used to denote canonical operators.

Similarly,

$$\begin{aligned}
\langle \psi_{n'}^{(\hat{k}')} | e^{-i2\hat{x}} | \psi_n^{(\hat{k})} \rangle &= \lim_{t\to+\infty} \int_{-t}^{t} \mathrm{d}x \Psi_{n'}^{*(\hat{k}')}(\hat{x})\ e^{-i2\hat{x}}\ \Psi_n^{(\hat{k})}(\hat{x}) \\
&= \sum_{m} \psi_{n'}^{*(\hat{k}+2m-1)} \psi_n^{(\hat{k}+2m)}.
\end{aligned} \tag{2.35}$$

2.4 Dispersion

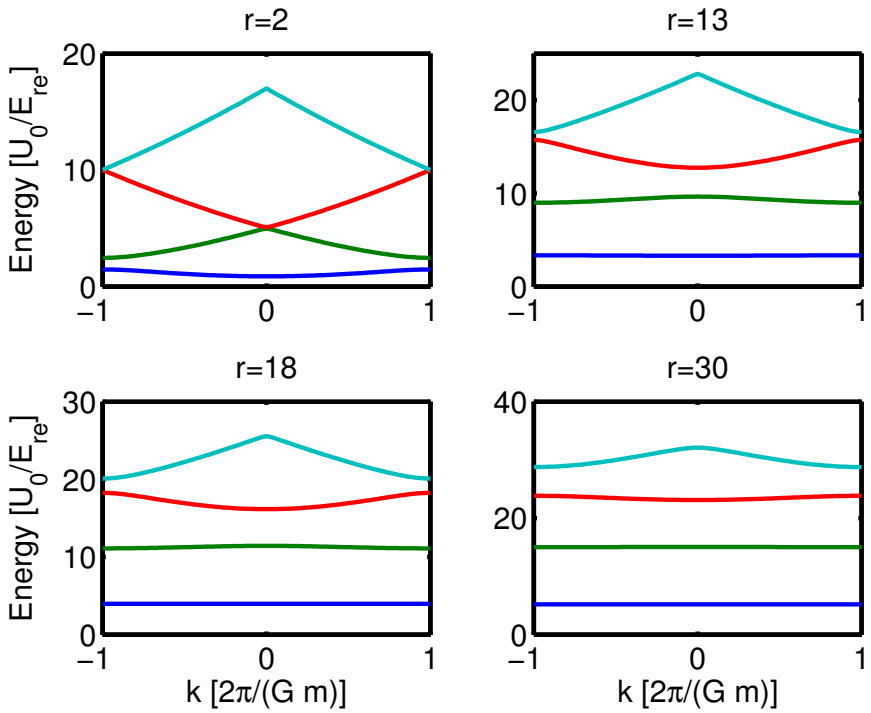

Figure 2.2: The first four energy 1-D band structures are shown in the momentum basis for four different potential depths r. The lower potential depth $r = 2$ (top left) shows the largest amount of energy dispersion and the closest energy crossings. The depth $r = 30$ (bottom right) shows a lesser amount of dispersion and larger energy splittings.

According to the model of the system outlined above, states with different quasimomenta will evolve independently so the system can be treated as an ensemble of non-interacting particles. Since the eigenenergies of this system depends on quasimomentum, there will be dispersion in the resonance frequencies across the range of quasimomenta. In other words, the resonant frequencies of excitations associated with different vertical transitions are not the same: see Fig. 2.2. This dispersion is characterized by the quantity

$$\mathcal{D} = 1 - \frac{\Delta E_{01}^{(1)}}{\Delta E_{01}^{(0)}}, \tag{2.36}$$

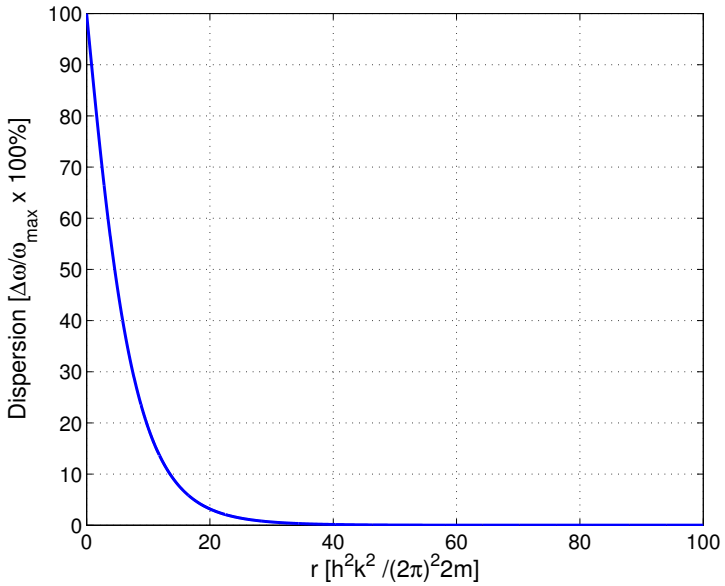

Figure 2.3: The dispersion between the first two energy bands in the 1-D optical lattice as a function of the potential depth.

where $\Delta E_{01}^{(k)} = E_1^{(k)} - E_0^{(k)}$.

The main consequence of the dispersion is that a single harmonic excitation cannot simultaneously excite all possible quasimomenta transitions, which poses a difficult challenge for controlling an ensemble with high dispersion. For the optical lattice, the amount of energy dispersion decreases with an increase in the strength of potential since the atoms become more localized, as shown in Fig. 2.3. The dispersion can be fitted to an exponential function for $r < 100$ to show its exponentially decreasing dependence on increasing potential as follows

$$\mathcal{D}(r) = 1.045e^{-0.1676r}. \tag{2.37}$$

Unfortunately the anharmonicity of the lattice, which is essential to resolve different transition frequencies, decreases polynomially with increasing potential depth (see Fig. 2.4). For $k = 0$ the relative anharmonicity can be characterized as

$$\delta(r) = -1.075e^{-0.0655r} - 0.04103e^{0.00521r}, \tag{2.38}$$

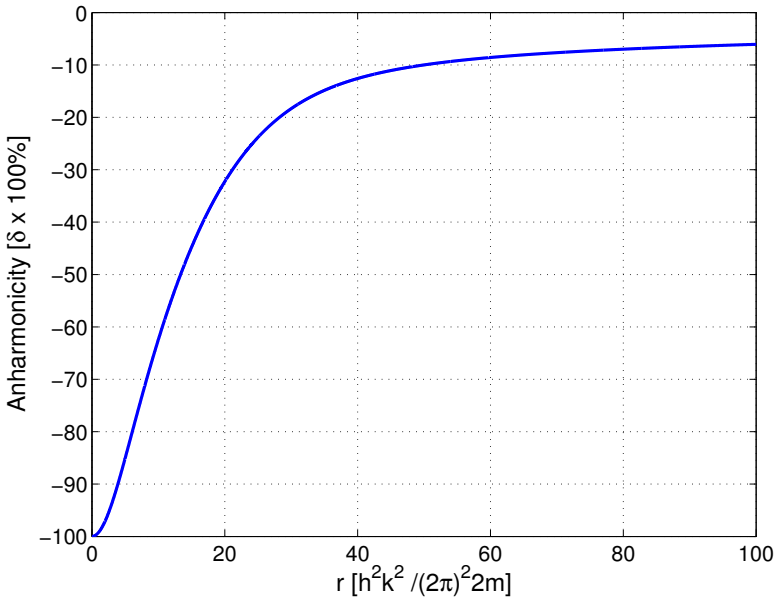

Figure 2.4: The anharmonicity of the first two energy levels at $k = 0$ as a function of the potential depth r.

where

$$\delta = 1 - \frac{\Delta\omega_{12}(k=0)}{\Delta\omega_{01}(k=0)} \tag{2.39}$$

signifies the deviation of the eigenenergies from harmonic energies. This leads to a trade-off when choosing the depth of the lattice between dispersion and anharmonicity.

In addition to the dispersion in the eigenenergies, there is significant dispersion over the quasimomentum space for the coupling matrix elements that represent the controls. This dispersion also decreases with the strength of the potential, and is higher for couplings to further neighbouring states, as shown Fig. 2.5. In addition, odd neighbouring coupling matrix elements such as the first and third nearest neighbour couplings have an opposite sign between one half of the first Brillouin zone and the other (see Appendix A for more detail and figures on the coupling bands). As a result, rotation operations between states separated by odd quantum numbers in the one dimensional optical lattice will be performed in opposing directions. Thus, with the addition of inhomogeneity in the couplings, it is a non-trivial task to develop controls sequences to account for both energy and coupling dispersion.

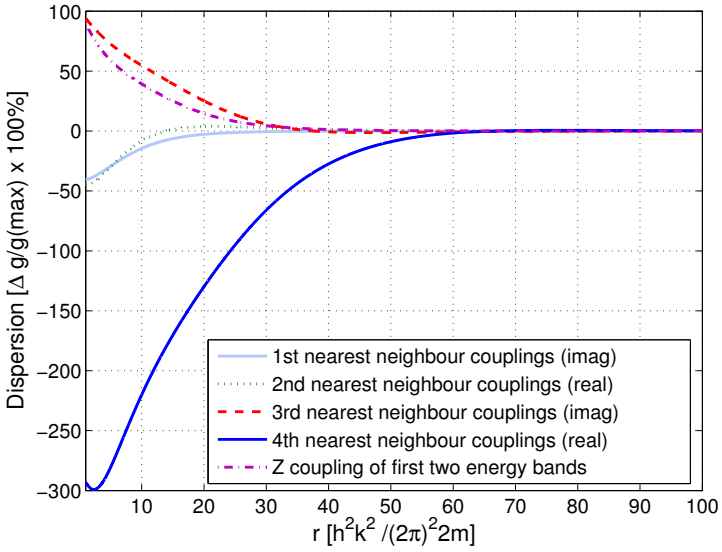

Figure 2.5: The dispersion in the real and imaginary coupling matrix elements (for $k > 0$) between the ground state and an excited state as a function of the trapping potential depth r. Here, the n^{th} nearest neighbour coupling level denotes the dispersion in coupling between the ground state and the n^{th} excited state.

2.5 Relation to the charge qubit (transmon)

Other systems can fit the model of the optical lattice as outlined in this chapter. One such system is the superconducting transmon qubit, allowing the results from the study of the 1-D optical lattice to be directly applicable to this system with minor modifications, as explained in this section.

The transmon is a device which contains a single charge qubit (Cooper-pair box) [11, 83] placed within a microwave coplanar waveguide cavity, providing shielding from r.f. noise and allowing for reduced sensitivity to charge noise [65]. The advantage to using this device is its insensitivity to critical current and flux noise compared to other superconducting qubit devices such as phase and flux qubits [110]. As a result, dephasing times are increased. The addition of the cavity also allows for dispersive readout to be performed. Reduction in charge sensitivity is achieved by the use of a very large capacitor placed within the cavity, thus increasing the Josephson to charging energy ratio. Typically, this ratio is $E_J/E_C \approx 20 - 50$, allowing for very low energy dispersions [50]. The charge qubit can be modelled similarly to the optical lattice. The simplified Hamiltonian of this system takes the form

$$\hat{H}^{(n_g)} = 4E_C(\hat{n} - n_g)^2 - E_J \cos\hat{\phi} \tag{2.40}$$

where $\hat{n}$ is the number of Cooper pairs on the superconducting islands, $\hat{\phi}$ is the phase difference to the island, E_C and E_J are the charging and Josephson energy, respectively and $n_g = C_g U/2e$ is the effective offset charge.

Since $\hat{n}$ and $\hat{\phi}$ are canonically conjugate variables, we can directly map this Hamiltonian onto that of the optical lattice by letting

$$\hat{n} \to p, \quad \hat{\phi} \to x \quad \text{and} \quad \frac{E_J}{E_C} \to \frac{r}{2}. \tag{2.41}$$

The only remaining component is to let the gate charge, n_g, play the role of the quasimomenta [95]. In this case, the gate charge would have a single value, unlike the ensemble in the one-dimensional optical lattice, but has uncertainty due to noise from fluctuating charges and voltages [51]. In order to control the charge qubit we must account for this inherent spread over n_g. The optimization techniques for these two systems will be identical, even though the causes of the dispersion are very different: ensemble averaging or parameter uncertainty. Pulse sequences such as CORPSE [24] has been applied to minimize fluctuations of the energy splittings [22] in superconducting qubits. This has been investigated to a greater extent numerically [80].

Chapter 3

Optimal Control Theory

3.1 Introduction

Control theory pertains to the control of a dynamical system given a static and dynamical description of that system, the effect of the control sequence on the system, and possibly the effects of an external system not controlled directly by the controls [55]. In quantum computation, it is a necessity to have control and as a consequence be able to control a quantum system.

The objective of control theory is to use a set of controls that make it possible for a system to perform a dynamic operation as best as possible given its dynamics and constraints whereas finding solutions analytically to perform the same operation to the desired degree of precision would be impossible. Often, the best control sequence can only be found through numerical techniques in limits where analytic approximations breakdown. However, in practice it may be impossible to find an optimal solution given limited computational resources for systems with complex dynamics.

There are essentially two general implementations of control on a system: open-loop and closed-loop feedback control. Closed-loop feedback involves controls that are adjusted according to measurements of the response of the system in order to manipulate it appropriately. This is valuable in controlling a system whereby the effects of the control is somewhat unpredictable due to imperfect control hardware, external effects of the environment, and lack of knowledge of the dynamic response of the system itself. Open-loop feedback control does not rely on physically measuring the response of a system during the application of control. As a result, the response of a system to a control application must

be well-known. If the response is not well-known a range of possible responses must be accounted for. The advantage here in using open-loop feedback control is that undesirable effects on the system due to measurements made during the application of the control and issues with measurement precision is avoided.

Since the one-dimensional optical lattice model in this research is simple enough to be modelled computationally, open-loop time-optimal control techniques are sufficient to finding pulses for performing state transfer and gate operations for the purposes of quantum computation. The following section outlines the control techniques suitable for systems such as the one-dimensional optical lattice.

3.2 Time-optimal control using gradient-ascent pulse engineering

GRAPE (gradient-ascent pulse engineering) is a numerical optimization routine that searches for optimal control sequences of a fixed duration [59, 13, 75, 15, 90]. A fidelity function Φ is a measure of the performance of the controls for a desired operation. Using a fidelity function the control sequence $\mathbf{u}$ are optimized using a gradient search over the fidelity landscape. In GRAPE, fidelity functions are made preferable to other measures of performance since taking the gradient of a fidelity is in general tractable.

A closed system with P degrees of freedom for control can be described by the Hamiltonian,

$$H(t) = H_0 + \sum_{p=1}^{P} u_p(t) H_p, \tag{3.1}$$

with H_0 and H_p being the drift and control Hamiltonians, respectively and $u_p(t)$ the control parameters for each degree of freedom. The unitary describing the evolution of the system is

$$U = \mathcal{T}\left[e^{-i\int_0^T H(t)\mathrm{d}t}\right], \tag{3.2}$$

where $\mathcal{T}$ is the time-ordering parameter.

The control sequence is initially $\mathbf{u}^{(0)}$ and is updated after each iterative optimization step r following the rule

$$\mathbf{u}^{(r+1)} = \mathbf{u}^{(r)} + \epsilon \nabla_u \Phi, \tag{3.3}$$

where ϵ is a step parameter that may be changed between iterations for faster convergence, and $\nabla_u \Phi$ is the gradient of the fidelity with respect to the controls. This gradient will

update the controls in an efficient manner that maximizes the fidelity. The iteration can continue until a desired minimum fidelity is reached. As a note, finding a global optimum is not guaranteed with this protocol. However, finding high-fidelity control sequences is possible by optimizing a number of different initial controls.

There are two different classes of fidelity functions considered here: performance of state transfers and performance of unitary operations (otherwise known as quantum gates).

Unitary operation

We consider a quantum system with a Hilbert space of dimension d. We apply the controls over a time T and discretize it as a series of N square pulses each with duration Δt so that $\mathbf{u_p} = \sum_n^N u_{p,n}$. The most common method of measuring the fidelity between the gates realized with these controls and the desired gate is

$$\Phi = \left| \frac{1}{d} \operatorname{Tr}[\ V^\dagger U(T)\ ] \right|^2, \tag{3.4}$$

where V is the desired gate. With a control sequence that is a set of square-pulses, the evolution unitary operator for the system can be written as

$$U_j = \exp\left\{ -i\Delta t \left(H_0 + \sum_{p=1}^{P} u_{p,j} H_p \right) \right\}. \tag{3.5}$$

Thus the realized gate at the end of the control sequence is

$$U(T) = U_N U_{N-1} \cdots U_2 U_1. \tag{3.6}$$

The gradient of the fidelity with respect to the controls can thus be calculated,

$$\begin{aligned} \frac{\partial \Phi}{\partial u_{p,j}} &= \frac{\partial}{\partial u_{p,j}} \left| \frac{1}{d} \operatorname{Tr}[V^\dagger U_N \cdots U_1] \right|^2 \\ &= \frac{1}{d^2} \frac{\partial}{\partial u_{p,j}} \left(\operatorname{Tr}[V^\dagger U_N \cdots U_1] \operatorname{Tr}[U_1^\dagger \cdots U_N^\dagger V] \right), \end{aligned} \tag{3.7}$$

where the cyclic permutation property of trace has been used. For simplicity, let the

backward and forward evolution propagators, respectively, be

$$\begin{aligned} P_j &= U_{j+1}^\dagger \cdots U_N^\dagger V \\ X_j &= U_j \cdots U_1, \end{aligned} \tag{3.8}$$

giving,

$$\begin{aligned} \frac{\partial \Phi}{\partial u_{p,j}} &= \frac{1}{d^2} \frac{\partial}{\partial u_{p,j}} (\mathrm{Tr}[P_j^\dagger X_j] \, \mathrm{Tr}[X_j^\dagger P_j]) \\ &= \frac{1}{d^2} \bigg(\mathrm{Tr} \left[P_j^\dagger \frac{\partial X_j}{\partial u_{p,j}} \right] \mathrm{Tr} \left[X_j^\dagger P_j \right] + \mathrm{Tr} \left[P_j^\dagger X_j \right] \mathrm{Tr} \left[\frac{\partial X_j^\dagger}{\partial u_{p,j}} P_j \right] \bigg) \\ &= \frac{1}{d^2} \bigg(\mathrm{Tr} \left[P_j^\dagger \frac{\partial U_j}{\partial u_{p,j}} U_{j-1} \cdots U_1 \right] \mathrm{Tr} \left[X_j^\dagger P_j \right] + \mathrm{Tr} \left[P_j^\dagger X_j \right] \mathrm{Tr} \left[U_1^\dagger \cdots U_{j-1}^\dagger \frac{\partial U_j^\dagger}{\partial u_{p,j}} P_j \right] \bigg). \end{aligned} \tag{3.9}$$

The derivative of the time evolution unitary of time step j is

$$\frac{\partial U_j}{\partial u_{p,j}} = \frac{\partial}{\partial u_{p,j}} \exp \bigg\{ -i\Delta t \bigg(H_0 + \sum_{p=1}^{P} u_{p,j} H_p \bigg) \bigg\}. \tag{3.10}$$

In order for this to be solved, we refer to the BCH lemma [48] which states:

$$\frac{\mathrm{d}}{\mathrm{d}x} e^{A+xB} \bigg|_{x=0} = e^A \int_0^1 e^{A\tau} B e^{-A\tau} \mathrm{d}\tau, \tag{3.11}$$

or

$$\frac{\mathrm{d}}{\mathrm{d}u_{p,j}} e^{-i\Delta t (H_0 + \sum_{p=1}^{P} u_{p,j} H_p)} = -i\Delta t U_j \bigg(\frac{1}{\Delta t} \int_0^{\Delta t} U_j(\tau) H_p U_j(-\tau) \mathrm{d}\tau \bigg), \tag{3.12}$$

where

$$U_j(\tau) = \exp \bigg\{ -i\tau \bigg(H_0 + \sum_{p=1}^{P} u_{p,j} H_p \bigg) \bigg\}. \tag{3.13}$$

Here, let $\bar{H}_p$ be the average Hamiltonian defined as the expression in the parenthesis of

Eq. (3.12). The gradient then simplifies to,

$$\begin{aligned}\frac{\partial \Phi}{\partial u_{p,j}} &= \frac{1}{d^2}\Bigg(\mathrm{Tr}\left[P_j^\dagger(-i\Delta t)\bar{H}_p U_j \cdots U_1\right] \mathrm{Tr}\left[X_j^\dagger P_j\right] + \mathrm{Tr}\left[P_j^\dagger X_j\right] \mathrm{Tr}\left[U_1^\dagger \cdots U_j^\dagger \bar{H}_p^\dagger i\Delta t P_j\right]\Bigg) \\ &= -\frac{i\Delta t}{d}\Bigg(\mathrm{Tr}\left[P_j^\dagger \bar{H}_p X_j\right] \mathrm{Tr}\left[X_j^\dagger P_j\right] - \mathrm{Tr}\left[P_j^\dagger X_j\right] \mathrm{Tr}\left[X_j^\dagger \bar{H}_p^\dagger P_j\right]\Bigg) \\ &= \frac{2\Delta t}{d}\mathrm{Im}\Bigg(\mathrm{Tr}\left[P_j^\dagger \bar{H}_p X_j\right] \mathrm{Tr}\left[X_j^\dagger P_j\right]\Bigg).\end{aligned} \tag{3.14}$$

The average Hamiltonian can be solved either explicitly or by approximation. In the first order approximation, assume that $\Delta t << ||H_0 + \sum_{p=1}^{P} u_{p,j} H_p||^{-1}$. Thus $U_j(\tau) \approx \mathbf{I}$ for $\tau \varepsilon [0,\ \Delta t]$ and using the approximation as $\Delta t << ||H(t)||^{-1}$, the average Hamiltonian becomes

$$\begin{aligned}\bar{H}_p &= \frac{1}{\Delta t}\int_0^{\Delta t} U_j(\tau) H_p U_j(-\tau) \mathrm{d}\tau \\ &\approx \frac{1}{\Delta t}\int_0^{\Delta t} \mathbf{I} H_p \mathbf{I} \mathrm{d}\tau \\ &= H_p.\end{aligned} \tag{3.15}$$

Thus, the derivative of the unitary with respect to the control can be approximated as

$$\frac{\partial U_j^\dagger}{\partial u_{p,j}} \approx -i\Delta t H_p U_j. \tag{3.16}$$

The advantage of the first order approximation to $\bar{H}_p$ is that it requires less computation than the explicit solution. However, there is potential for convergence problems during optimization since the gradient provided is not precise. For optimization over complex topological landscapes, it is advantageous to use the the explicit solution at the expense of a possible increase in computation. The difficulty in calculating the integral explicitly in Eq. (3.12) analytically is the exponentiated matrices. However, using similarity transformations (diagonalization) of the contents of the exponentiated expression in the time evolution unitary $U_j(\tau)$, the integral can be greatly simplified in this basis since the

unitaries become diagonal. Expanding the integral expression we have:

$$\bar{H}_p = \frac{1}{\Delta t}\int_0^{\Delta t} \exp\{-i\tau H_j\} H_p \exp\{i\tau H_j\} \mathrm{d}\tau, \tag{3.17}$$

where $H_j = H_0 + \sum_{p=1}^{P} u_{p,j} H_p$.

We now do a change of basis on Eq. (3.17) above using the basis transformation T_j that diagonalizes H_j. Letting $D = T_j^\dagger H_j T_j$ gives

$$T_j^\dagger \bar{H}_p T_j = \frac{1}{\Delta t}\int_0^{\Delta t} \exp\{-i\tau D\}\ T_j^\dagger H_p T_j\ \exp\{i\tau D\} \mathrm{d}\tau. \tag{3.18}$$

Using the vector set $|m\rangle\langle m|$ to represent the new basis, the diagonal matrix becomes $D = \sum_m \lambda_m |m\rangle\langle m|$ where λ_m is an eigenvalue of H_j. If we use bra-ket notation to write out the matrix elements of $\bar{H}_p$, we get:

$$\begin{aligned}
\langle m|\bar{H}'_p|n\rangle &= \langle m|T_j^\dagger \bar{H}_p T_j|n\rangle \\
&= \langle m|\frac{1}{\Delta t}\int_0^{\Delta t} e^{-i\tau\sum_{m'}\lambda_{m'}|m'\rangle\langle m'|}\ T_j^\dagger H_p T_j\ e^{i\tau\sum_{n'}\lambda_{n'}|n'\rangle\langle n'|} d\tau |n\rangle \\
&= \langle m|\frac{1}{\Delta t}\int_0^{\Delta t} \sum_{m'} e^{-i\tau\lambda_{m'}}|m'\rangle\langle m'|\ T_j^\dagger H_p T_j\ \sum_{n} e^{i\tau\lambda_{n'}}|n'\rangle\langle n'| d\tau |n\rangle \\
&= \sum_{m'n'}\frac{1}{\Delta t}\int_0^{\Delta t} e^{-i\tau\lambda_{m'}}\langle m|m'\rangle\langle m'|\ T_j^\dagger H_p T_j\ e^{i\tau\lambda_{n'}}|n'\rangle\langle n'|n\rangle d\tau \\
&= \sum_{m'n'}\frac{1}{\Delta t}\int_0^{\Delta t} e^{-i\tau\lambda_{m'}}\ \langle m'|T_j^\dagger H_p T_j|n'\rangle\ e^{i\tau\lambda_n}\delta_{m'm}\delta_{n'n} d\tau \\
&= \frac{1}{\Delta t}\int_0^{\Delta t} e^{-i\tau(\lambda_m-\lambda_n)}\ \langle m|T_j^\dagger H_p T_j|n\rangle\ d\tau \\
&= \begin{cases} \langle m|T_j^\dagger H_p T_j|n\rangle & \text{if } n = m \\ \frac{i}{\Delta t(\lambda_m-\lambda_n)}(e^{-i\Delta t(\lambda_m-\lambda_n)}-1)\ \langle m|T_j^\dagger H_p T_j|n\rangle & \text{if } n \neq m. \end{cases}
\end{aligned} \tag{3.19}$$

We must transform this solution back to the computational basis by undoing the similarity transformation so that we have the final solution for the average Hamiltonian. To calculate the analytic gradient, we use the same gradient as Eq. (3.14) with the appropriate

average Hamiltonian, i.e.

$$\frac{\partial \Phi}{\partial u_{p,j}} = \frac{2\Delta t}{d} \mathrm{Im}\Big(\mathrm{Tr}\left[P_j^\dagger (T_j \bar{H}'_p T_j^\dagger) X_j \right] \mathrm{Tr}\left[X_j^\dagger P_j \right] \Big). \tag{3.20}$$

State transfer

Following the previous section, GRAPE can also be applied to the task of preparing desired states from an initial state for a quantum system, i.e. state transfer. Essentially any state transfer can be generalized as a unitary operation. However, using state transfer optimization techniques allows the pulse to be designed to utilize the population of higher levels for more efficient transfer than is possible with a general gate [60].

The most common measure of state fidelity is

$$\Phi = \frac{1}{d} \mathrm{Tr}[\ C^\dagger \rho(T)\ ] \tag{3.21}$$

where C is the desired state, d is the dimension of the system, and $\rho(T)$ is the realized state at the end of the control sequence.

In similar fashion to the calculation shown in the previous section, the gradient of the fidelity with respect to the controls is computed to be

$$\frac{\partial \Phi}{\partial u_{p,j}} = -i \frac{\Delta t}{d} \mathrm{Tr}(\lambda_j^\dagger [\bar{H}_p, \rho_j]) \tag{3.22}$$

where the backward and forward propagators, λ_j and ρ_j respectively, are defined as

$$\begin{aligned} \lambda_j &= U_{j+1}^\dagger \cdots U_N^\dagger C U_N \cdots U_{j+1} \\ \rho_j &= U_j \cdots U_1 \rho_0 U_1^\dagger \cdots U_j^\dagger \end{aligned} \tag{3.23}$$

where the evolution unitary U_j at time j is defined as in Eq. (3.5), and the average Hamiltonian is defined as either Eq. (3.15) or Eq. (3.19).

Penalty functions

The simplest manner to optimize a pulse with restrictions on the controls such as total power or amplitude is to place penalty functions on the fidelity. These penalty functions

are added as an extra term in the fidelity and the appropriate term is added to the gradient of the fidelity. Eg., if the amplitude of the controls is preferred to be small, penalties for large amplitudes may be placed so that the fidelity becomes

$$\Phi' = \Phi - \sum_{p=1}^{P}\sum_{j=1}^{N}(|u_{p,j}|^2 - \alpha_p), \tag{3.24}$$

and the corresponding gradient is

$$\frac{\partial\Phi'}{\partial u_{p,j}} = \frac{\partial\Phi}{\partial u_{p,j}} - 2|u_{p,j}|, \tag{3.25}$$

where α_p is the strength of the penalties.

Strict amplitude restrictions may also be put in place for a control so that $|u_{p,j}| < \alpha_p$. With such restrictions, the fidelity becomes

$$\Phi' = \Phi - \sum_{p=1}^{P}\sum_{j=1}^{N}\left(\frac{1}{2}|u_{p,j}|^2 - \alpha_p|u_{p,j}|\right), \tag{3.26}$$

with gradient

$$\frac{\partial\Phi'}{\partial u_{p,j}} = \frac{\partial\Phi}{\partial u_{p,j}} - (|u_{p,j}| - \alpha_p). \tag{3.27}$$

3.3 Robust GRAPE

Robust GRAPE pertains to a set of global controls for a system that are optimized to be robust to at least one variable parameter which will henceforth be called an ensemble parameter. This parameter can be represented as noise, energy dispersion, uncertainty in system parameters, etc. To numerically optimize robust controls, a discrete sample of Hamiltonians over a range of the different varying parameters must be taken. For simplicity, in this subsection only one ensemble parameter, k, is considered. The framework in the previous section is continued here.

3.3.1 Discrete ensemble sampling for optimization

Pulses of finite time have a measurable frequency bandwidth thus the system to which it is applied will respond to a wide-band of available excitation frequencies. This property allows discrete optimization to work for a continuous ensemble parameter k.

Consider a simple two-state system with dipole coupling between levels and a simple π-on control pulse $f(x) = \alpha\cos(\omega_0 t)$ to perform a NOT gate. For a pulse applied for infinite time the Fourier transform would give the spectral function for frequency ω

$$\begin{aligned} F(\omega) &= \int_0^\infty \alpha f(x) e^{-i\omega t} dt \\ &= \alpha\sqrt{\frac{\pi}{2}}\delta(\omega-\omega_0) + \alpha\sqrt{\frac{\pi}{2}}\delta(\omega+\omega_0). \end{aligned} \tag{3.28}$$

For a finite duration of time T, the spectral function for the simple pulse would be

$$F(\omega;T) = \frac{A}{\omega^2-\omega_0^2}\left|\omega - e^{-iT\omega}(\omega\cos(\omega_0 T) + i\omega_0\sin(\omega_0 T))\right|, \tag{3.29}$$

where A is a normalization factor. This corresponds to a symmetrical spectrum that is peaked about the frequency ω_0, however the bandwidth of the spectrum is finite and the frequency is less well-defined with decreasing duration. The unitary time evolution as a function of the rotation angle θ for a fast, simple dipole interaction is

$$U[\theta] = e^{-i\sigma_X\frac{\theta}{2}} = \mathbf{I}\cos(\theta/2) - i\sigma_X\sin(\theta/2). \tag{3.30}$$

where σ_X is the Pauli-spin matrix representation of the dipole coupling. The unitary representing the evolution of the system with frequency response ω after some time T is

$$U[\pi F(\omega;T)] = \mathbf{I}\cos(F(\omega;T)\pi/2) - i\sigma_X\sin(F(\omega;T)\pi/2) \tag{3.31}$$

Using the fidelity function from Eq. (3.4) to measure the response of the physical system to the pulse, the fidelity can be expressed as

$$\Phi(\theta) = \left|\frac{1}{d}\,\mathrm{Tr}[\ V^\dagger U(\theta)\ ]\right|^2 \tag{3.32}$$

or with respect to Eq. (3.31)

$$\Phi(\omega) = \left| \frac{1}{d} \mathrm{Tr}[\ V^{\dagger} U(\pi F(\omega))\ ] \right|^2. \tag{3.33}$$

For a system with an ensemble parameter that results in varying resonance frequencies $\omega(k)$, the fidelity response would be

$$\Phi(k) = \left| \frac{1}{d} \mathrm{Tr}[\ V^{\dagger} U(\pi F(\omega(k)))\ ] \right|^2. \tag{3.34}$$

Since the bandwidth of the spectrum increases with decreasing pulse duration, Eq. (3.34) shows that the bandwidth of the response of the system also increases.

When choosing discrete points of the ensemble parameter k to optimize a system, the bandwidth should be large enough such that systems with intermediate ensemble parameters will also precisely perform the desired operation. Otherwise the time duration would have to be shortened or the distance between sampled k values would have to be decreased by sampling more points. This will become important in the description in Section 4.5.

The Nyquist sampling rate states that to sufficiently sample a function, the ideal sampling frequency must be at least twice the frequency bandwidth of the response [23]. Thus, for the specific fidelity function, given some time T, there will be a bandwidth b of the fidelity response as a function of the ensemble parameter k so that the sampling rate for optimization would be $\nu = 2b$. However, this is not completely necessary as using a proper fidelity function will design controls to be robust, as explained near the end of this subsection.

Unitary operation

The general Hamiltonian of a closed system with a dependence on an ensemble parameter is

$$H^{(k)}(t) = H_0^{(k)} + \sum_{p=1}^{P} u_p(t) H_p^{(k)}. \tag{3.35}$$

The system with the varying parameter will be treated as an ensemble of systems. We define the robust time evolution unitary operator as

$$U^{(k)} = \mathcal{T}\left[e^{-i \int_0^T H^{(k)}(t) \mathrm{d}t} \right], \tag{3.36}$$

where $\mathcal{T}$ is the time-ordering operator.

A suitable fidelity must be chosen so that its gradient is tractable. Choosing the fidelity function in Eq. (3.4) for each sampled value of the ensemble parameter is suitable. Thus, the overall fidelity function across the ensemble is

$$\Phi = \frac{1}{d^2}\left|\int \mathrm{d}k\ c(k)\,\mathrm{Tr}\left(V^\dagger U^{(k)}\right)\right|^2, \tag{3.37}$$

where d is the dimension of each system, V is the desired gate, and $c(k)$ is the distribution of the ensemble parameter. For numerical analysis, a discrete number of systems in the ensemble must be sampled with values $k_1, k_2, \ldots k_M$, where M is the number of systems sampled in the ensemble. Thus, the overall discretely sampled fidelity across the ensemble becomes

$$\Phi = \frac{1}{(dM)^2}\left|\sum_{l=1}^{M} c(k_l)\,\mathrm{Tr}\left(V^\dagger U^{(k_l)}\right)\right|^2. \tag{3.38}$$

For GRAPE, the gradient with respect to the controls, $\nabla_u \Phi$, must be provided. Using the property $|a|^2 = 2\mathrm{Re}(a)$, the corresponding gradient for the ensemble sampled fidelity is

$$\begin{aligned}\frac{\partial \Phi}{\partial u_{p,j}} =& \frac{2}{(dM)^2}\mathrm{Re}\left(\sum_{l=1}^{M} c(k_l)\,\mathrm{Tr}\left[V^\dagger \frac{\partial U^{(k_l)}}{\partial u_{p,j}}\right] \times \sum_{l'=1}^{M} c(k_l)\,\mathrm{Tr}\left[V^\dagger U^{(k_l')}\right]^*\right) \\ =& \frac{2}{(dM)^2}\mathrm{Re}\left(\mathrm{Tr}\left[V^\dagger \sum_{l=1}^{M} c(k_l)\frac{\partial U^{(k_l)}}{\partial u_{p,j}}\right] \times \sum_{l'=1}^{M} c(k_l)\,\mathrm{Tr}\left[V^\dagger U^{(k_l')}\right]^*\right),\end{aligned} \tag{3.39}$$

where

$$\frac{\partial U_j^{(k_l)}}{\partial u_{p,j}} = -i\Delta t U_j^{(k_l)} \bar{H}_p^{(k_l)}. \tag{3.40}$$

Here the average Hamiltonian can be approximated as $\bar{H}_p^{(k_l)} \approx H_p^{(k_l)}$ or expressed analytically as $\bar{H}_p^{(k_l)} = T_j^{(k_l)} \bar{H}_p^{(k_l)\prime} T_j^{(k_l)\dagger}$, where $T_j^{(k_l)}$ diagonalizes the Hamiltonian $H_j^{(k_l)}$ and

$$\langle m|\bar{H}_p^{(k_l)\prime}|n\rangle = \begin{cases} \langle m|T_j^{(k_l)\dagger} H_p^{(k_l)} T_j^{(k_l)}|n\rangle & \text{if } n = m \\ \frac{i}{\Delta t(\lambda_m - \lambda_n)}(e^{-i\Delta t(\lambda_m - \lambda_n)} - 1)\ \langle m|T_j^{(k_l)\dagger} H_p^{(k_l)} T_j^{(k_l)}|n\rangle & \text{if } n \neq m. \end{cases} \tag{3.41}$$

For a d-dimensional system, the computational-scaling for calculating the gradient for M

different evolutions scales by a factor of M compared to standard GRAPE. This is an improvement over representing the discrete ensemble as a dM-dimension Hilbert space since $d \times d$ matrix multiplication scales with $\mathcal{O}(d^3)$.

For simplicity, let the backward and forward propagators be defined, respectively, as

$$\begin{aligned} P_j^{(k_l)} &= {U_{j+1}^{(k_l)}}^\dagger \cdots {U_N^{(k_l)}}^\dagger V \\ X_j^{(k_l)} &= U_j^{(k_l)} \cdots U_1^{(k_l)}. \end{aligned} \tag{3.42}$$

Using Eq. (3.40) and Eq. (3.42), the gradient of the sample fidelity Eq. (3.39) can be expressed as

$$\begin{aligned} \frac{\partial \Phi}{\partial u_{p,j}} &= \frac{2}{(dM)^2} \mathrm{Re}\Bigg(\sum_{l=1}^{M} c(k_l) \,\mathrm{Tr}\left[P_j^{\dagger(k_l)} \frac{\partial X_j^{(k_l)}}{\partial u_{p,j}} \right] \sum_{l'=1}^{M} c(k_l) \,\mathrm{Tr}\left[X_j^{\dagger(k'_l)} P_j^{(k'_l)} \right] \Bigg) \\ &= \frac{2}{(dM)^2} \mathrm{Re}\Bigg(\sum_{l=1}^{M} c(k_l) \,\mathrm{Tr}\left[P_j^{\dagger(k_l)} \frac{\partial U_j^{(k_l)}}{\partial u_{p,j}} X_{j-1}^{(k_l)} \right] \sum_{l'=1}^{M} c(k_l) \,\mathrm{Tr}\left[X_j^{\dagger(k'_l)} P_j^{(k'_l)} \right] \Bigg) \\ &= \frac{2}{(dM)^2} \mathrm{Re}\Bigg(\sum_{l=1}^{M} c(k_l) \,\mathrm{Tr}\left[P_j^{\dagger(k_l)} \big(-i\Delta t \bar{H}_p^{(k_l)} \big) X_j^{(k_l)} \right] \sum_{l'=1}^{M} c(k_l) \,\mathrm{Tr}\left[X_j^{\dagger(k'_l)} P_j^{(k'_l)} \right] \Bigg) \\ &= \frac{2\Delta t}{(dM)^2} \mathrm{Im}\Bigg(\sum_{l=1}^{M} c(k_l) \,\mathrm{Tr}\left[P_j^{\dagger(k_l)} \bar{H}_p^{(k_l)} X_j^{(k_l)} \right] \sum_{l'=1}^{M} c(k_l) \,\mathrm{Tr}\left[X_j^{\dagger(k'_l)} P_j^{(k'_l)} \right] \Bigg). \end{aligned} \tag{3.43}$$

There are a variety of other fidelity functions that could be used for robust GRAPE

and provide suitable gradients such as:

$$\Phi_1 = \frac{1}{(dM)^2} \sum_{l=1}^{M} \left| c(k_l) \operatorname{Tr}\left(V^\dagger U^{(k_l)}\right) \right|^2 \tag{3.44a}$$

$$\Phi_2 = \frac{1}{dM} \operatorname{Re}\left(\sum_{l=1}^{M} c(k_l) \operatorname{Tr}\left(V^\dagger U^{(k_l)}\right) \right) \tag{3.44b}$$

$$\Phi_3 = \frac{1}{dM} \operatorname{Im}\left(\sum_{l=1}^{M} c(k_l) \operatorname{Tr}\left(V^\dagger U^{(k_l)}\right) \right) \tag{3.44c}$$

$$\Phi_4 = \frac{1}{dM} \left| \sum_{l=1}^{M} c(k_l) \operatorname{Tr}\left(V^\dagger U^{(k_l)}\right) \right| \tag{3.44d}$$

$$\Phi_5 = \frac{1}{dM} \sum_{l=1}^{M} c(k_l) \left| \operatorname{Tr}\left(V^\dagger U^{(k_l)}\right) \right| \tag{3.44e}$$

Remarks

The fidelity function in Eq. (3.38) is different from just a simple average of the standard gate fidelity over the ensemble. This fidelity function is particularly important in that it accounts for phase differences across the sampled fidelities and optimizes the controls to minimize this difference. At first glance it would seem that the phase in $U^{(k)}$ is not relevant, however it's phase ensures that intermediate regions between sampled ensemble points evolve in the same manner. This resolves the issue of having to ensure that pulse durations must be short enough for their broadband frequencies to perform operations in the intermediate regions of the ensemble that were not directly optimized. Following an example given by Dr. Seth Merkel, consider evolutions on all traceless Hamiltonians. The unitary group representing all available evolution operators are $SU(d)$, thus all unitary evolution operators have $\det(U) = 1$. Assuming $\det(V) = 1$, there are only a finite set of unitary maps that maximize $|\operatorname{Tr}(V^\dagger U)|$. These unitary operators can admit a determinate of $U = e^{i2\pi q/d} V$ where $q = 1 \ldots d$. For intermediate regions in quasimomentum space between two different phases, there may be poor fidelity since $U^{(k)}$ can not change instantaneously due to the nature of broadband pulses (see Subsection 3.3.1). For a physical system such as a one-dimensional optical lattice, the evolutions are not all $SU(d)$, however it is suspected that similar arguments can be made for the requirement of global phase matching of $U^{(k)}$ although this requires further investigation. In practice, the optimization will be trapped in local maxima of poor fidelity if global phase is neglected. This is evident

when points sampled in k space for optimization have higher fidelities than intermediate regions between two sampled points. The fidelity that has been chosen for optimization of the ensemble accounts for this phase to ensure that it is uniform throughout the ensemble parameter space.

State transfer

Using the derivations of the previous section, robust state transfer is summarized with a modified phase constrained fidelity function based on Eq. (3.21). Using the definitions from the previous section, this can be expressed as

$$\Phi = \frac{1}{dM}\left|\sum_{l=1}^{M} c(k_l)\,\mathrm{Tr}\left(C^{\dagger}\rho^{(k_l)}\right)\right|. \tag{3.45}$$

where C is the desired state. The corresponding gradient of the fidelity is

$$\frac{\partial\Phi}{\partial u_{p,j}} = \frac{2\Delta t}{d}\mathrm{Im}\left(\sum_{l=1}^{M} c(k_l)\,\mathrm{Tr}(\lambda_j^{\dagger(k_l)}[\bar{H}_p^{(k_l)},\rho_j^{(k_l)}])\right) \tag{3.46}$$

where the backward and forward propagators are defined, respectively, as

$$\begin{aligned}\lambda_j^{(k_l)} &= U_{j+1}^{\dagger(k_l)}\cdots U_N^{\dagger(k_l)} C U_N^{\dagger(k_l)}\cdots U_{j+1}^{\dagger(k_l)}\\ \rho_j^{(k_l)} &= U_j^{(k_l)}\cdots U_1^{(k_l)}\rho_0^{(k_l)} U_1^{\dagger(k_l)}\cdots U_j^{\dagger(k_l)}.\end{aligned} \tag{3.47}$$

3.3.2 Advanced optimization techniques

There are many techniques that can be used to carry out gradient search-based optimization more effectively in order to find the best control pulses. One of the problems with using GRAPE is how to efficiently utilize computational resources to find good solutions and handle local maxima traps which cause convergence issues. One of the main approaches to this problem involves an algorithmic approach to adapting the gradient step parameter ϵ and in managing convergence issues. However, one must consider that different algorithmic approaches have different computational complexities and performances in handling traps [25]. In general, algorithms should be investigated and chosen appropriately. In this section, the most comprehensive algorithm used for generating robust controls is reviewed and described. In addition, techniques for dealing with convergence issues are briefly overviewed.

Comprehensive Algorithm

At first glance, it appears that the comprehensive algorithm requires the most resources to implement however it is the most likely to converge to a solution, as shown in Fig. 3.1. The idea behind it is to ensure that any steps taken with the gradient in modifying the controls will increase fidelity in an efficient manner. The step parameter ϵ is changed adaptively; being increased when the controls have increased the fidelity and decreased otherwise. The first iteration will have the fidelity Φ_{before} and its gradient calculated. A second fidelity Φ_0 is calculated again after the controls are updated using the gradient.

The next step is to ensure that the updated controls have increased the fidelity, thus indicating that the controls are being optimized. First, the fidelity for each ensemble parameter is checked to see if it has exceeded the desired fidelity Φ_{max}. Checking the fidelity $\Phi_0^{(l)}$ of each ensemble parameter l rather than the fidelity of the entire ensemble Φ_0 is done in the interest of having an operation performed with the minimum fidelity for all sampled points in the ensemble. Exceeding Φ_{max} for all sampled $\Phi_0^{(l)}$ signifies the successful optimization of the control sequence.

If the control has not been successfully optimized, the next step is to check if there is a change in the current fidelity from the previous fidelity. It is not possible to further optimize the control if the change in fidelity is no longer detectable due to finite precision in numerical computation. As a result, the best possible solution is the previous control.

With the success of the previous check, the next check is to ensure that the ensemble fidelity Φ_0 has increased from the previous iteration. If it is has increased, then the controls are updated with the gradient. The gradient step parameter ϵ is then adaptively increased and the next iteration begins. If it has not increased, this may be a result of too large of a modification of the controls by the gradient. The step parameter ϵ is then decreased by $\alpha\ \epsilon(0,1)$ until an increase in the fidelity is detected. If an increase is not detected when the step parameter is below the threshold μ, then it is considered unreasonable to continue to search for a convergent solution.

Miscellaneous Techniques

For systems and desired operations that are complex, using numerical optimization techniques to attain control sequences may be difficult. The optimization process may often not be able to return convergent controls with reasonable resources due to the inherent complexity of the fidelity landscape [88]. As a result, additional techniques may be employed in optimization. Such techniques include: simulated annealing on the control landscape

for situations when the control sequence will not converge to a solution, appropriately changing the step parameter ϵ, choosing random initial controls, and choosing intuitive initial controls based on analytic techniques. These techniques are adapted to the system of interest and the desired operation. In this thesis, all such techniques were employed except for simulated annealing, which was avoided due to the instability of finding good solutions that occurs when coordinates on a fidelity landscape are randomized.

It is not a precise science to use the techniques described above, it often requires knowledge and experience to employ a successful strategy. However, a hybrid of GRAPE with highly adaptive genetic algorithms has been proposed to complement the weaknesses of gradient ascent algorithms [70].

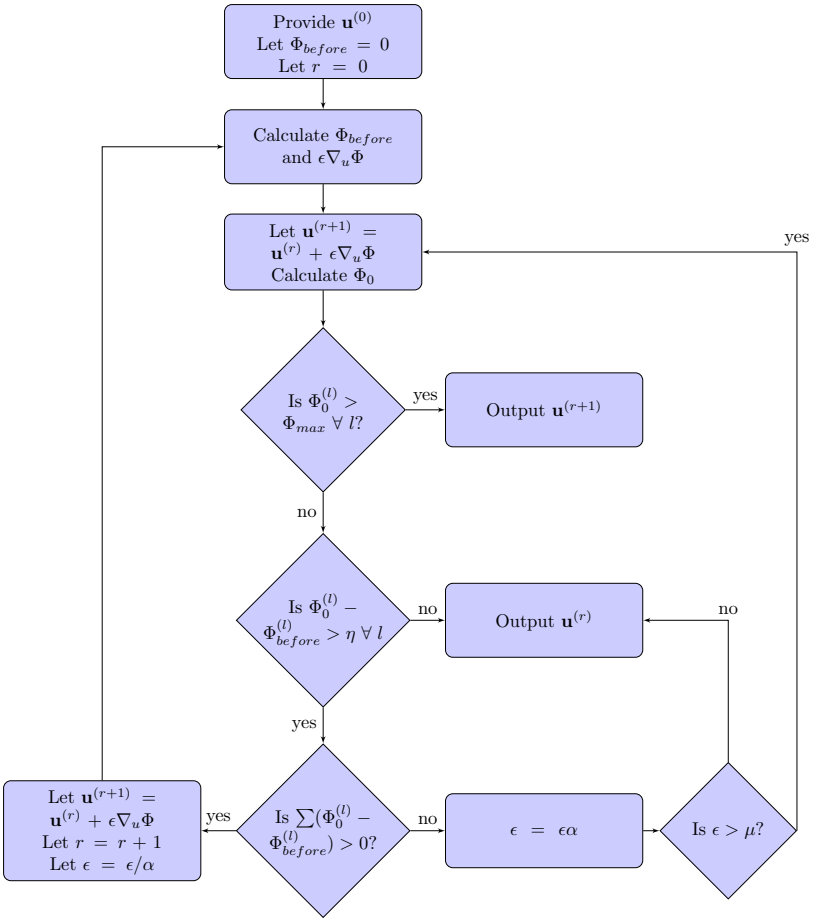

Figure 3.1: A flowchart showing the comprehensive algorithm for implementing robust gradient ascent numerical optimization with discrete sampling over an ensemble parameter. First, as standard with numerical optimization, a control pulse $\mathbf{u}^{(r+1)}$ is provided. Here, r is the iteration counter. The next step is to calculate the fidelity and its gradient with respect to the control. The controls are then updated and the fidelity from the updated controls is calculated. The first condition is to check if the updated fidelity Φ_0 has reached the desired precision for each ensemble point l, otherwise to continue. The second condition checks if any individual fidelities $\Phi_0^{(l)}$ of each point in the ensemble has changed from before. If not, the optimization is discontinued. The third condition checks if the fidelities of each point has increased from before on average. If not, the gradient step size ϵ is reduced and the step of updating the controls is repeated. If the gradient step size is smaller than μ the optimization is halted. Otherwise if the third condition is true, the updated controls are kept and the optimization is reiterated.

Chapter 4

Results

This chapter summarizes the numerical simulations that were performed using optimized pulses and the performance of these optimizations. Using the numerical techniques outlined in Ch. 3, control parameters were optimized for the one-dimensional optical lattice Hamiltonian in Eq. (2.4) for varying potential depths and pulse durations. The main target gate was a NOT gate on the first two energy bands of the one-dimensional horizontal optical lattice. For initial controls, we considered both a π-on Rabi pulse (assuming no dispersion) and bounded randomly generated controls fields. In general, the evolution due to the controls were simulated using a model limited to the first six energy bands and typically sampling over 10 values of the quasimomenta. In this discussion, it has been assumed that the lattice wave number $k_L = 1$ so that $K = 2$, and boundaries of the first Brillouin zone are from $k = -1$ to $k = 1$ with the distribution function being constant $c(k) = 1$. The optimization was sampled over only a limited number of values of the quasimomenta k, typically 10 points, in order to perform the numerical search efficiently using the fidelity in Eq. (3.38). The number of control fields was fixed for the number of full free oscillations at $k = 0$ and was typically 100 per free oscillation. Ideally, the gradient search will halt when a local maxima in the fidelity is reached but this may take a considerable amount of computational resources. All optimizations were halted after 10^5 updates in the control parameters and in some cases after a fidelity of 0.99 was obtained. After obtaining the optimized controls, the final fidelity was calculated using the fidelity function in Eq. (3.4) by simulating the system over a finer sample of quasimomenta, typically with 100 uniformly sampled points.

For the following sections in this chapter, examples are shown for resulting optimized controls with amplitude restrictions that would be present in a typical experimental setup in order to observe what performance was possible for preparing states (Section 4.1). Ex-

amples are shown for performing NOT gates for optimizing one half (Section 4.2) and the entire (Section 4.3) first Brillouin zone. Performance results are shown for robust GRAPE for a range of dispersions and times for optimization on half (Subsection 4.4.1) and the entire (Subsection 4.4.2) first Brillouin zone. This shows that it is possible to perform operations of reasonable fidelity in reasonable times for a system with inhomogeneity. This is a proof of the theoretical minimum performance possible and that higher fidelities and shorter times are achievable. Although the results for control of the entire lattice are what this research aimed for, the results for control of half the lattice is significant nonetheless since it deals with the same dispersion in eigenenergy but without the anti-symmetry of the coupling matrix elements about k=0. Thus, the complications in adding anti-symmetry in couplings can be observed.

In addition, it is found that the pulses for performing gates on the entire lattice are palindromic. An explanation of this effect is given in Section 4.6. A comparison of using the phase restricted fidelity function in Eq. (3.38) and a partially phase restricted fidelity in Eq. (3.44b) is presented in Subsection 4.4.3. Finally, it is observed in Section 4.5 that the lattice responds favourably to shorter simple pulses due to pulse bandwidth arguments from Subsection 3.3.1.

4.1 State transfer optimization with penalty functions

For controls that can be directly applied to the lab, physical constraints and boundary conditions on the controls must be accounted for. Such constraints translate to constraints on the controls. For a simple 1-D optical lattice experiment with the control setup described in Section 2.3, a typical experimental setup shows that the potential depth of the laser controls must lie within the range of $r = 18$ to $r = 40$. In order to keep atoms trapped in an experiment on a one-dimensional vertical lattice the translation control must not shift the lattice by a phase of $\pm\pi/2$, or equivalently a distance of $\pm\frac{\pi}{4k_L}$, and the duration for each pulse must not be less than 1 μs [82].

Here, an example of an optimized pulse for state transfer with a potential depth of $r = 25$ (1.38% dispersion) with the aforementioned constraints is shown in Fig. 4.1. The pulse was optimized for a system with four levels using the fidelity function from Eq. (3.45) modified with the penalty function described in Eq. (3.24). The restrictions that the phase and amplitude modulation must not exceed a shift of $\pi/2$ and $r \pm 3$, respectively, were placed. The optimization was halted when all optimization sampled points in quasimomentum performed with gate error of less than 1%. It is observed that the pulse is well-behaved

for a time of 1.15 ms which is on the order of several free oscillations. The corresponding average gate error is 0.35%, and is fairly flat across the quasimomentum.

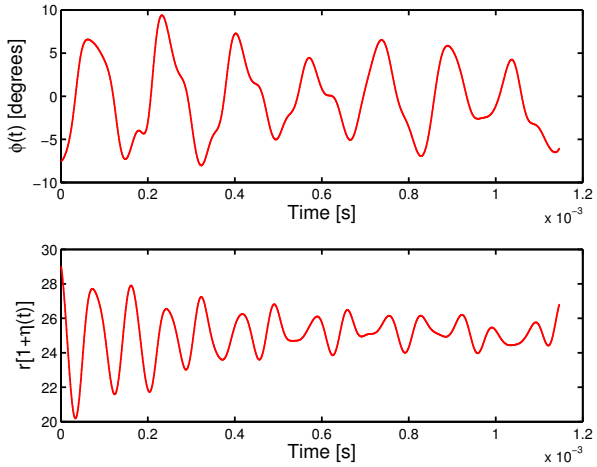

Figure 4.1: Well-behaved controls for transfer of the ground to the first excited band of the 1-D optical lattice for a potential depth of r=25 with 1.38% dispersion. The pulse is optimized with the constraint that the phase control $\phi(t)$ shifts within $\pi/2$ and the amplitude control $r[1+\eta(t)]$ modulates within the range r=22-28. The pulse sequence is sampled at a rate of 1 μs with a total duration of 1.15 ms (7 free oscillations measured at k=0).

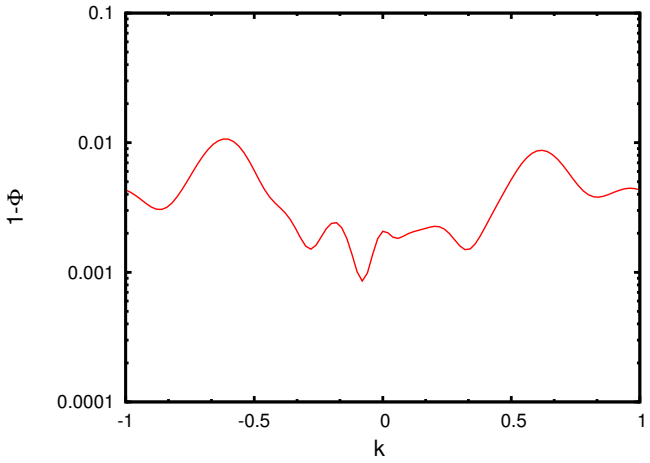

Figure 4.2: The corresponding gate error of the pulse optimized in Fig. 4.1. The gate error is no greater than 1% and is 0.35% on average.

4.2 Example of NOT gate controls for half lattice (k$\geq$ 0)

Here are two examples of optimized controls for performing NOT gates on the first two energy bands of the optical lattice model from Chapter 2 limited to the first six energy bands. One is a control for a system with potential depth $r = 7$ (which corresponds to a dispersion of 32.7%), as shown in Fig. 4.3. The duration of this control was 5 free oscillations (when measured at k=0). The gate error across the ensemble was less than 2% with the exception of particles with quasimomentum near the edges of the Brillouin zone, see Fig. 4.4. Even with such high dispersions in the energies and control Hamiltonians gates with reasonable fidelities can be found.

The second control in Fig. 4.3 is for a system with potential depth of $r = 2$ and thus a dispersion of 75.7%. The average fidelity for the optimized points was 96.0% but after finer examination of the fidelity across the quasimomenta it was found to have an average of 50.0%, as shown in Fig. 4.4. Thus a more cautious approach should be taken with regards to optimizing a coarse sampling over the quasimomenta space. These limitations can be overcome by finer sampling over the range of quasimomenta, however this can become computationally expensive.

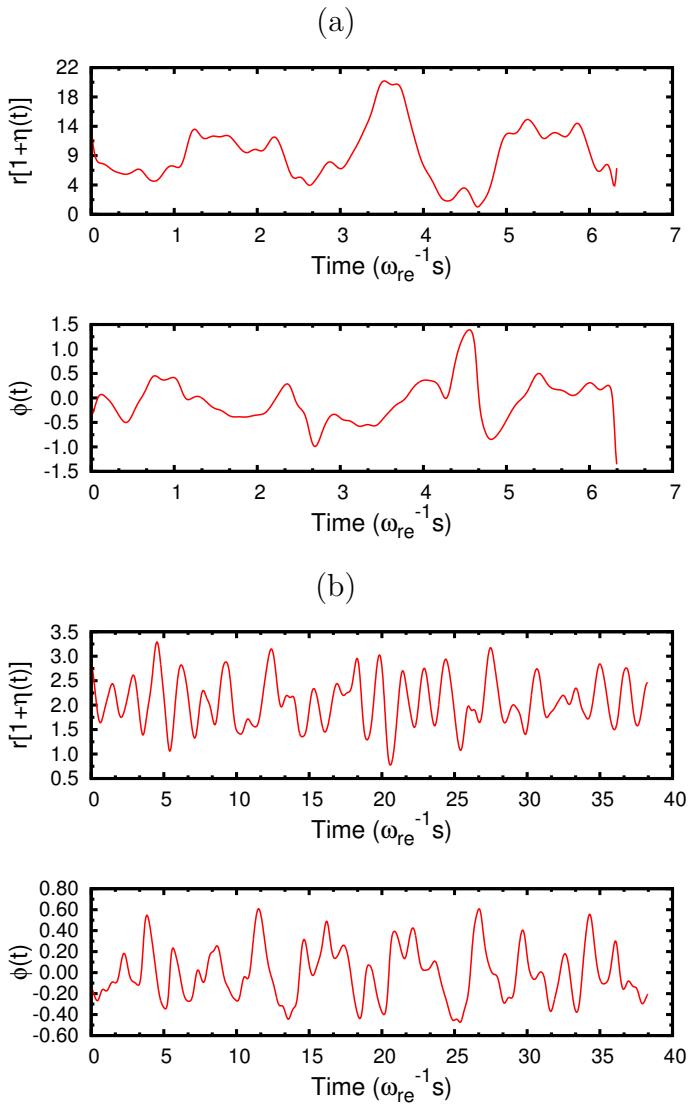

Figure 4.3: Comparison of two optimized controls for preparing a NOT gate for one half of the first Brillouin zone (k$\geq$ 0) when the optimization uses only ten points in quasimomentum space. Both pulses are well-behaved in the sense that they don't translate the lattice by a full lattice site or change rapidly from the initial value for r. (a) An optimized pulse for a potential depth $r = 7$ with 32.7% dispersion and fidelity 98.7% which is calculated by sampling over 100 quasimomentum values. The duration of the pulse is 5 free oscillations (at k=0). (b) An optimized pulse for potential depth $r = 2$ and dispersion 75.7% with an averaged sample fidelity of only 50.0%. The time duration of the pulse is 25 free oscillations (at k=0).

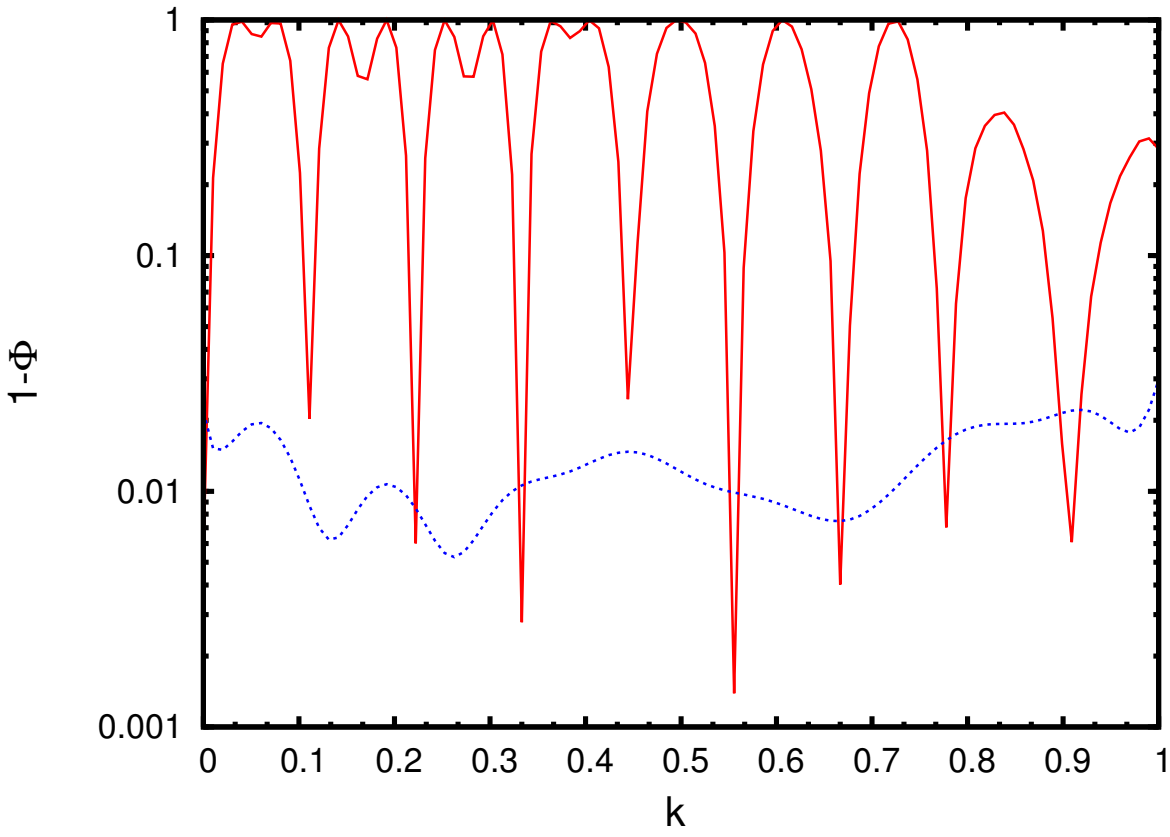

Figure 4.4: Comparison of gate error for well-behaved optimized controls in Fig. 4.3 where the blue dotted line corresponds to control sequence (a) and the red solid line to (b). For (a) the gate error is at most 3% across the possible quasimomenta and the average gate error is 1.3%. In (b) the gate error has been minimized for the quasimomenta points that were sampled for optimization but was 50.0% on average when sampled over 100 points.

4.3 Example of NOT gate controls for full lattice

Here, examples for some of the best pulses for performing gates over the entire lattice are described. The defining characteristic of the optimized pulses were that they were palindromic, i.e. the pulse sequences were symmetric in time about the centre of their duration. An example of two such pulses is shown Fig. 4.5. Here, one optimized control performs very well for a lattice depth of r=30 (a dispersion of 0.63%), and is robust to any quasimomentum to within 0.4% error. The duration of the pulse is moderate, with 10 free oscillations (measured at k=0). The second pulse is for a shallower lattice depth of r=12 with an energy dispersion of 13.2%. The duration of the pulse was relatively short at 2.5 free oscillations (measured at k=0). The fidelity response to both optimized pulses is shown in Fig. 4.6. It is observed that gates with low quasimomenta would perform poorly with this pulse. This was expected since the coupling element dispersion changes rapidly near k=0 (see Appendix A).

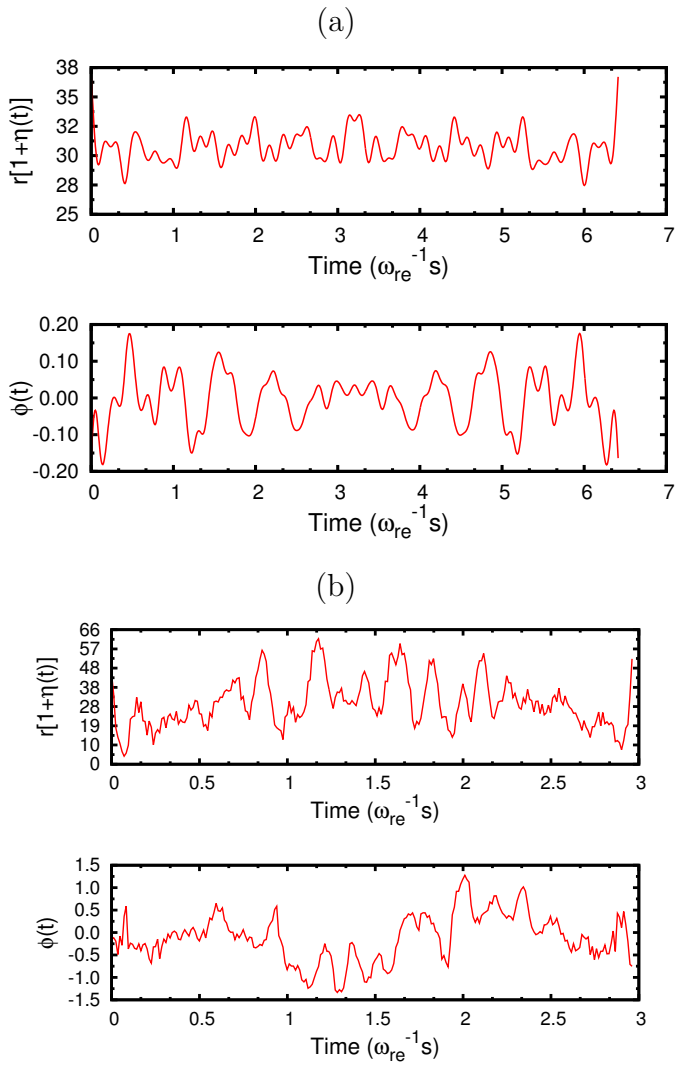

Figure 4.5: Comparison of two optimized controls for preparing a NOT gate for k$\geq$ 0 when the optimization uses only ten uniformly sampled points in quasi momentum space. Both pulses are well-behaved in the sense that they don't translate the lattice by a full lattice site or change rapidly from the initial value for r. (a) An optimized pulse for a potential depth $r = 30$ with 0.63% dispersion and fidelity 99.6% which is calculated by sampling over 200 quasimomentum values. The duration of the pulse was 10 free oscillations (measured at k=0). (b) An optimized pulse for potential depth $r = 12$ and dispersion 13.2% with a sampled fidelity of 97.6% . The time duration of the pulse was 2.5 free oscillations (measured at k=0). The controls are palindromic due to a π-angle phase shift in the control Hamiltonians between $k > 0$ and $k < 0$.

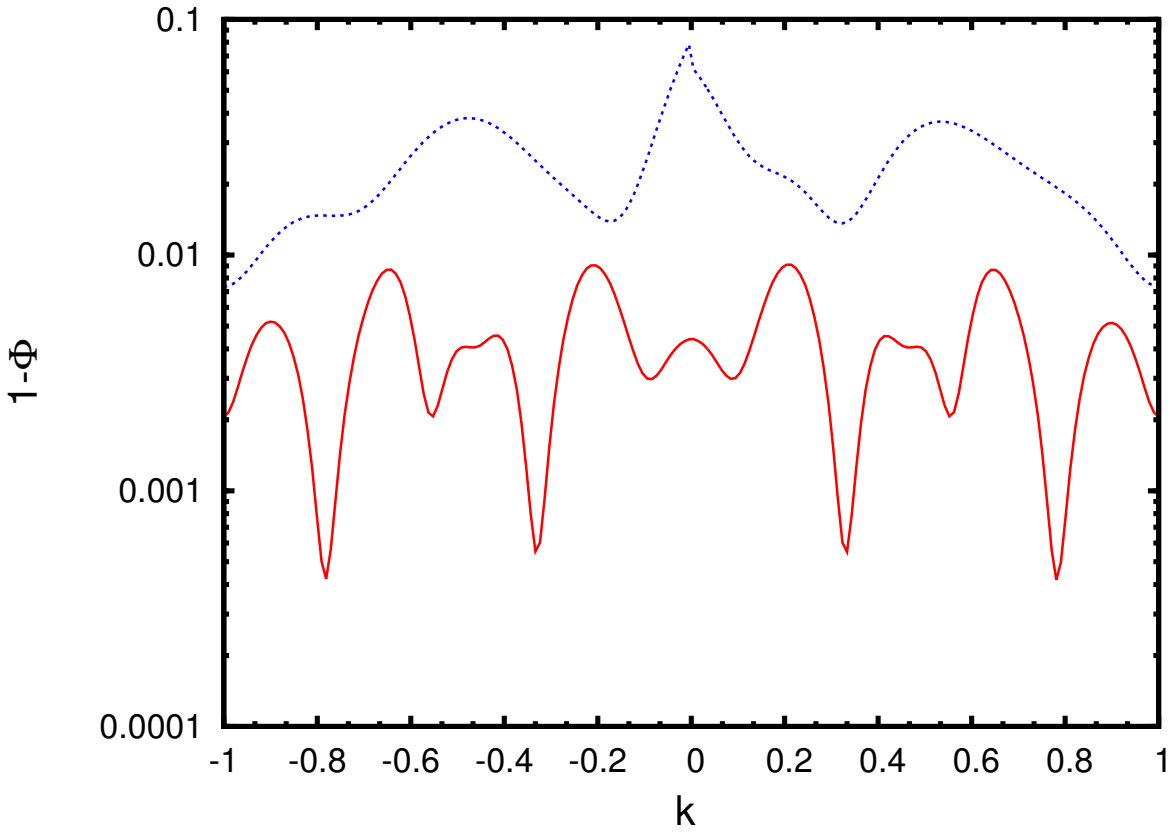

Figure 4.6: Comparison of gate error for optimized controls in Fig. 4.5 where the red solid line corresponds to control sequence (a) and the blue dotted line to (b). Due to the optimized control being palindromic for (a) and somewhat palindromic for (b), the response of the lattice is nearly symmetrical about k=0. (a) The gate error is less than 1% across the possible quasimomenta and the average gate error is 0.41%. In (b) the gate error for the quasimomenta points that were sampled is less than 8% and is 2.4% on average when sampled uniformly over 200 points.

4.4 Performance of robust NOT gate

4.4.1 Performance for half the lattice

The relationship between the maximum fidelity of the solutions and the level of dispersion of the Hamiltonian for half of the first Brillouin zone (k$\geq$ 0) was observed. Although the maximum iterations for optimization was in place (10^5 iterations), for short times (Fig. 4.7) excellent control fields were found ($\Phi > 0.99$ for potentials as shallow as r=17, i.e. potentials with 5.36% dispersion) for the entire range of potential depths that were considered, $0.25 \leq r \leq 110$.

In general, for long gate times, the maximum fidelity solution for NOT gates became lower as the dispersion was increased, see Fig. 4.8. The optimization becomes more difficult with higher dispersion due to the vast number of control fields that must be optimized and the inherent limits of broadband control. As a result, broadband pulses must be tailored to accommodate a greater range of possible energies and couplings for optimization.

In addition, the fidelity becomes deficient as the gate times increase. This may seem counterintuitive, but it is due to the fact that as the gate time increases the amount that the fidelity varies as a function of k increases. For very short gate times, the fidelity is fairly constant across quasimomentum space, but for long gates the fidelity is often found to be high only for the specific points that were optimized, and dips to almost zero in the intermediate regimes, as seen in Fig. 4.4.

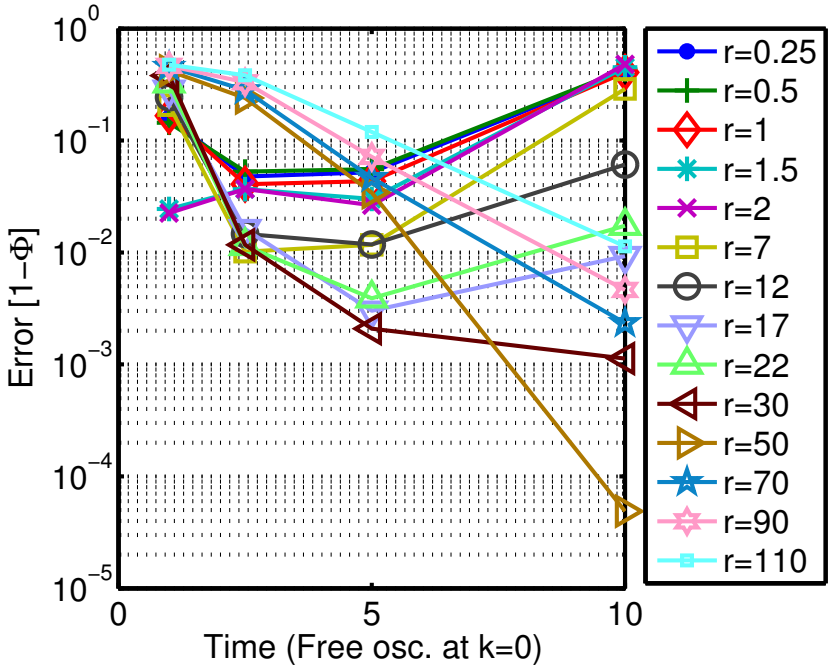

Figure 4.7: The maximum fidelity for an optimized pulse over a range of times, from 1 to 10 free oscillations (measured at k=0), preparing a NOT gate on half of the first Brillouin zone (where $k > 0$) as a series of different potential depths. The potential depth ranged from $r = 0.25$ to $r = 110$, giving a dispersion ranging from 96.9% to 0.01%, respectively. Each point is an average of optimized pulses from 1 Rabi and 10 random initial pulses.

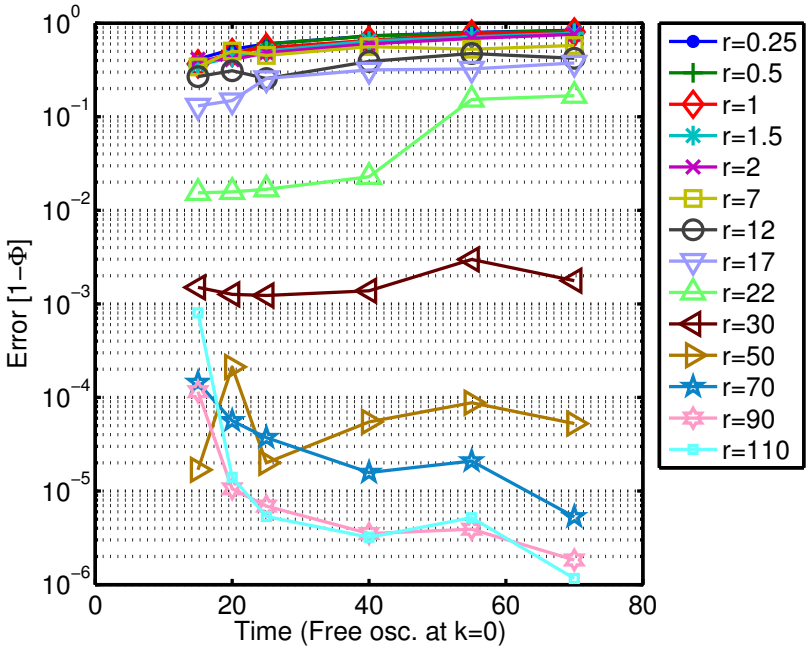

Figure 4.8: Same as Fig. 4.7 but with times from 15 to 70 free oscillations (at k=0).

4.4.2 Performance for the whole lattice

The relationship for the maximum fidelity of NOT gates optimized over the entire first Brillouin zone for different durations was observed for a series of potential depths (giving a range of dispersions). The optimization was performed in a manner similar to Subsection 4.4.1. As such, the range of lattice depths observed was $0.25 \leq r \leq 110$. Here, Fig. 4.9 shows that fidelities of $\Phi > 0.99$ were only observed with potential depths of r=30 (0.63% dispersion) and greater.

In comparison to the maximum fidelities observed for half the Brillouin zone, optimizing over the full Brillouin zone resulted in fidelities that showed similar trends over long times (15 to 70 free oscillations measured at k=0) with a slight decrease in fidelity (Fig. 4.10). At short times with 1 to 10 free oscillations (measured at k=0), similar trends to Fig. 4.7 were observed, however for lattice depths of r=17 and lower the fidelity has decreased significantly (Fig. 4.9).

The significant decrease in fidelity observed for highly dispersive energies and couplings when optimizing for the full lattice was due to a phase difference of π in some coupling matrix elements with quasimomenta of $-k$ and $+k$ within the first Brillouin zone (see Appendix A). This adds additional complexity to any gradient search algorithm as there are significantly fewer available sets of unitary maps that result in the gate versus having symmetric coupling elements.

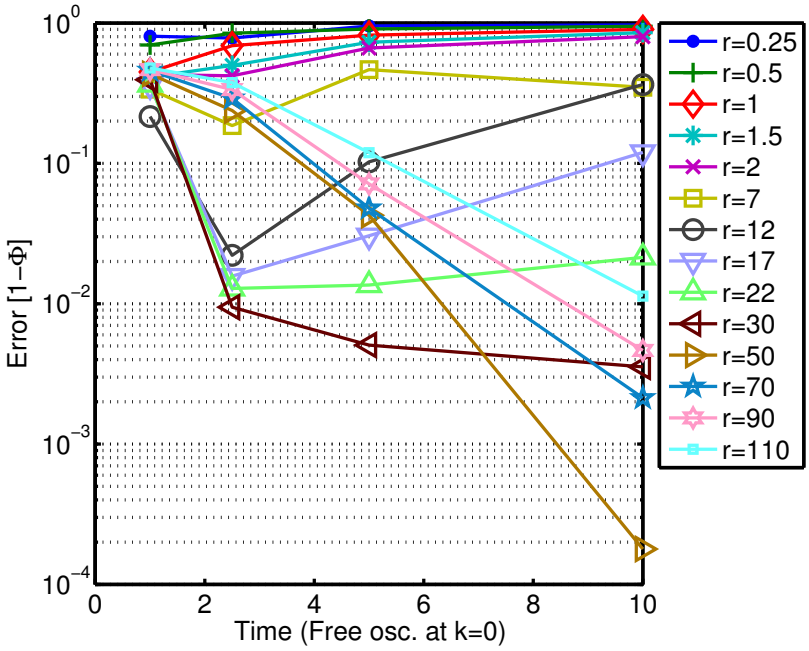

Figure 4.9: The maximum fidelity for an optimized pulse over a range of times, from 1 to 10 free oscillations (at k=0), preparing a NOT gate on the entire Brillouin zone as a series of different potential depths. The potential depth ranged from $r = 0.25$ to $r = 110$, giving a dispersion ranging from 96.9% to 0.01%, respectively. Each point is an average of optimized pulses from 1 Rabi and 10 random initial pulses.

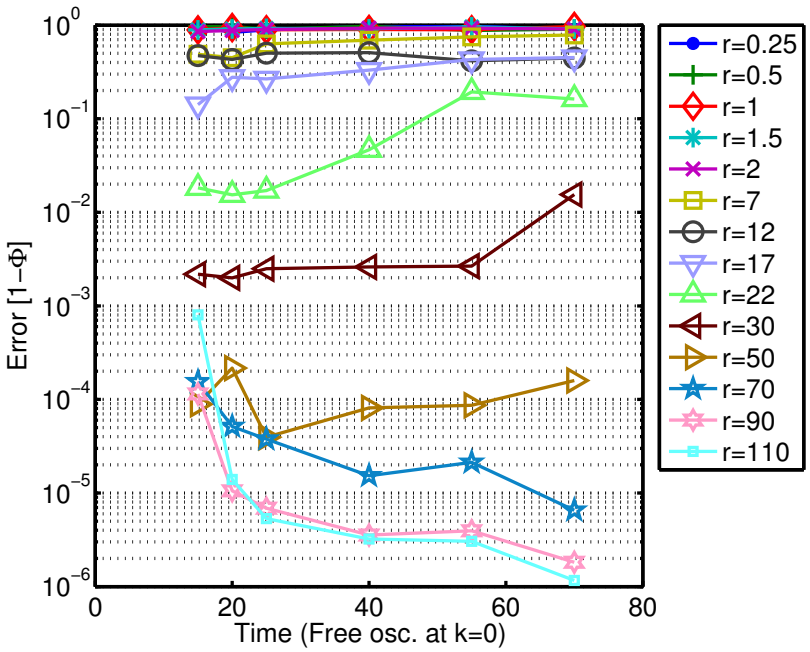

Figure 4.10: Same as Fig. 4.9 but with times from 15 to 70 free oscillations (at k=0).

4.4.3 Comparison of optimization between phase constrained and partially phase constrained ensemble fidelity

In choosing the fidelity of Eq. (3.38) for optimizing gate control pulses due to a favourable property, it is appropriate to compare it empirically with another fidelity function that lacks this property. This particular fidelity was chosen since it constrained the relative phase between the fidelities sampled for each ensemble parameter (i.e. quasimomentum) in the range considered over fidelities with unconstrained phase.

For ease of comparison, the maximum fidelities for the fully phase constrained fidelity in Eq. (3.38) are shown in Fig. 4.11, along with the results for the partially phase constrained fidelity, where only the real component of the fidelity was taken in Eq. (3.44b) (see Fig. 4.12) for performing NOT gates on the full optical lattice. Both fidelities are shown as a function of pulse durations from 2 to 55 free oscillations (measured at k=0) for a series of potential depths $2 \geq r \geq 50$. The maximum fidelities of both plots were calculated as consistent to the method described in the beginning of this chapter, where each of the 200 observed quasimomentum has a corresponding fidelity calculated using Eq. (3.4). As such, phase constrained ensemble fidelity is shown empirically to be superior to partially constrained ensemble fidelity for determining gate controls for the considered optical lattice model. Thus, it can be concluded that optimization with a completely phase constrained fidelity would result in pulses with better performance than a phase unconstrained fidelity.

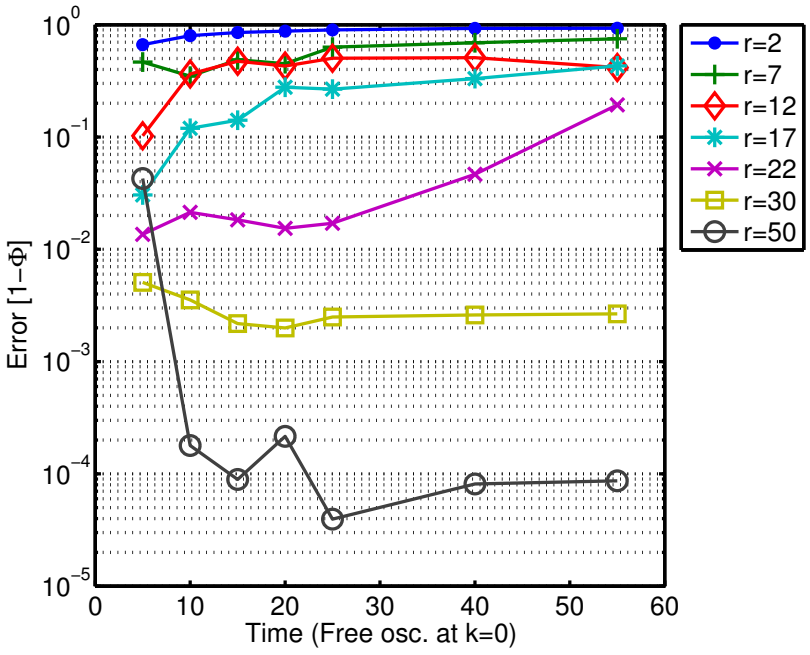

Figure 4.11: The maximum fidelity for a pulse optimized using the phase constrained fidelity function over a range of times, from 2 to 55 free oscillations (measured at k=0), preparing a NOT gate on the entire Brillouin zone as a series of different potential depths. The potential depth ranged from $r = 2$ to $r = 50$, giving a dispersion ranging from 75.7% to 0.04%, respectively. Each point is a maximum of optimized pulses from 1 Rabi and 10 random initial pulses.

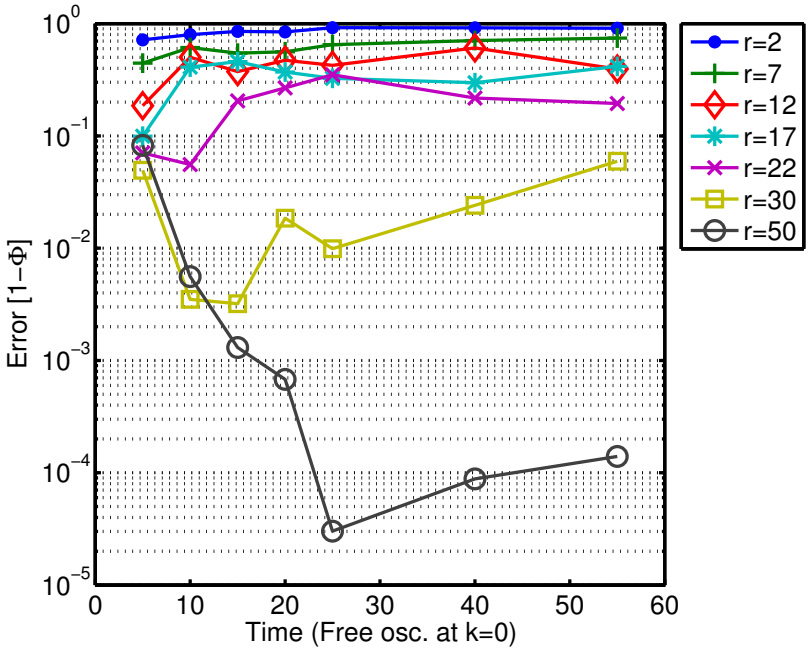

Figure 4.12: The maximum fidelities as observed similarly to Fig. 4.11, with the exception that only the partially phase constrained fidelity of Eq. (3.44b) was used to optimize the controls.

4.5 Bandwidth considerations

The connection between gate duration and the rate of change of fidelity can be observed through the simulation described in Fig. 4.13. Here, GRAPE is performed for exactly one value of the quasimomentum. The performance of this control field across k is then observed. It was found that as the gate time was decreased the fidelity response became more broad about the single value of quasimomentum that was optimized. As a result, fewer points in quasimomenta would need to be sampled for shorter times in order to have a favourable response for the entire lattice.

In principle, there should always be higher fidelity control fields at longer gate times but finding these fields becomes increasingly computationally expensive. Considering the fidelity landscape as a function of the amplitude of the control fields, increasing the number of control fields essentially increases the dimension of this landscape, thus making it increasingly more complex with many local maxims. Good solutions may exist, however localized searches over a landscape where many false maxims exist make it increasingly difficult to search for a good solution. In other words, finding good control fields becomes computationally expensive as the need to sample more values in quasimomentum space or to simply run the algorithm from many different initial conditions increases as one expects to see a flat high fidelity response across the quasimomentum space.

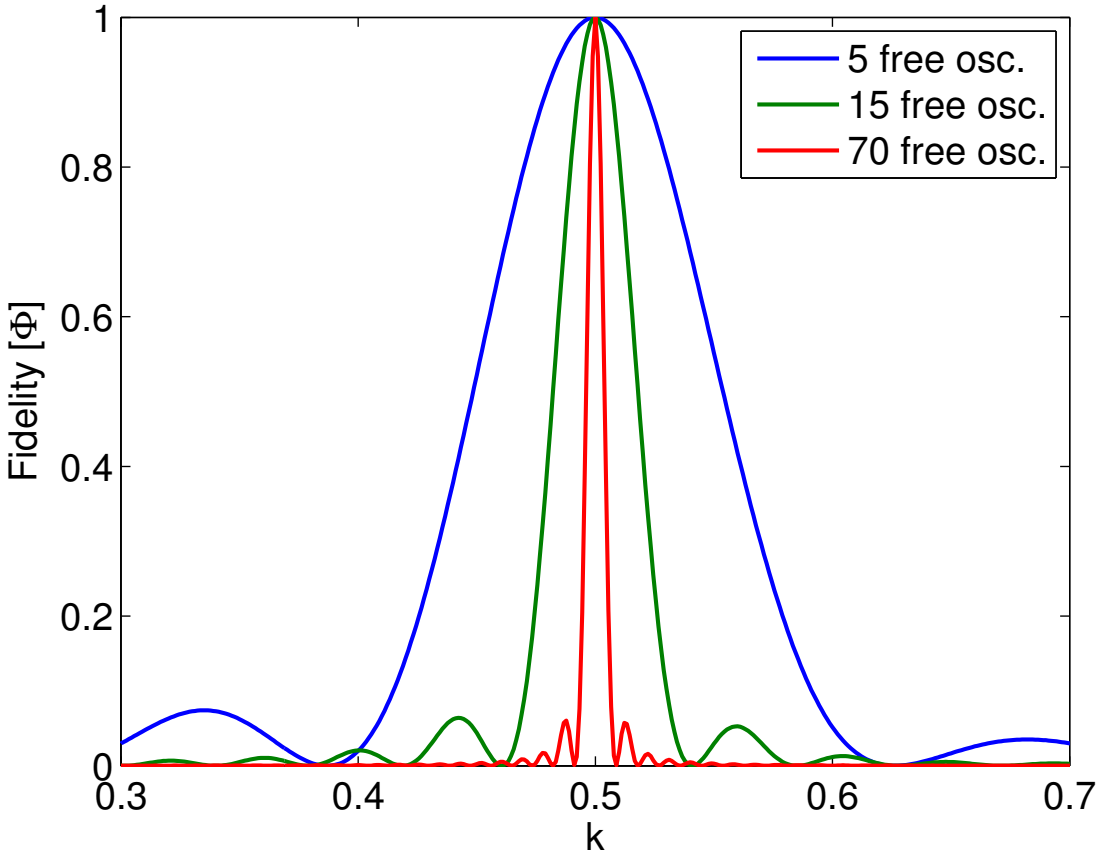

Figure 4.13: The fidelity response over quasimomenta is shown for pulses for performing NOT gates at a potential depth of $r = 2$ for three different times that were optimized specifically for k=0.5. This shows the effect of the bandwidth limit of the pulses on fidelity. Shorter pulses have larger spectral bandwidth and thus affect a larger range of quasimomenta so that relatively fewer points in quasimomenta would need to be sampled for optimization of the ensemble.

4.6 Palindromic Controls Analysis

In controlling the optical lattice, there is an additional complication. When the system Hamiltonian with quasimomentum $+|k|$ is compared to the system Hamiltonian with quasimomentum $-|k|$ within the same Brillouin zone, the eigenenergy remains the same however the control may be changed due to anti-symmetry. In particular, the function for the imaginary computational component of the control Hamiltonian $H_I = i(e^{ikx} - e^{-ikx})$ is an odd function so that changing the sign of the quasimomentum changes the sign of the control. This effect can be seen in the Figures of Appendix A. Since the imaginary Hamiltonian is responsible for the 1st and 3rd nearest-neighbour matrix coupling elements, these coupling elements will be anti-symmetric about k=0 (refer to Fig. A.2 and Fig. A.4). As a result, rotations made using these couplings for $+|k|$ will cause reverse rotations to occur with $-|k|$. With the additional effect of the drifting of the Hamiltonian and controls that work on the time-scale of these drift rotations, a set of controls that is robust to one half of the Brillouin will not perform properly for the other half since the evolutions are different. Thus, the need for focused robust control arises.

Here, a control pulse for a simple scenario can be developed to show that one ideal solution would be to have palindromic pulses, that is pulses that are symmetric about the time of half its duration. Examine a simple two state system where we have assumed that robust controls for performing simple rotations is at our disposal. Also assume that there is anti-symmetry in the X-rotation about $k = 0$. The goal would be to perform a simple state transfer from the ground to first excited state. One of the simplest control pulses to control both halves of the Brillouin zone involves techniques derived from Hahn spin-echo [46].

For a pulse of duration T, there are two phases in the sequence, one half for time $0 \leq t < T/2$ and the second half for time $T/2 \leq t < T$. The second half of the control sequence will be the time reversal of the first half. For the first half of the sequence, the pulse begins with a $X_{\pi/2}$ rotation (where X_ϕ denotes a rotation about the x-axis of angle ϕ) of the ground state into the uniform superposition state, as visualized on the Bloch sphere in part (a) of Fig. 4.14. This is allowed to precess for some time allowing for a total accumulated phase of $e^{i\pi/2}$. For the negative half of the Brillouin zone, the response to the rotation is in the reverse direction, as observed in Fig. 4.15.

For the second half of the pulse sequence, the exact reverse of the sequence for the first half would then be performed. This begins by allowing the system to drift and accumulate another phase $e^{i\pi/2}$. Then a $X_{-\pi/2}$ rotation is performed which would result in the state for the positive half of the Brillouin zone being in the excited state. The drift for the negative

half of the Brillouin zone would occur as it did in the second half, however its response to the X-rotation would be reversed and it would also end in the excited state. Thus, the states of particles on both halves of the Brillouin zone would be focused at the end of the pulse sequence using a palindromic control.

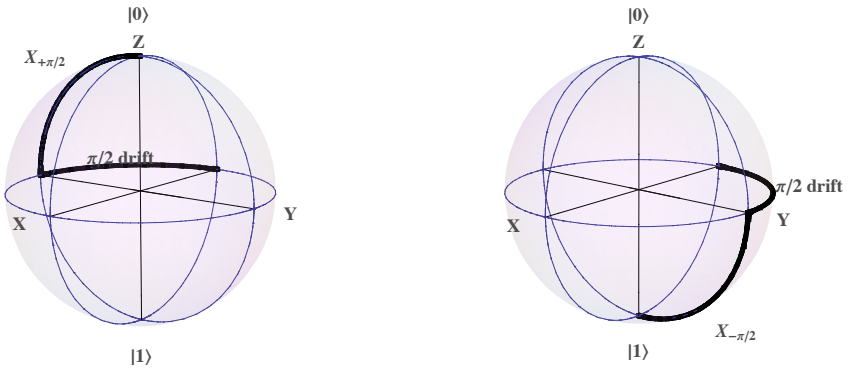

(a) $0 \leq t < T/2$. (b) $T/2 \leq t < T$.

Figure 4.14: The evolution of a two state system with positive σ_x coupling elements (such as in the positive half of the Brillouin zone with $k > 0$) with a palindromic pulse for preparing the excited state from the ground state. (a) At time $0 \leq t < T/2$ a $X_{\pi/2}$ rotation pulse is applied followed by a drift to allow a rotation about the Z-axis of $\pi/2$. (b) At time $T/2 \leq t < T$, the exact reverse pulse sequence in the first half is applied. Here, the system is allowed to drift about the Z-axis by $\pi/2$, followed by a $X_{-\pi/2}$ rotation pulse.

For time-optimal controls on a complex system that we have considered, simple control techniques are not sufficient. Fast pulses would utilize the many interactions between different states in order to prepare a state or gate in a relatively short time. In addition, rotations would not occur without drift as assumed in the simple example above. As a result, the design of control sequences would be non-trivial, especially with a system requiring robustness. Thus, the need for optimal control in order to develop proper high-precision control sequences.

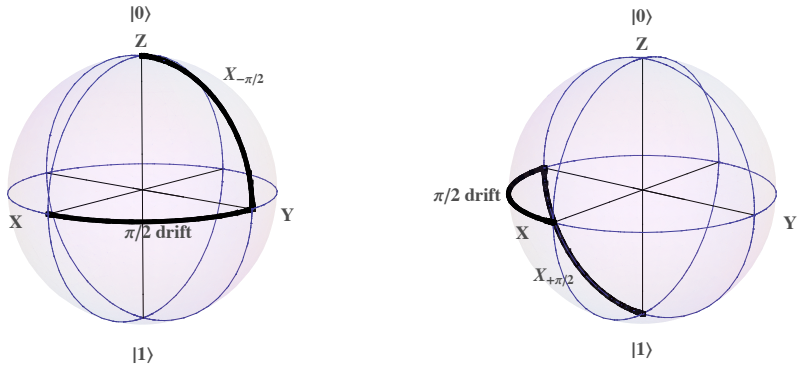

(a) $0 \leq t < T/2$. (b) $T/2 \leq t < T$.

Figure 4.15: The evolution of a two state system with negative σ_x coupling elements (such as in the negative half of the Brillouin zone with $k < 0$) with the exact same palindromic pulse applied in Fig. 4.14 for preparing the excited state from the ground state. In this regime, because the control couplings have been phase shifted by π, the system will respond in the opposite manner to controlled rotations than it would for positive couplings. (a) At time $0 \leq t < T/2$ a $X_{\pi/2}$ rotation pulse (which appears as $X_{-\pi/2}$ for $k < 0$) is applied followed by a drift to allow a rotation about the Z-axis of $\pi/2$. (b) At time $T/2 \leq t < T$, the exact reverse pulse sequence in the first half is applied. Here, the system is allowed to drift about the Z-axis by $\pi/2$, followed by a $X_{-\pi/2}$ rotation pulse (which appears as $X_{\pi/2}$ for $k < 0$).

Chapter 5

Conclusions

In 1965, a prophetic prediction known as Moore's law, which has been widely accepted by the microchip industry, states that for a fixed cost, the complexity of integrated electronic components would double every two years. As physical constraints such as the quantum effects of noise and most notably tunneling effects pose a limit to the ability in continuing the miniaturization of devices, thus threatening an end to Moore's law, the need to develop new technologies becomes more apparent. What makes quantum computers remarkable in comparison to traditional classical computers is that they would utilize these otherwise oppressive quantum effects to not only surpass the computational power of classical computers, but provide an entirely new paradigm of information processing. This paradigm provides the potential for algorithms that would be significantly faster than any classical algorithm and provide secure communications, all to the extent that it is worth pursuing the goal of a functioning quantum computer. Thus, with the goal and challenges in mind, researchers have pursued discoveries in all avenues related to the processing of information using quantum effects which include: quantum algorithms, complexity theory, quantum cryptography and communications, quantum fault-tolerance and error correction, topological quantum computing, physical quantum devices, quantum control, etc.

This thesis is focused on the study of time-optimal robust control for the one-dimensional optical lattice. A working quantum computer must be stable against the effects of dispersion, fluctuations in parameters, and uncertainty in parameters. Demonstrating the ability to design robust control for a system as difficult and challenging to control as the optical lattice shows that it is possible to develop the controls to perform operations with the necessary stability and precision. The control techniques discussed in this thesis can be applied to other devices for quantum computers such as superconducting qubits which includes the quantronium, flux, charge, phase, and the transmon qubits. These techniques

can even be applied to other systems for physical or chemical study in the research of NMR or condensed matter systems.

In this thesis, the physical model that was considered for controlling the one-dimensional optical lattice with two global lasers to shift the trapping potential and to adjust the height of the potential was discussed in Chapter 2. The optimal control techniques using gradient-ascent pulse engineering that were developed to design controls for the optical lattice that were robust to it's energy dispersion, control dispersion, and control anti-symmetry was discussed in Chapter 3. Finally, the results of simulations for optimized controls was shown and discussed in Chapter 4. These results showed that it was indeed reasonably possible to produce controls that could robustly control the optical lattice with a precision of at least 99% for dispersions in the vibrational energies of 0.6%. The results showed that our technique of using the phase-constrained fidelity function proved superior to phase-unconstrained fidelity functions. It was also observed that palindromic pulses were produced by optimization due to the anti-symmetries of the controls.

With concluding remarks, it can be said that with further optimization, it is possible to tailor the controls to the desired precision. Future work for improved control design can also be explored as an extension of the concepts in this work, such as a hybrid method of gradient-ascent pulse engineering and genetic algorithms in order to unite the advantages of their unique ability for local and global searches [70], or the use of a new proposal of real-embedding [49].

APPENDICES

Appendix A

Coupling bands for the optical lattice

Here, in the same manner that the eigenenergy bands were shown in Fig. 2.2 of Section 2.4, the dispersion of the coupling strength across the Brillouin zone for the ground and 1st excited states of the 1-D optical lattice are shown for a range of lattice potential depths. The important property of the energy couplings (coupling matrix elements) to consider are that they may be either symmetrical or anti-symmetrical about the zero quasimomentum in the first Brillouin zone. The consequence of having anti-symmetric coupling elements in quasimomenta adds to the complexity of the control challenge as driving a qubit rotation for atoms with positive quasimomenta will perform the opposite rotation for atoms with negative quasimomenta. To add to the difficulty of control, the coupling elements also have increasing gradients with respect to quasimomenta as the trapping potential depth is decreased.

The Z-couplings (σ_X matrix elements) in Fig. A.1 show a smooth symmetrical curve for the first two states with the exception of a dip near k=0 for low lattice depths. Both the 1st and 3rd nearest-neighbour couplings (where the n^{th} nearest-neighbour coupling denotes the coupling matrix element from one state to the n^{th} higher state) for the first two states show anti-symmetry with a discontinuity about k=0, shown in Fig. A.2 and Fig. A.4 respectively. In addition, with shallower trapping potential depths the amount of dispersion in the coupling elements increases. Such couplings are responsible for the need of time-reversal invariant control pulses to perform gates on the optical lattice [43]. The 2nd and 4th nearest-neighbour couplings in Fig. A.3 and Fig. A.5, respectively, show steep changes in strength near k=0 and in quasimomenta near the boundaries of the Brillouin zone. This effect is more pronounced with shallower trapping potential depths.

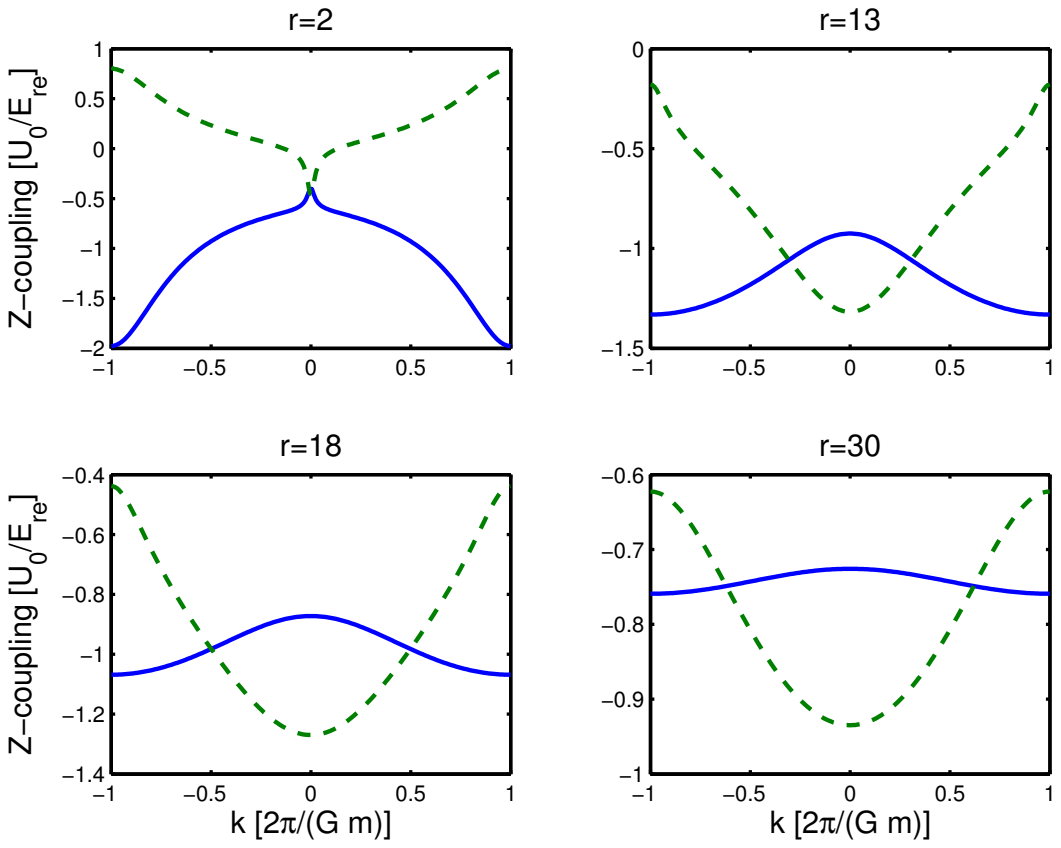

Figure A.1: The Z-coupling (σ_X matrix elements) strength is shown for the ground state (blue solid) and the first excited state (green dashed) across the quasimomentum within the first Brillouin zone of the 1-D optical lattice for varying trapping potential depths.

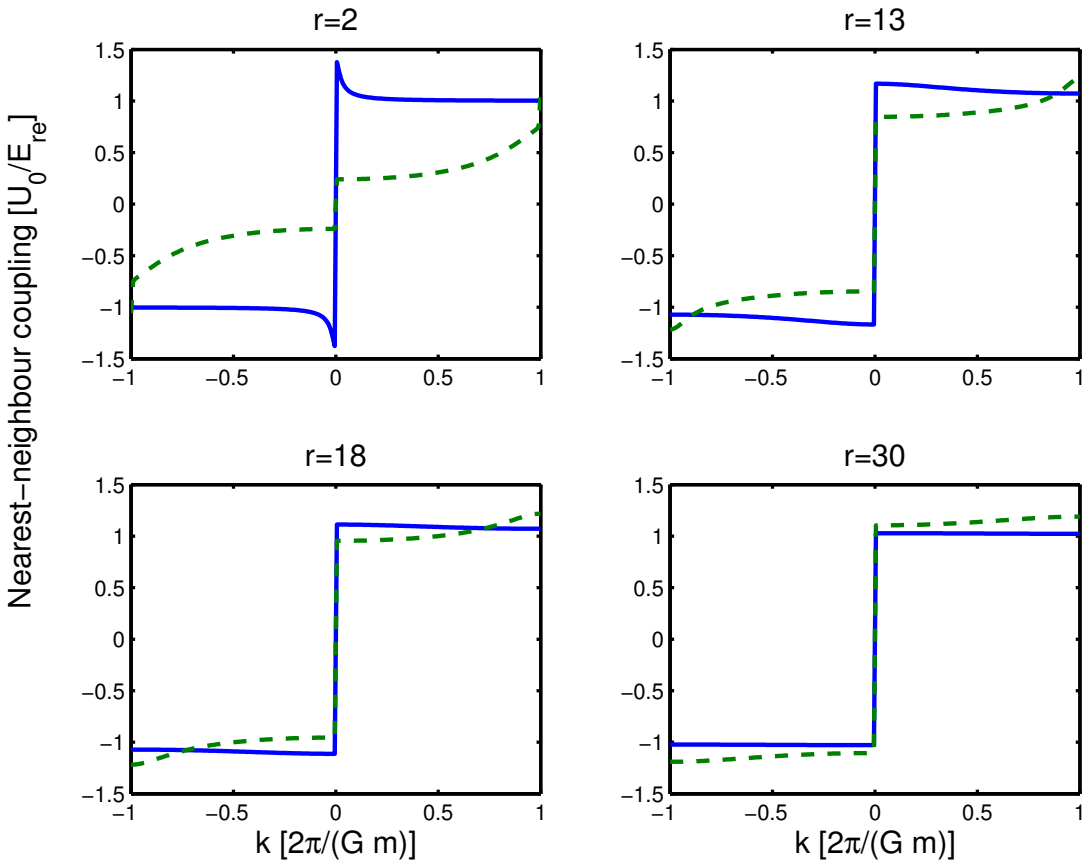

Figure A.2: The nearest-neighbour coupling strength (matrix coupling element to the first higher state) is shown for the ground state (blue solid) and the first excited state (green dashed) across the quasimomentum within the first Brillouin zone of the one-dimensional optical lattice for varying trapping potential depths. The coupling strengths are anti-symmetric about k=0.

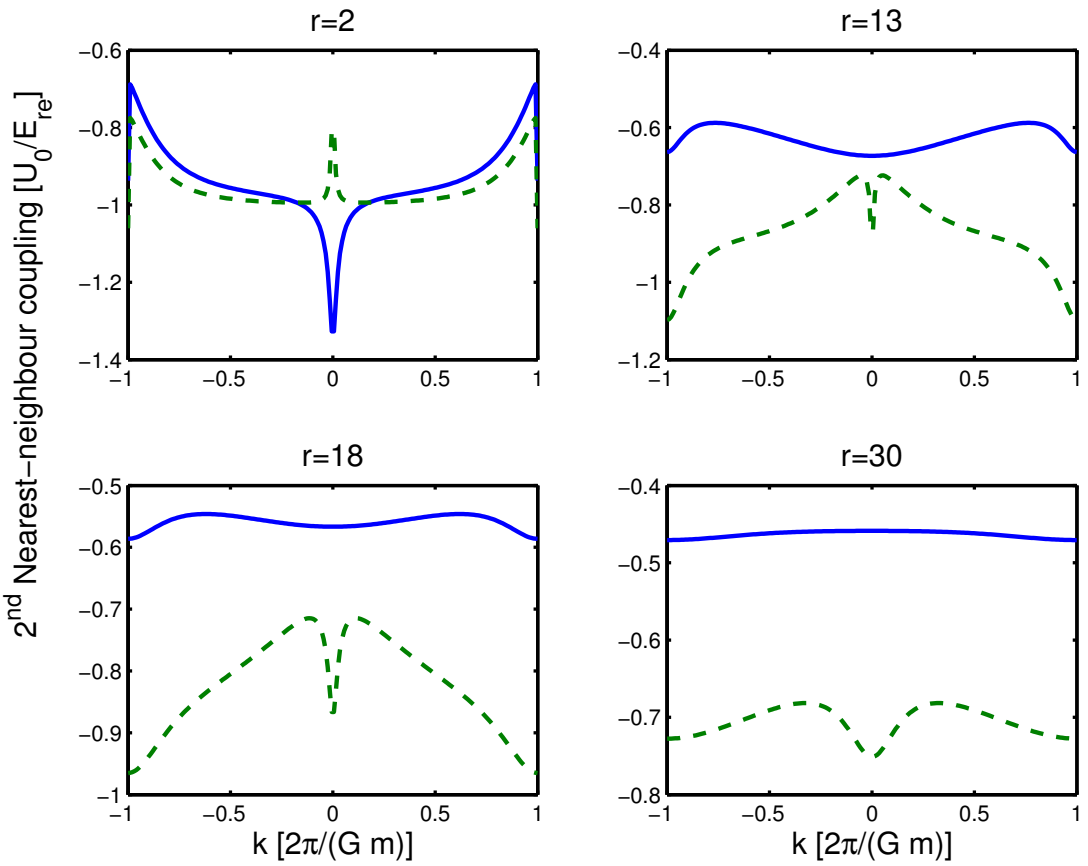

Figure A.3: The 2nd nearest-neighbour coupling strength (matrix coupling element to the second higher state) is shown for the ground state (blue solid) and the first excited state (green dashed) across the quasimomentum within the first Brillouin zone of the one-dimensional optical lattice for varying trapping potential depths. The coupling for the second excited state exhibits rapid change near k=0. At r=2, the coupling for the first excited state also exhibits this effect.

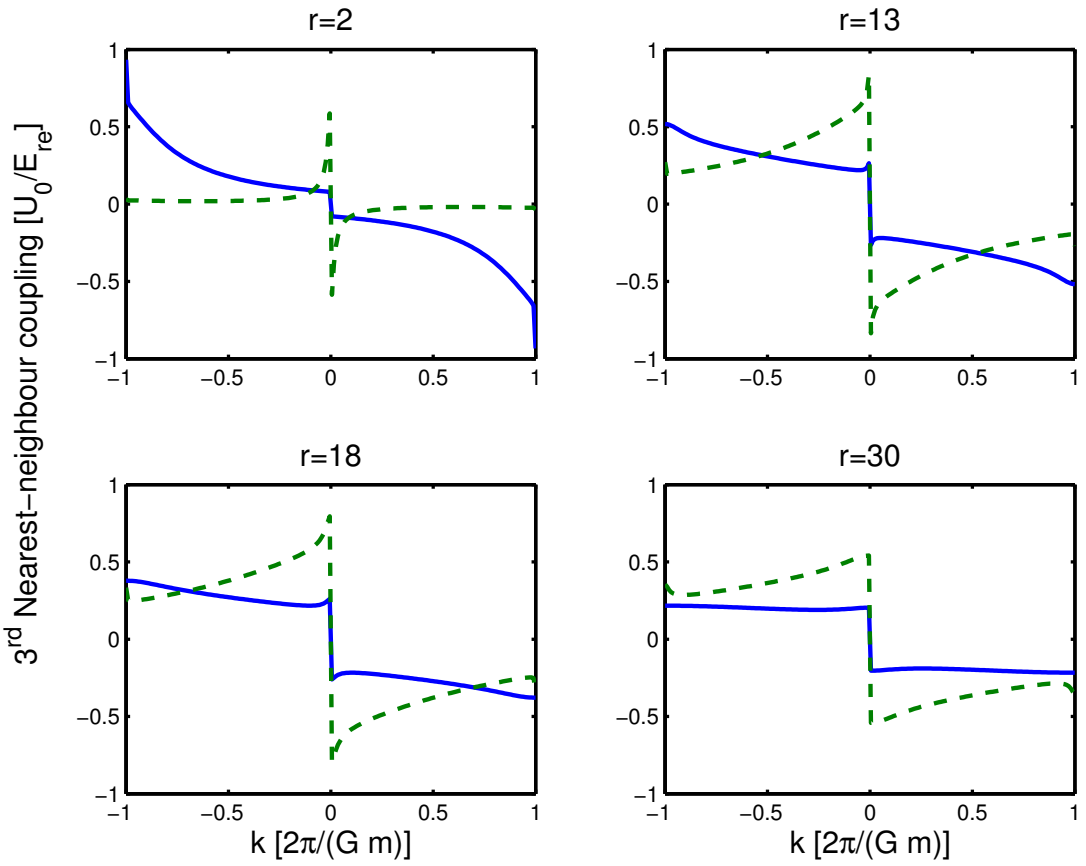

Figure A.4: The 3rd nearest-neighbour coupling strength (matrix coupling element to the third higher state) is shown for the ground state (blue solid) and the first excited state (green dashed) across the quasimomentum within the first Brillouin zone of the one-dimensional optical lattice for varying trapping potential depths. The coupling strengths are anti-symmetric about k=0.

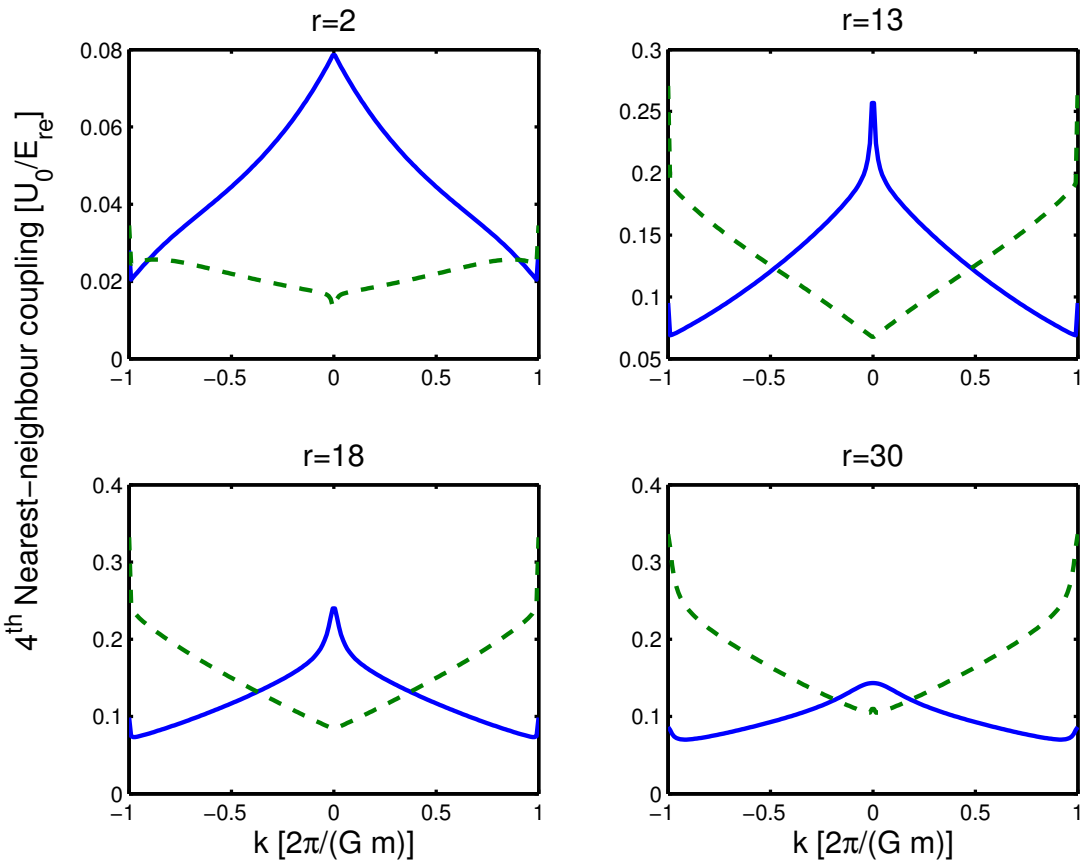

Figure A.5: The 4th nearest-neighbour coupling strength (matrix coupling element to the fourth higher state) is shown for the ground state (blue solid) and the first excited state (green dashed) across the quasimomentum within the first Brillouin zone of the one-dimensional optical lattice for varying trapping potential depths. The coupling strength has increasing gradient near k=0 for lower potential depths.

Appendix B

Performance of robust controls for NOT gates supplement

B.1 Performance for the whole lattice

Here supplementary information is provided for the results of the performance of optimized pulses shown in Subsection 4.4.2. The supplement provided are the average and median fidelities for optimized NOT gates versus the duration of the pulse for a series of potential depths along with the maximum fidelity (minimum error) for very short durations. There are three sets of gate durations shown: very short (0.1 to 0.75 free oscillations at k=0), short (1 to 10 free oscillations at k=0), and long (15 to 70 free oscillations at k=0). The NOT gates were optimized for the whole one-dimensional optical lattice (i.e. the entire first Brillouin zone).

B.1.1 Very short times

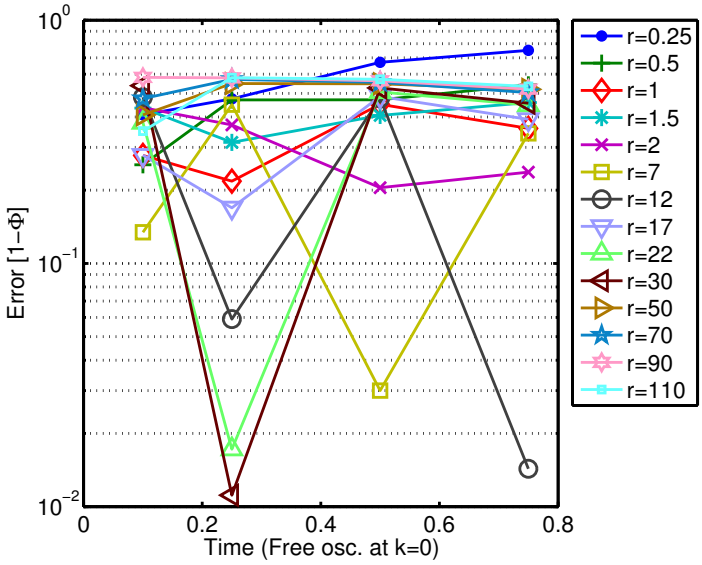

Figure B.1: The maximum fidelity for an optimized pulse over a range of times, from 0.1 to 0.75 free oscillations (at k=0), preparing a NOT gate on the entire Brillouin zone as a series of different potential depths. The potential depth ranged from $r = 0.25$ to $r = 110$, giving a dispersion ranging from 96.9% to 0.01%, respectively. Each point is a maximum of optimized pulses from 1 Rabi and 10 random initial pulses.

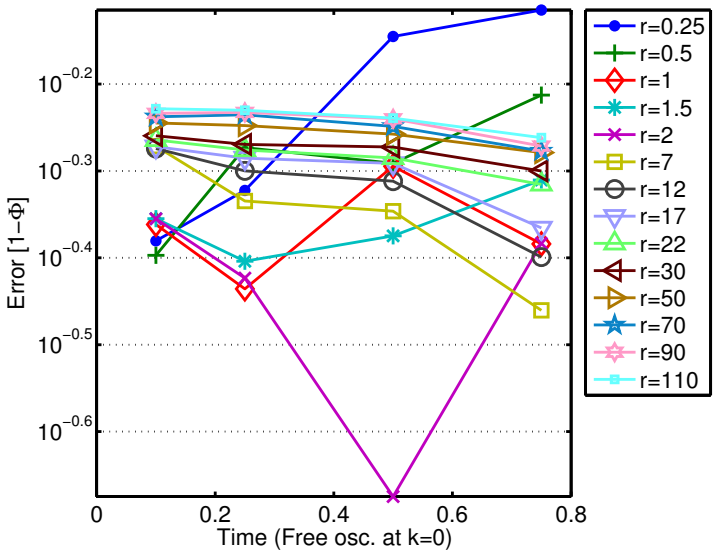

Figure B.2: Same as Fig. B.1 but with each point a median of the error with optimized pulses from 1 Rabi and 10 random initial pulses.

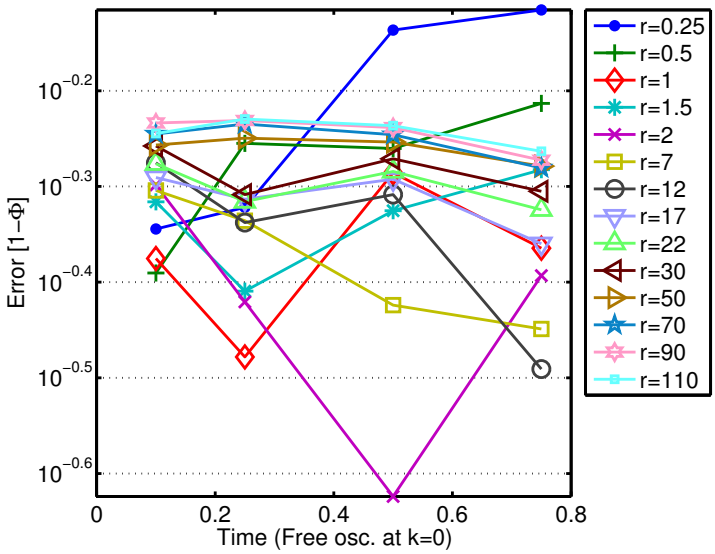

Figure B.3: Same as Fig. B.1 but with each point an average of the error with optimized pulses from 1 Rabi and 10 random initial pulses.

B.1.2 Short times

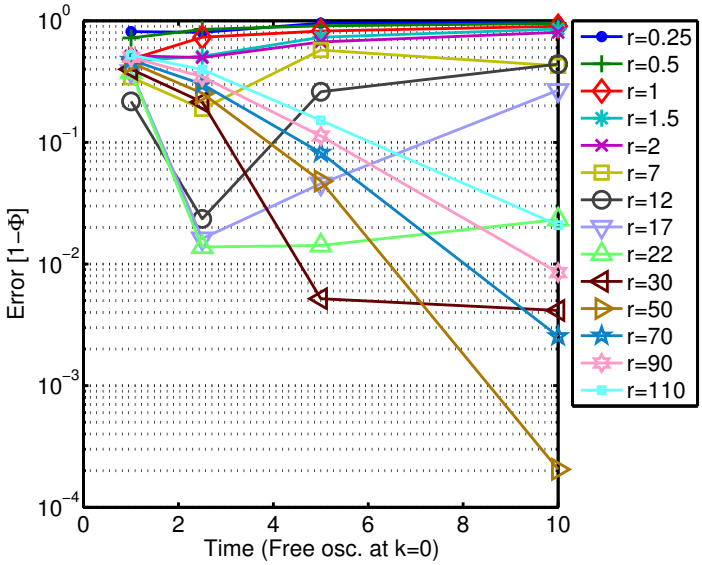

Figure B.4: The median fidelity for an optimized pulse over a range of times, from 1 to 10 free oscillations (at k=0), preparing a NOT gate on the entire Brillouin zone as a series of different potential depths. The potential depth ranged from $r = 0.25$ to $r = 110$, giving a dispersion ranging from 96.9% to 0.01%, respectively. Each point is a median of optimized pulses from 1 Rabi and 10 random initial pulses.

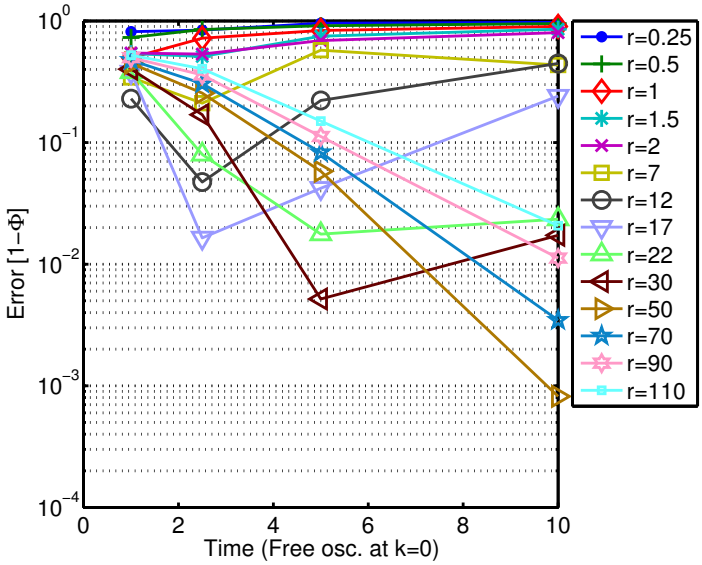

Figure B.5: Same as Fig. B.4 but with each point an average of the error with optimized pulses from 1 Rabi and 10 random initial pulses.

B.1.3 Long times

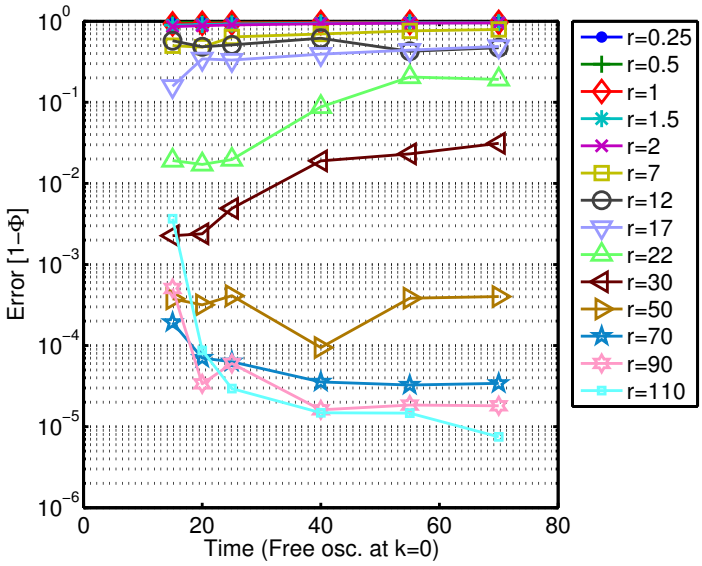

Figure B.6: The median fidelity for an optimized pulse over a range of times, from 15 to 70 free oscillations (at k=0), preparing a NOT gate as a series of different potential depths. The potential depth ranged from $r = 0.25$ to $r = 110$, giving a dispersion ranging from 96.9% to 0.01%, respectively. Each point is a median of optimized pulses from 1 Rabi and 10 random initial pulses.

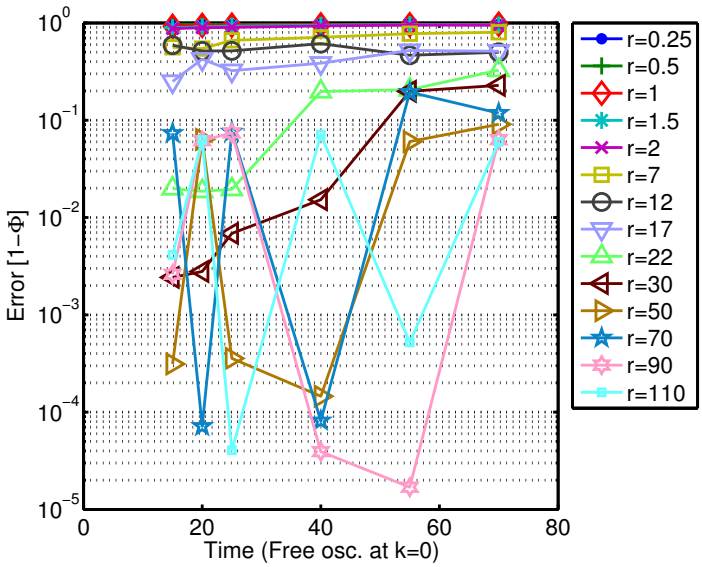

Figure B.7: Same as Fig. B.6 but with each point an average of the error with optimized pulses from 1 Rabi and 10 random initial pulses.

B.2 Performance for the whole lattice with k=0 optimized

The results for optimization of pulses for performing NOT gates on the full optical lattice Hamiltonian in a manner almost precisely to Section 4.4.2 are shown. The exception in these particular pulses were that 11 quasimomentum points were evenly sampled in the first Brillouin zone for optimization. This was performed to allow k=0 to be sampled in the optimization, whereas it was not sampled in Section 4.4.2 and thus some pulses showed higher gate errors around that point. The results for sampling the Hamiltonian with k=0 for optimization did not show significant improvement. Here, the minimum, median, and average gate errors are shown for very short (0.1 to 0.75 free oscillations at k=0), short (1 to 10 free oscillations at k=0), and long (15 to 70 free oscillations at k=0) times.

B.2.1 Very short times

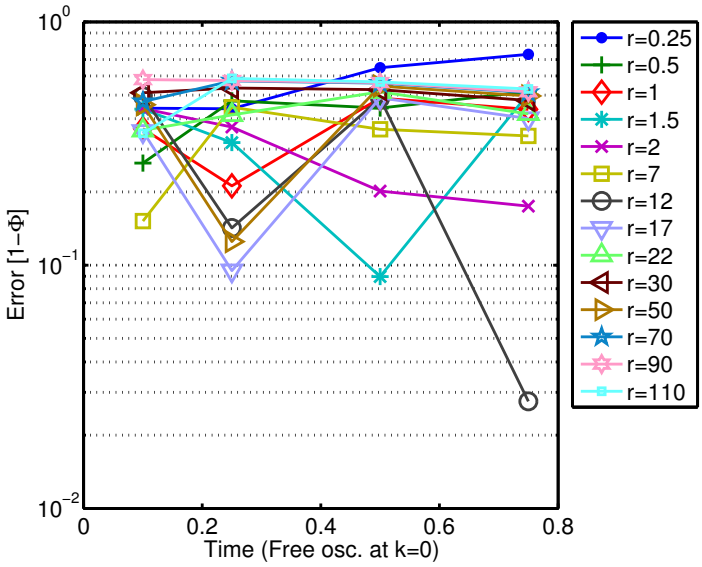

Figure B.8: The maximum fidelity for an optimized pulse over a range of times, from 0.1 to 0.75 free oscillations (at k=0), preparing a NOT gate as a series of different potential depths. The potential depth ranged from $r = 0.25$ to $r = 110$, giving a dispersion ranging from 96.9% to 0.01%, respectively. Here, the k=0 was a sampled point included for optimization. Each point is a maximum from optimized pulses initialized from 1 Rabi and 10 random pulses.

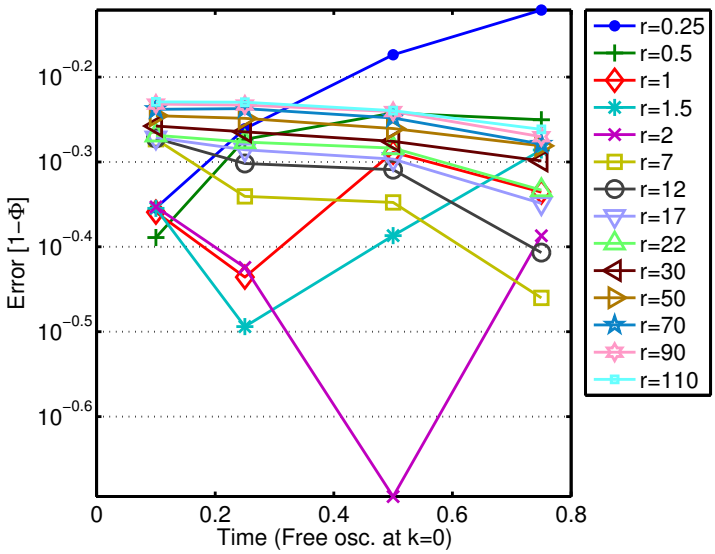

Figure B.9: Same as Fig. B.8 but with each point a median of the error with optimized pulses from 1 Rabi and 10 random initial pulses.

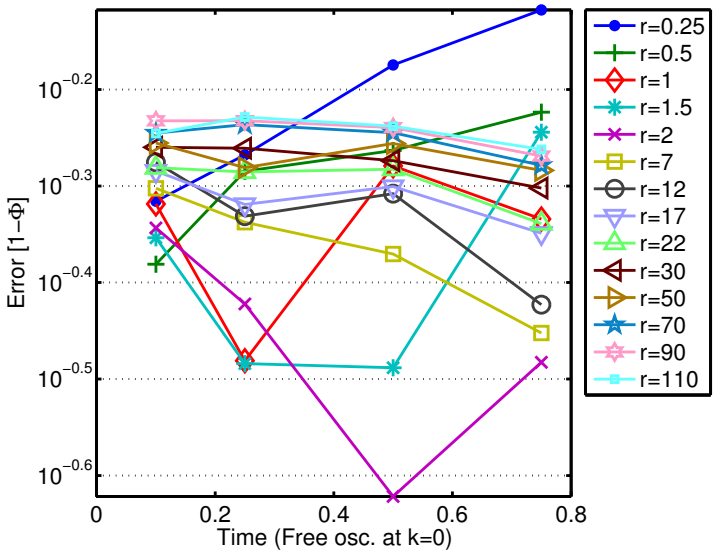

Figure B.10: Same as Fig. B.8 but with each point an average of the error with optimized pulses from 1 Rabi and 10 random initial pulses.

B.2.2 Short times

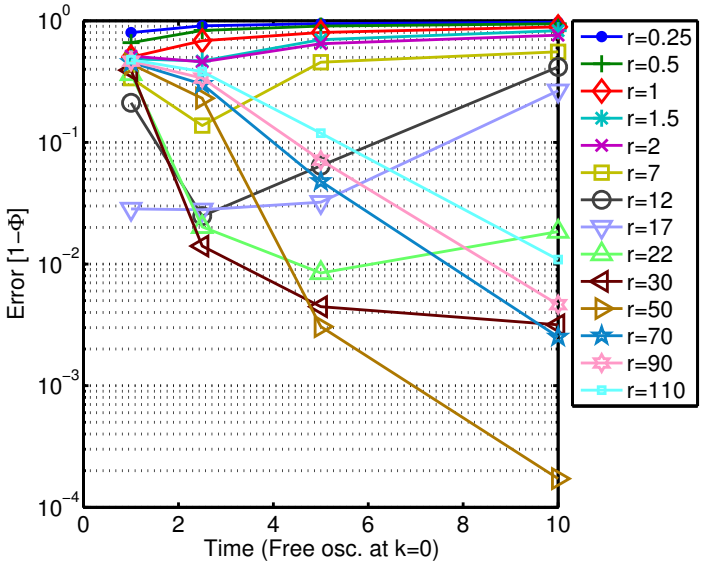

Figure B.11: The maximum fidelity for an optimized pulse over a range of times, from 1 to 10 free oscillations (at k=0), preparing a NOT gate as a series of different potential depths. The potential depth ranged from $r = 0.25$ to $r = 110$, giving a dispersion ranging from 96.9% to 0.01%, respectively. Here, the k=0 was a sampled point included for optimization. Each point is a maximum of optimized pulses from 1 Rabi and 10 random initial pulses.

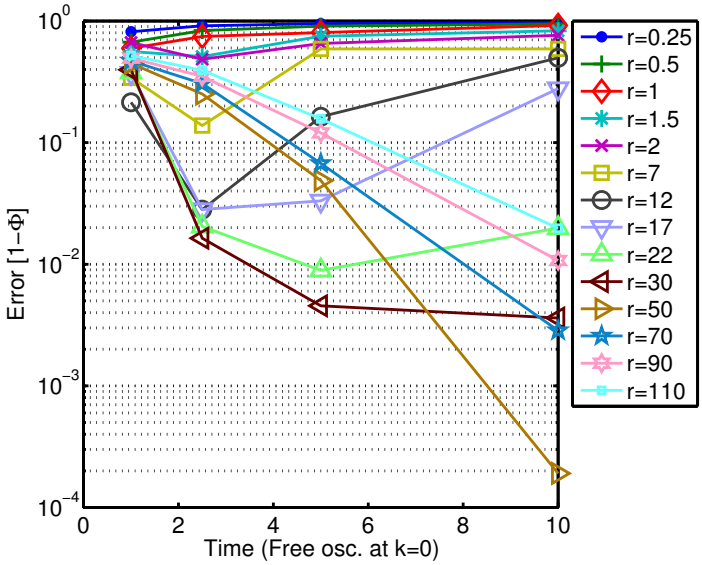

Figure B.12: Same as Fig. B.11 but with each point a median of the error with optimized pulses from 1 Rabi and 10 random initial pulses.

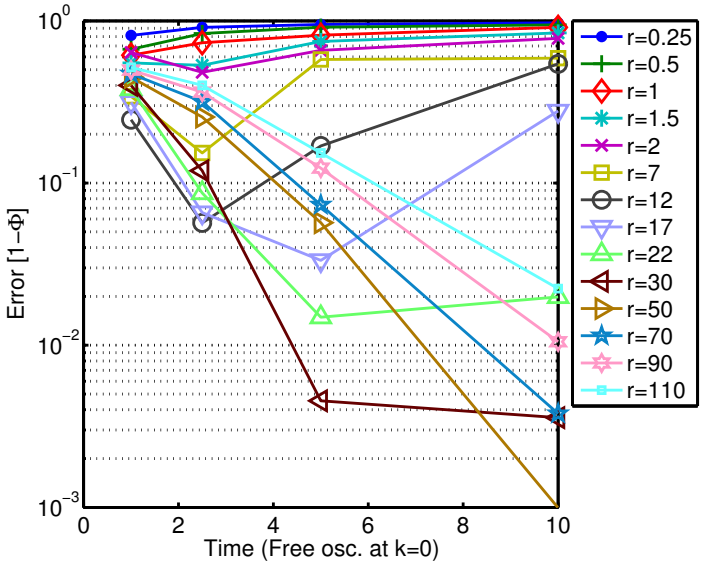

Figure B.13: Same as Fig. B.11 but with each point an average of the error with optimized pulses from 1 Rabi and 10 random initial pulses.

B.2.3 Long times

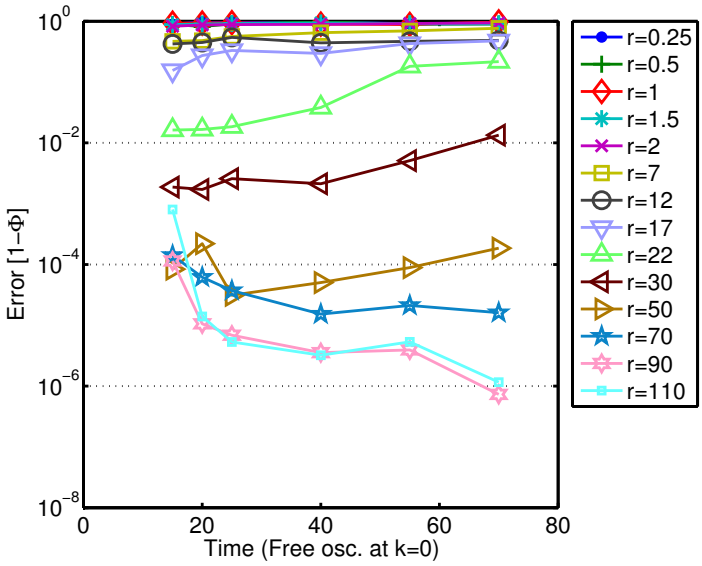

Figure B.14: The maximum fidelity for an optimized pulse over a range of times, from 15 to 70 free oscillations (at k=0), preparing a NOT gate as a series of different potential depths. The potential depth ranged from $r = 0.25$ to $r = 110$, giving a dispersion ranging from 96.9% to 0.01%, respectively. Here, the k=0 was a sampled point included for optimization. Each point is a maximum of optimized pulses from 1 Rabi and 10 random initial pulses.

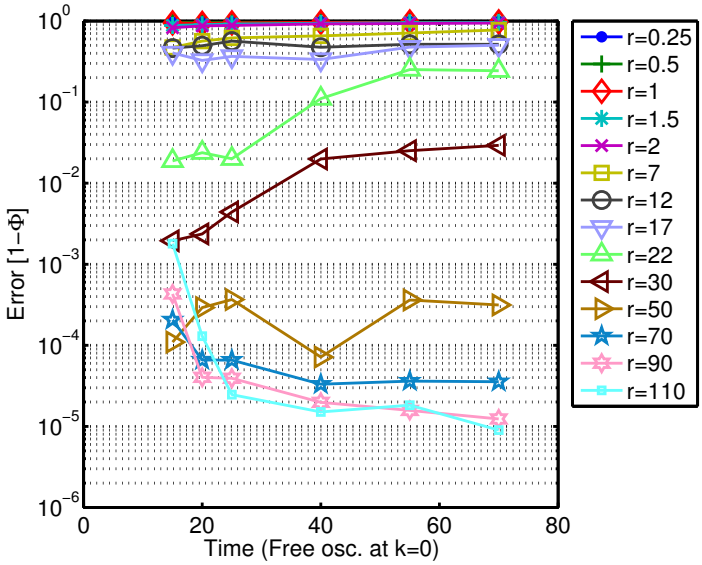

Figure B.15: Same as Fig. B.14 but with each point a median of the error with optimized pulses from 1 Rabi and 10 random initial pulses.

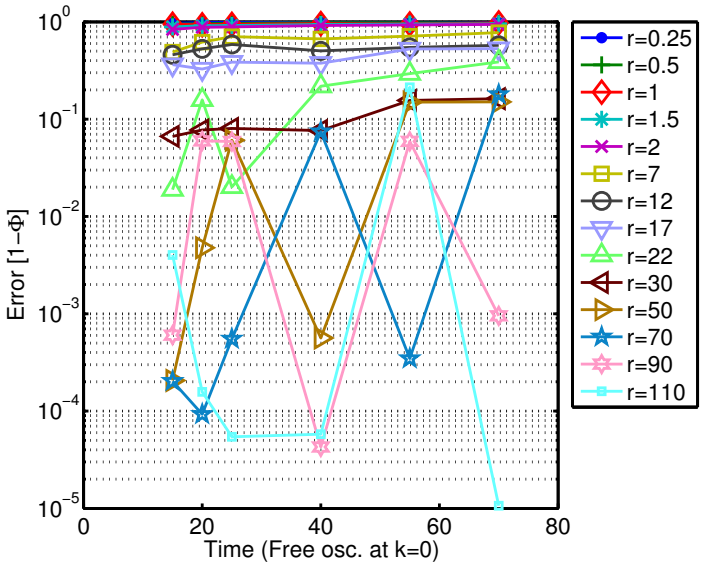

Figure B.16: Same as Fig. B.14 but with each point an average of the error with optimized pulses from 1 Rabi and 10 random initial pulses.

References

[1] Abragam. *The principles of nuclear magnetism*. Clarendon Press Oxford University Press, Oxford Oxfordshire New York, 1983. 3

[2] Neil W. Ashcroft and N. David Mermin. *Solid State Physics*. Brooks Cole, 1976. 12, 14

[3] Jonathan Baugh, Osama Moussa, Colm A. Ryan, Raymond Laflamme, Chandrasekhar Ramanathan, Timothy F. Havel, and David G. Cory. Solid-state nmr three-qubit homonuclear system for quantum-information processing: Control and characterization. *Phys. Rev. A*, 73(2):022305, Feb 2006. 3

[4] Robert Beals. Quantum computation of fourier transforms over symmetric groups. In *ACM Symposium on Theory of Computing*, pages 48–53, 1997. 2

[5] Q. Beaufils, G. Tackmann, X. Wang, B. Pelle, S. Pelisson, P. Wolf, and F. Pereira dos Santos. Laser controlled tunneling in a vertical optical lattice. *Phys. Rev. Lett.*, 106(21):213002, May 2011. 9

[6] P. Bertet, I. Chiorescu, G. Burkard, K. Semba, C. J. P. M. Harmans, D. P. DiVincenzo, and J. E. Mooij. Dephasing of a superconducting qubit induced by photon noise. *Phys. Rev. Lett.*, 95(25):257002, Dec 2005. 5

[7] I. Bloch. Quantum coherence and entanglement with ultracold atoms in optical lattices. *Nature (insight)*, 453:1016, 2008. 7

[8] Immanuel Bloch, Jean Dalibard, and Wilhelm Zwerger. Many-body physics with ultracold gases. *Rev. Mod. Phys.*, 80(3):885–964, Jul 2008. 7

[9] Robin Blume-Kohout, Hui Khoon Ng, David Poulin, and Lorenza Viola. Characterizing the structure of preserved information in quantum processes. *Phys. Rev. Lett.*, 100(3):030501, Jan 2008. 4

[10] T.W. Borneman, M.D. Hürlimann, and D.G. Cory. Application of optimal control to cpmg refocusing pulse design. *Journal of Magnetic Resonance*, 207(2):220–233, 2010. 6

[11] V. Bouchiat, D. Vion, P. Joyez, D. Esteve, and M.H. Devoret. Quantum coherence with a single cooper pair. *Physica Scripta*, 1998(T76):165, 1998. 23

[12] Gavin K. Brennen, Carlton M. Caves, Poul S. Jessen, and Ivan H. Deutsch. Quantum logic gates in optical lattices. *Phys. Rev. Lett.*, 82(5):1060–1063, Feb 1999. 7

[13] P. Brumer and M. Shapiro. *Principles of the Quantum Control of Molecular Processes*. Wiley, 2003. 25

[14] J. Bylander, S. Gustavsson, F. Yan, F. Yoshihara, K. Harrabi, G. Fitch, D. G. Cory, Y. Nakamura, J.-S. Tsai, and W. D. Oliver. Dynamical decoupling and noise spectroscopy with a superconducting flux qubit. *ArXiv e-prints*, January 2011. 4

[15] R. Chakrabarti and H. Rabitz. Quantum control landscapes. *Intl. Rev. Phys. Chem.*, 26:671, 2007. 25

[16] G. Chen, D.A. Church, B-G. Englert, C. Henkel, B. Rohwedder, M.O. Scully, and M.S. Zubairy. *Quantum Computing Devices: Principles, Designs, and Analysis*. Chapman and Hall/CRC, Boca Raton, 2006. 7

[17] Andrew M. Childs, Edward Farhi, and Sam Gutmann. An example of the difference between quantum and classical random walks. *Quantum Information Processing*, 1:35–43, 2002. 10.1023/A:1019609420309. 2

[18] J.M. Chow, L. DiCarlo, J.M. Gambetta, F. Motzoi, L. Frunzio, S.M. Girvin, and R.J. Schoelkopf. Implementing optimal control pulse shaping for improved single-qubit gates. *Phys. Rev. A*, 82:040305(R), 2010. 8

[19] J.M. Chow, J.M. Gambetta, L. Tornberg, J. Koch, L.S. Bishop, A.A. Houck, B.R. Johnson, L. Frunzio, S.M. Girvin, and R.J. Schoelkopf. Randomized benchmarking and process tomography for gate errors in a solid-state qubit. *Phys. Rev. Lett.*, 102:090502, 2009. 8

[20] J. I. Cirac and P. Zoller. Quantum computations with cold trapped ions. *Phys. Rev. Lett.*, 74(20):4091–4094, May 1995. 2

[21] John Clarke and Frank K. Wilhelm. Superconducting quantum bits. *Nature*, 453(7198):1031–1042, 06 2008. 2, 4

[22] E. Collin, G. Ithier, A. Aassime, P. Joyez, D. Vion, and D. Esteve. Nmr-like control of a quantum bit superconducting circuit. *Phys. Rev. Lett.*, 93:157005, 2004. 23

[23] Leon Couch. *Digital and analog communication systems*. Macmillan Collier Macmillan, New York London, 1990. 33

[24] H.K. Cummins and J.A. Jones. Use of composite rotations to correct systematic errors in nmr quantum computation. *New J. Phys.*, 2:6, 2000. 23

[25] P. de Fouquieres and S. G. ˜Schirmer. Quantum Control Landscapes: A Closer Look. *ArXiv e-prints*, April 2010. 37

[26] D. Deutsch. Quantum theory, the church-turing principle and the universal quantum computer. *Proceedings of the Royal Society of London. Series A, Mathematical and Physical Sciences*, 400(1818):pp. 97–117, 1985. 1, 2

[27] Ivan H. Deutsch, Gavin K. Brennen, and Poul S. Jessen. Quantum computing with neutral atoms in an optical lattice. *Fortschr. Phys.*, 48(9-11):925–943, 2000. 5, 7

[28] D. P. DiVincenzo and D. Loss. Quantum information is physical. *Superlattices and Microstructures*, 23(3-4):419 – 432, 1998. 1

[29] David P. DiVincenzo. Quantum computation. *Science*, 270(5234):pp. 255–261, 1995. 1

[30] David P. DiVincenzo and Peter W. Shor. Fault-tolerant error correction with efficient quantum codes. *Phys. Rev. Lett.*, 77(15):3260–3263, Oct 1996. 3

[31] P. Domokos, J. M. Raimond, M. Brune, and S. Haroche. Simple cavity-qed two-bit universal quantum logic gate: The principle and expected performances. *Phys. Rev. A*, 52(5):3554–3559, Nov 1995. 2

[32] Mark Ettinger and Peter Høyer. On quantum algorithms for noncommutative hidden subgroups. *Advances in Applied Mathematics*, 25(3):239 – 251, 2000. 2

[33] Richard Feynman. Simulating physics with computers. *International Journal of Theoretical Physics*, 21:467–488, 1982. 10.1007/BF02650179. 1

[34] Richard Feynman. Quantum mechanical computers. *Foundations of Physics*, 16:507–531, 1986. 10.1007/BF01886518. 1

[35] Ray Freeman. Shaped radiofrequency pulses in high resolution nmr. *Progress in Nuclear Magnetic Resonance Spectroscopy*, 32(1):59 – 106, 1998. 3

[36] D Frenkel and R Portugal. Algebraic methods to compute mathieu functions. *Journal of Physics A: Mathematical and General*, 34(17):3541, 2001. 10

[37] A. Galiautdinov, A. N. Korotkov, and J. M. Martinis. Resonator/zero-Qubit architecture for superconducting qubits. *ArXiv e-prints*, May 2011. 5

[38] J. M. Gambetta, F. Motzoi, S. T. Merkel, and F. K. Wilhelm. Analytic control methods for high-fidelity unitary operations in a weakly nonlinear oscillator. *Phys. Rev. A*, 83(1):012308, Jan 2011. 4

[39] Helen Geen and Ray Freeman. Band-selective radiofrequency pulses. *Journal of Magnetic Resonance (1969)*, 93(1):93 – 141, 1991. 4

[40] Nicolas Gisin, Grégoire Ribordy, Wolfgang Tittel, and Hugo Zbinden. Quantum cryptography. *Rev. Mod. Phys.*, 74(1):145–195, Mar 2002. 1

[41] D. Gottesman. *Stabilizer codes and quantum error correction*. PhD thesis, California Institute of Technology, 1997. 3

[42] M. Greiner, O. Mandel, T. Esslinger, T.W. Hänsch, and I. Bloch. Quantum phase transition from a superfluid to a mott insulator in a gas of ultracold atoms. *Nature*, 415:39, 2002. 7

[43] C. Griesinger, C. Gemperle, and O.W. Sørensen. Symmetry in coherence transfer. *Molecular Physics*, 62(2):295–332, 1987. 68

[44] Rudolf Grimm, Matthias Weidemüller, and Yurii B. Ovchinnikov. Optical dipole traps for neutral atoms. In Benjamin Bederson and Herbert Walther, editors, *Optical Dipole Traps for Neutral Atoms*, volume 42 of *Advances In Atomic, Molecular, and Optical Physics*, pages 95 – 170. Academic Press, 2000. 2

[45] Lov K. Grover. Quantum computers can search rapidly by using almost any transformation. *Phys. Rev. Lett.*, 80(19):4329–4332, May 1998. 2

[46] E. L. Hahn. Spin echoes. *Phys. Rev.*, 80(4):580–594, Nov 1950. 62

[47] L. Hales and S. Hallgren. An improved quantum fourier transform algorithm and applications. In *Proceedings of the 41st Annual Symposium on Foundations of Computer Science*, pages 515–, Washington, DC, USA, 2000. IEEE Computer Society. 2

[48] Brian Hall. *Lie groups, Lie algebras, and representations : an elementary introduction*. Springer, New York, 2003. 27

[49] Tyler Holden. *Time-Optimal Control of Quantum Systems: Numerical Techniques and Singular Trajectories*. PhD thesis, University of Waterloo, 2011. 4, 66

[50] A. A. Houck, J. A. Schreier, B. R. Johnson, J. M. Chow, Jens Koch, J. M. Gambetta, D. I. Schuster, L. Frunzio, M. H. Devoret, S. M. Girvin, and R. J. Schoelkopf. Controlling the spontaneous emission of a superconducting transmon qubit. *Phys. Rev. Lett.*, 101(8):080502, Aug 2008. 23

[51] A.A. Houck, J. Koch, M.H. Devoret, S.M. Girvin, and R.J. Schoelkopf. Life after charge noise: recent results with transmon qubits. *Quant. Inf. Proc.*, 8:105, 2009. 23

[52] S. Das Sarma J. P. Kestner. A proposed spin qubit cnot gate robust against noisy coupling. *arXiv:1103.1379v1*, 2011. 4

[53] D. Jaksch, C. Bruder, C.W. Gardiner, J.I. Cirac, and P. Zoller. Cold bosonic atoms in optical lattices. *Phys. Rev. Lett.*, 82:1975, 1999. 7

[54] H. Jirari, F.W.J. Hekking, and O. Buisson. Optimal control of superconducting n-level quantum systems. *EPL*, 87:28004, 2009. arXiv:0903.4028. 8

[55] A. Bryson Jr and Y.-C. Ho. *Applied Optimal Control*. Hemisphere, Washington, DC, 1975. 6, 24

[56] Richard S. Judson and Herschel Rabitz. Teaching lasers to control molecules. *Phys. Rev. Lett.*, 68:1500–1503, Mar 1992. 4

[57] J.F. Kanem, S. Maneshi, S.H. Myrskog, and A.M. Steinberg. Phase space tomography of classical and nonclassical vibrational states of atoms in an optical lattice. *Journal of Optics B: Quantum and Semiclassical Optics*, 7(12):S705, 2005. 9

[58] C. Yalçn Kaya, Stephen K. Lucas, and Sergey T. Simakov. Computations for bang–bang constrained optimal control using a mathematical programming formulation. *Optimal Control Applications and Methods*, 25(6):295–308, 2004. 4

[59] Navin Khaneja, Timo Reiss, Cindie Kehlet, Thomas Schulte-Herbrüggen, and Steffen J. Glaser. Optimal control of coupled spin dynamics: design of nmr pulse sequences by gradient ascent algorithms. *Journal of Magnetic Resonance*, 172(2):296 – 305, 2005. 4, 6, 25

[60] B. Khani, J. M. Gambetta, F. Motzoi, and F. K. Wilhelm. Optimal generation of fock states in a weakly nonlinear oscillator. *Physica Scripta*, 2009(T137):014021, 2009. 30

[61] Kaveh Khodjasteh and Lorenza Viola. Dynamical quantum error correction of unitary operations with bounded controls. *Phys. Rev. A*, 80(3):032314, Sep 2009. 4

[62] Charles Kittel. *Introduction to solid state physics*. Wiley, Hoboken, NJ, 2005. 14, 16

[63] E. Knill, R. Laflamme, and G. J. Milburn. A scheme for efficient quantum computation with linear optics. *Nature*, 409(6816):46–52, 01 2001. 2

[64] Emanuel Knill and Raymond Laflamme. Theory of quantum error-correcting codes. *Phys. Rev. A*, 55(2):900–911, Feb 1997. 3

[65] Jens Koch, Terri M. Yu, Jay Gambetta, A. A. Houck, D. I. Schuster, J. Majer, Alexandre Blais, M. H. Devoret, S. M. Girvin, and R. J. Schoelkopf. Charge-insensitive qubit design derived from the cooper pair box. *Phys. Rev. A*, 76(4):042319, Oct 2007. 3, 23

[66] V.F. Krotov. *Global Methods in Optimal Control*. Marcel Decker, New York, 1996. 4, 6

[67] I. L. Chuang L. M. K. Vandersypen. Nmr techniques for quantum control and computation. *Reviews of Modern Physics*, 76(4):1037–1069, October 2004. 3, 4

[68] T. D. Ladd, F. Jelezko, R. Laflamme, Y. Nakamura, C. Monroe, and J. L. O'Brien. Quantum computers. *Nature*, 464(7285):45–53, 03 2010. 1, 5, 7

[69] R. Landauer. Irreversibility and heat generation in the computing process. *IBM Journal of Research and Development*, 5(3):183 –191, july 1961. 1

[70] Riccardo Leardi, editor. *Nature-inspired methods in chemometrics : genetic algorithms and artificial neural networks*. Elsevier, Amsterdam Boston, 2003. 39, 66

[71] Maciej Lewenstein, Anna Sanpera, Veronica Ahufinger, Bogdan Damski, Aditi Sen, and Ujjwal Sen. Ultracold atomic gases in optical lattices: mimicking condensed matter physics and beyond. *Advances in Physics*, 56(2):243–379, 2007. 7

[72] Jr-Shin Li and Navin Khaneja. Control of inhomogeneous quantum ensembles. *Phys. Rev. A*, 73(3):030302, Mar 2006. 4, 6

[73] Jr-Shin Li, Justin Ruths, Tsyr-Yan Yu, Haribabu Arthanari, and Gerhard Wagner. Optimal pulse design in quantum control: A unified computational method. *PNAS*, 108(5):1879–1884, Feb 2011. 8

[74] D. A. Lidar and K. B. Whaley. Decoherence-Free Subspaces and Subsystems. In F. Benatti & R. Floreanini, editor, *Irreversible Quantum Dynamics*, volume 622 of *Lecture Notes in Physics, Berlin Springer Verlag*, pages 83–120, 2003. 4

[75] S. Machnes, U. Sander, S. J. Glaser, P. de Fouquieres, A. Gruslys, S. Schirmer, and T. Schulte-Herbrüggen. Comparing, optimising and benchmarking quantum control algorithms in a unifying programming framework. *arXiv:1011.4874v2*, 2010. 25

[76] Samansa Maneshi, Jalani F. Kanem, Chao Zhuang, Matt Partlow, and Aephraim M. Steinberg. Efficient vibrational state coupling in an optical tilted-washboard potential via multiple spatial translations and application to pulse echoes. *Phys. Rev. A*, 77(2):022303, Feb 2008. 7, 9, 10

[77] Samansa Maneshi, Chao Zhuang, Christopher R. Paul, Luciano S. Cruz, and Aephraim M. Steinberg. Coherence freeze in an optical lattice investigated via pump-probe spectroscopy. *Phys. Rev. Lett.*, 105:193001, Nov 2010. 9

[78] B. Misra and E. C. G. Sudarshan. The zeno's paradox in quantum theory. *Journal of Mathematical Physics*, 18(4):756–763, 1977. 4

[79] K. Mitra and C. A. R. S. de Melo. Enhancing decoherence times in superconducting qubits via circuit design. *arXiv:1001.1701v2*, January 2010. 3

[80] M. Möttönen, R. de Sousa, J. Zhang, and K.B. Whaley. High fidelity one-qubit operations under random telegraph noise. *Phys. Rev. A*, 73:022332, 2006. 4, 23

[81] F. Motzoi, J.M. Gambetta, P. Rebentrost, and F.K. Wilhelm. Simple pulses for elimination of leakage in weakly nonlinear qubits. *Phys. Rev. Lett*, 103:110501, 2009. 4, 8

[82] S. H. Myrskog, J. K. Fox, M. W. Mitchell, and A. M. Steinberg. Quantum process tomography on vibrational states of atoms in an optical lattice. *Phys. Rev. A*, 72(1):013615, Jul 2005. 9, 16, 42

[83] Y. Nakamura, Yu. A. Pashkin, and J. S. Tsai. Coherent control of macroscopic quantum states in a single-cooper-pair box. *Nature*, 398(6730):786–788, 04 1999. 23

[84] Chetan Nayak, Steven H. Simon, Ady Stern, Michael Freedman, and Sankar Das Sarma. Non-abelian anyons and topological quantum computation. *Rev. Mod. Phys.*, 80(3):1083–1159, Sep 2008. 2

[85] H. Paik, D. I. Schuster, L. S. Bishop, G. Kirchmair, G. Catelani, A. P. Sears, B. R. Johnson, M. J. Reagor, L. Frunzio, L. Glazman, and R. J. Schoelkopf. How coherent are Josephson junctions? *ArXiv e-prints*, May 2011. 5

[86] S. Pasini, P. Karbach, C. Raas, and G. S. Uhrig. Optimized pulses for the perturbative decoupling of a spin and a decoherence bath. *Phys. Rev. A*, 80(2):022328, Aug 2009. 4

[87] F. Platzer, F. Mintert, and A. Buchleitner. Optimal dynamic control of many-body entanglement. *Physical Review Letters*, 105(2), 2010. 6

[88] H. Rabitz, T.-S. Ho, M. Hsieh, R. Kosut, and M. Demiralp. Topology of optimally controlled quantum mechanical transition probability landscapes. *Phys. Rev. A*, 74(1):012721, Jul 2006. 38

[89] P. Rebentrost and F.K. Wilhelm. Optimal control of a leaking qubit. *Phys. Rev. B*, 79:060507(R), 2009. arXiv:0808.2680. 8

[90] S.A. Rice and M. Zhao. *Optimal Control of Molecular Dynamics*. Wiley, 2000. 6, 25

[91] D. Rossini, P. Facchi, R. Fazio, G. Florio, D. A. Lidar, S. Pascazio, F. Plastina, and P. Zanardi. Bang-bang control of a qubit coupled to a quantum critical spin bath. *Phys. Rev. A*, 77(5):052112, May 2008. 4

[92] S. Safaei, S. Montangero, F. Taddei, and R. Fazio. Optimized single-qubit gates for josephson phase qubits. *Phys. Rev. B*, 79:064524, 2009. 8

[93] R.S. Said and J. Twamley. Robust control of entanglement in a nitrogen-vacancy center coupled to a c 13 nuclear spin in diamond. *Physical Review A - Atomic, Molecular, and Optical Physics*, 80(3), 2009. 6

[94] P-I. Schneider and A. Saenz. Quantum computation with ultracold atoms in a driven optical lattice. arXiv:1103.4950, 2011. 6, 7

[95] Gerd Schön and A. D. Zaikin. Quantum coherent effects, phase transitions, and the dissipative dynamics of ultra small tunnel junctions. *Physics Reports*, 198(5-6):237 – 412, 1990. 23

[96] P. W. Shor. Algorithms for quantum computation: discrete logarithms and factoring. In *Proceedings of the 35th Annual Symposium on Foundations of Computer Science*, pages 124–134, Washington, DC, USA, 1994. IEEE Computer Society. 1

[97] Jonathan Simon, Waseem S. Bakr, Ruichao Ma, M. Eric Tai, Philipp M. Preiss, and Markus Greiner. Quantum simulation of antiferromagnetic spin chains in an optical lattice. *Nature*, 472(7343):307–312, 04 2011. 7

[98] T.E. Skinner, M. Braun, K. Woelk, N.I. Gershenzon, and S.J. Glaser. Design and application of robust rf pulses for toroid cavity nmr spectroscopy. *Journal of Magnetic Resonance*, 209(2):282–290, 2011. 6

[99] Thomas E. Skinner, Timo O. Reiss, Burkhard Luy, Navin Khaneja, and Steffen J. Glaser. Application of optimal control theory to the design of broadband excitation pulses for high-resolution nmr. *Journal of Magnetic Resonance*, 163(1):8 – 15, 2003. 4

[100] Charles Slichter. *Principles of magnetic resonance*. Springer-Verlag, Berlin New York, 1990. 3

[101] M. Steffen, J.M. Martinis, and I.L. Chuang. Accurate control of josephson phase qubits. *Phys. Rev. B*, 68:224518, 2003. 8

[102] M. J. Storcz, J. Vala, K. R. Brown, J. Kempe, F. K. Wilhelm, and K. B. Whaley. Full protection of superconducting qubit systems from coupling errors. *Phys. Rev. B*, 72(6):064511, Aug 2005. 4

[103] Q. A. Turchette, C. J. Hood, W. Lange, H. Mabuchi, and H. J. Kimble. Measurement of conditional phase shifts for quantum logic. *Phys. Rev. Lett.*, 75(25):4710–4713, Dec 1995. 2

[104] Götz S. Uhrig. Keeping a quantum bit alive by optimized π-pulse sequences. *Phys. Rev. Lett.*, 98(10):100504, Mar 2007. 4

[105] Lorenza Viola. Quantum control via encoded dynamical decoupling. *Phys. Rev. A*, 66(1):012307, Jul 2002. 4

[106] Lorenza Viola and Seth Lloyd. Dynamical suppression of decoherence in two-state quantum systems. *Phys. Rev. A*, 58(4):2733–2744, Oct 1998. 4

[107] D. Vion, A. Aassime, A. Cottet, P. Joyez, H. Pothier, C. Urbina, D. Esteve, and M. H. Devoret. Manipulating the quantum state of an electrical circuit. *Science*, 296(5569):886–889, 2002. 5

[108] M. Wallquist, V. S. Shumeiko, and G. Wendin. Selective coupling of superconducting charge qubits mediated by a tunable stripline cavity. *Phys. Rev. B*, 74(22):224506, Dec 2006. 5

[109] X. Wang, A. Bayat, S.G. Schirmer, and S. Bose. Robust entanglement in antiferromagnetic heisenberg chains by single-spin optimal control. *Physical Review A - Atomic, Molecular, and Optical Physics*, 81(3), 2010. 6

[110] J. Q. You, Xuedong Hu, S. Ashhab, and Franco Nori. Low-decoherence flux qubit. *Phys. Rev. B*, 75(14):140515, Apr 2007. 23

[111] Y. Zhang, M. Lapert, D. Sugny, M. Braun, and S.J. Glaser. Time-optimal control of spin 1/2 particles in the presence of radiation damping and relaxation. *Journal of Chemical Physics*, 134(5), 2011. 6

[112] Zhigang Zhang, Goong Chen, Zijian Diao, and Philip R. Hemmer. Nmr quantum computing. In *Advances in Applied Mathematics and Global Optimization*, volume 17 of *Advances in Mechanics and Mathematics*, pages 1–56. Springer US, 2009. 10.1007/978-0-387-75714-8_14. 2